



DIRECTION FINDING PERFORMANCE OF ANTENNA ARRAYS ON COMPLEX  
PLATFORMS USING NUMERICAL ELECTROMAGNETIC SIMULATION TOOLS

A THESIS SUBMITTED TO  
THE GRADUATE SCHOOL OF NATURAL AND APPLIED SCIENCES  
OF  
MIDDLE EAST TECHNICAL UNIVERSITY

BY

MUSTAFA ONUR ÖZEÇ

IN PARTIAL FULFILLMENT OF THE REQUIREMENTS  
FOR  
THE DEGREE OF MASTER OF SCIENCE  
IN  
ELECTRICAL AND ELECTRONICS ENGINEERING

SEPTEMBER 2011

Approval of the thesis:

**DIRECTION FINDING PERFORMANCE OF ANTENNA ARRAYS ON COMPLEX  
PLATFORMS USING NUMERICAL ELECTROMAGNETIC SIMULATION TOOLS**

submitted by **MUSTAFA ONUR ÖZEÇ** in partial fulfillment of the requirements for the degree of **Master of Science in Electrical and Electronics Engineering Department, Middle East Technical University** by,

Prof. Dr. Canan Özgen  
Dean, Graduate School of **Natural and Applied Sciences**

\_\_\_\_\_

Prof. Dr. İsmet Erkmn  
Head of Department, **Electrical and Electronics Engineering**

\_\_\_\_\_

Prof. Dr. T. Engin Tuncer  
Supervisor, **Electrical and Electronics Eng. Dept., METU**

\_\_\_\_\_

**Examining Committee Members:**

Assoc. Prof. Dr. Şimşek Demir  
Electrical and Electronics Eng. Dept., METU

\_\_\_\_\_

Prof. Dr. T. Engin Tuncer  
Electrical and Electronics Eng. Dept., METU

\_\_\_\_\_

Dr. Arzu Tuncay Koç  
Electrical and Electronics Eng. Dept., METU

\_\_\_\_\_

Dr. Fatih Kamışlı  
Electrical and Electronics Eng. Dept., METU

\_\_\_\_\_

Dr. Serkan Karakütük  
MİKES Inc.

\_\_\_\_\_

**Date:**

\_\_\_\_\_

**I hereby declare that all information in this document has been obtained and presented in accordance with academic rules and ethical conduct. I also declare that, as required by these rules and conduct, I have fully cited and referenced all material and results that are not original to this work.**

Name, Last Name: MUSTAFA ONUR ÖZEÇ

Signature :

# ABSTRACT

## DIRECTION FINDING PERFORMANCE OF ANTENNA ARRAYS ON COMPLEX PLATFORMS USING NUMERICAL ELECTROMAGNETIC SIMULATION TOOLS

Özeç, Mustafa Onur

M.Sc., Department of Electrical and Electronics Engineering

Supervisor : Prof. Dr. T. Engin Tuncer

September 2011, 124 pages

An important step for the design of direction finding systems is the performance evaluation using numeric electromagnetic simulation tools. In this thesis, a method is presented for both modeling and simulation in a numeric electromagnetic simulation tool FEKO. The method relies on the data generated by FEKO. The data is then processed by correlative interferometer algorithm. This process is implemented in a MATLAB environment. Different types of antenna arrays including dipole, monopole and discone antennas are used. The antenna arrays are mounted on a UAV and SUV in order to see the platform effects. The direction finding performance is evaluated for different scenarios. It is shown that the presented approach is an effective tool for understanding the direction finding characteristic of antenna arrays.

Keywords: Direction Finding, Correlative Interferometer, Numerical Electromagnetic Simulation Tools, Platform Effects

# ÖZ

## ANTEN DİZİLERİNİN KARMAŞIK PLATFORMLARDA NÜMERİK ELEKTROMANYETİK SİMÜLASYON YÖNTEMLERİYLE YÖN BULMA PERFORMANSLARININ İNCELENMESİ

Özeç, Mustafa Onur

Yüksek Lisans, Elektrik ve Elektronik Mühendisliği Bölümü

Tez Yöneticisi : Prof. Dr. T. Engin Tuncer

Eylül 2011, 124 sayfa

Yön Bulma sistemlerinin tasarımındaki önemli adımlardan biri Nümerik Elektromanyetik Simülasyon araçlarıyla Yön Bulma performanslarının değerlendirilmesidir. Bu tezde, Nümerik Elektromanyetik Simülasyon aracı olan FEKO programı vasıtasıyla modelleme ve simülasyon yöntemi geliştirilmiştir. Bu metod, FEKO programında oluşturulan verilere dayanmaktadır. FEKO'da elde edilen veriler Korelatif Enterferometre algoritması vasıtasıyla MATLAB ortamında Yön Bulma performansını belirlemek için kullanılmaktadır. Bu çalışmada dipol, monopol ve düşey konili anten dizileri kullanılmıştır. Anten dizileri, platform etkilerini gözlemlemek için UAV ve SUV araçlarına monte edilmiştir. Yön Bulma performansı değişik senaryolarda denenmiştir. Bu tezde geliştirilen simülasyon yönteminin anten dizilerinin yön bulma karakteristiklerini anlamada etkili olduğu gösterilmiştir.

Anahtar Kelimeler: Yön Bulma, Korelatif Enterferometre, Nümerik Elektromanyetik Simülasyon Yöntemleri, Platform Etkileri

*To my family*

## **ACKNOWLEDGMENTS**

I would like to thank my supervisor Prof. Dr. T. Engin Tuncer for his guidance, encouragement and patience throughout the completion of the thesis.

I would like to thank to Dr. Tansu Filik, Yılmaz Kalkan, Dr. Serkan Karakütük, Metin Aktaş and M. Fatih Bayramođlu for their support and friendship during my thesis work.

I would like to thank to Tübitak Bideb, for their financial support during my graduate study.

Finally, I would like to thank to my mother for her support to finish my thesis work.

# TABLE OF CONTENTS

ABSTRACT . . . . .	iv
ÖZ . . . . .	v
ACKNOWLEDGMENTS . . . . .	vii
TABLE OF CONTENTS . . . . .	viii
LIST OF TABLES . . . . .	xi
LIST OF FIGURES . . . . .	xii
CHAPTERS	
1 INTRODUCTION . . . . .	1
1.1 Direction Finding . . . . .	1
1.1.1 History of Direction Finding . . . . .	1
1.1.2 Classical and Modern Direction Finding Techniques . . . . .	2
1.2 Description of Thesis Work . . . . .	3
1.3 Organization . . . . .	5
2 DF SYSTEM COMPONENTS AND NUMERICAL ELECTROMAGNETIC COMPUTATIONAL TOOLS . . . . .	6
2.1 DF System Components . . . . .	6
2.1.1 Flow Chart of Simulation Methodology . . . . .	7
2.1.2 Signal Model . . . . .	9
2.1.3 Correlative Interferometer Method . . . . .	10
2.1.4 Flow Chart of Correlative Interferometer Methodology . . . . .	12
2.1.5 Cubic Spline Interpolation Method . . . . .	15
2.1.6 Multipath Effects . . . . .	17
2.2 Numerical Electromagnetic Computational Tools . . . . .	19
2.2.1 FEKO Tools and Simulation Settings . . . . .	20

3	WIDEBAND ANTENNA DF SYSTEM . . . . .	22
3.1	Antenna Models . . . . .	23
3.1.1	Discone Antenna Model . . . . .	23
3.1.2	Dipole Antenna Model . . . . .	30
3.1.2.1	Band-1 Dipole Antenna Model . . . . .	30
3.1.2.2	Band-2 Dipole Antenna Model . . . . .	32
3.2	Wideband Antenna Simulation Results . . . . .	35
3.2.1	Band-1 Simulations . . . . .	36
3.2.2	Band-2 Simulations . . . . .	45
3.3	Discussions . . . . .	53
4	DF SYSTEM ON UAV WITH DIPOLE ANTENNAS . . . . .	56
4.1	Dipole Antenna and UAV Model . . . . .	57
4.1.1	Dipole Antenna Model . . . . .	58
4.1.2	UAV Feko Model with Four Antenna . . . . .	59
4.1.3	UAV Feko Model with Eight Antenna . . . . .	62
4.2	Simulation Results for the UAV . . . . .	65
4.2.1	Four Antenna Model Simulation Results . . . . .	66
4.2.2	Eight Antenna Model Simulation Results . . . . .	74
4.3	Discussions . . . . .	82
5	DF SYSTEM ON SUV WITH MONOPOLE ANTENNAS . . . . .	84
5.1	SUV Model . . . . .	85
5.1.1	Antenna Model . . . . .	85
5.1.2	SUV Feko Model . . . . .	86
5.2	Simulation Results for the SUV . . . . .	91
5.2.1	Perfect Electric Conductor vs. Dielectric Medium . . . . .	92
5.3	Bias Analysis . . . . .	98
5.3.1	Perfect Electric Conductor vs Dielectric Medium-1 . . . . .	100
5.3.2	Perfect Electric Conductor vs Dielectric Medium-2 . . . . .	107
5.4	Discussions . . . . .	114

6	CONCLUSION . . . . .	116
	REFERENCES . . . . .	120

## LIST OF TABLES

### TABLES

Table 3.1	Discone antenna design parameters . . . . .	23
Table 3.2	Band-1 dipole antenna design parameters . . . . .	31
Table 3.3	Band-2 dipole antenna design parameters . . . . .	33
Table 4.1	Dipole antenna design parameters . . . . .	58
Table 5.1	Monopole antenna design parameters . . . . .	86

## LIST OF FIGURES

### FIGURES

Figure 2.1 Flow Chart of Simulation Pattern . . . . .	8
Figure 2.2 Flow Chart of Correlative Interferometer Method . . . . .	14
Figure 2.3 Reflection from smooth and conducting surface . . . . .	17
Figure 2.4 Plane Waves reflection from smooth and conducting surface . . . . .	18
Figure 3.1 Discone antenna dimensions . . . . .	24
Figure 3.2 Discone antenna array structure . . . . .	25
Figure 3.3 CADFEKO model of discone with four antennas . . . . .	25
Figure 3.4 CADFEKO model of discone with four antennas, three antennas separated by 120 degree, one antenna reversed, scaled by 0.5 and centered between three antennas . . . . .	26
Figure 3.5 CADFEKO model of discone with four antennas, three antennas separated by 120 degree, one antenna reversed and centered between three antennas . . . . .	26
Figure 3.6 CADFEKO model of discone with four antennas, three antennas separated by 135 degree, one antenna reversed and centered between three antennas . . . . .	27
Figure 3.7 CADFEKO model of discone with four antennas, antennas are reversed and have the same z-axis coordinates . . . . .	28
Figure 3.8 CADFEKO model of discone with four antennas, antennas are reversed and have different z-axis coordinates . . . . .	29
Figure 3.9 CADFEKO model of discone with five antennas, four of the antennas are on the same plane,one antenna is reversed and placed on top of x-axis antenna with a gap . . . . .	29
Figure 3.10 CADFEKO model of discone with five antennas with one dipole on the center of the four discone antennas lying on the same plane . . . . .	30

Figure 3.11 Band-1 dipole antenna dimensions . . . . .	31
Figure 3.12 Band-1 dipole antenna array structure . . . . .	32
Figure 3.13 CADFEKO model of band-1 dipole antenna . . . . .	32
Figure 3.14 Band-2 dipole antenna dimensions . . . . .	33
Figure 3.15 Band-2 dipole antenna array structure . . . . .	34
Figure 3.16 CADFEKO model of band-2 dipole antenna . . . . .	34
Figure 3.17 104 MHz, elevation angle is 72 degrees, comparison of DF performance of discone antennas (with 120 degree alignment and a 0.5 scaled discone on the center) and dipole antennas having four elements . . . . .	36
Figure 3.18 104 MHz, elevation angle is 90 degrees, comparison of DF performance of discone antennas (with 120 degree alignment and a 0.5 scaled discone on the center) and dipole antennas having four elements . . . . .	37
Figure 3.19 104 MHz, elevation angle is 108 degrees, comparison of DF performance of discone antennas (with 120 degree alignment and a 0.5 scaled discone on the center) and dipole antennas having four elements . . . . .	38
Figure 3.20 312 MHz, elevation angle is 72 degrees, comparison of DF performance of discone antennas (with 120 degree alignment and a 0.5 scaled discone on the center) and dipole antennas having four elements . . . . .	38
Figure 3.21 312 MHz, elevation angle is 90 degrees, comparison of DF performance of discone antennas (with 120 degree alignment and a 0.5 scaled discone on the center) and dipole antennas having four elements . . . . .	39
Figure 3.22 312 MHz, elevation angle is 108 degrees, comparison of DF performance of discone antennas (with 120 degree alignment and a 0.5 scaled discone on the center) and dipole antennas having four elements . . . . .	40
Figure 3.23 452 MHz, elevation angle is 72 degrees, comparison of DF performance of discone antennas (with 120 degree alignment and a 0.5 scaled discone on the center) and dipole antennas having four elements . . . . .	40
Figure 3.24 452 MHz, elevation angle is 90 degrees, comparison of DF performance of discone antennas (with 120 degree alignment and a 0.5 scaled discone on the center) and dipole antennas having four elements . . . . .	41

Figure 3.25 452 MHz, elevation angle is 108 degrees, comparison of DF performance of discone antennas (with 120 degree alignment and a 0.5 scaled discone on the center) and dipole antennas having four elements . . . . .	41
Figure 3.26 504 MHz, elevation angle is 72 degrees, comparison of DF performance of discone antennas (with 120 degree alignment and a 0.5 scaled discone on the center) and dipole antennas having four elements . . . . .	42
Figure 3.27 504 MHz, elevation angle is 90 degrees, comparison of DF performance of discone antennas (with 120 degree alignment and a 0.5 scaled discone on the center) and dipole antennas having four elements . . . . .	43
Figure 3.28 504 MHz, elevation angle is 108 degrees, comparison of DF performance of discone antennas (with 120 degree alignment and a 0.5 scaled discone on the center) and dipole antennas having four elements . . . . .	43
Figure 3.29 648 MHz, elevation angle is 72 degrees, comparison of DF performance of discone antennas (with 120 degree alignment and a 0.5 scaled discone on the center) and dipole antennas having four elements . . . . .	44
Figure 3.30 648 MHz, elevation angle is 90 degrees, comparison of DF performance of discone antennas (with 120 degree alignment and a 0.5 scaled discone on the center) and dipole antennas having four elements . . . . .	44
Figure 3.31 648 MHz, elevation angle is 108 degrees, comparison of DF performance of discone antennas (with 120 degree alignment and a 0.5 scaled discone on the center) and dipole antennas having four elements . . . . .	45
Figure 3.32 648 MHz, elevation angle is 72 degrees, comparison of DF performance of discone antennas (with 120 degree alignment and a 0.5 scaled discone on the center) and dipole antennas having four elements . . . . .	46
Figure 3.33 648 MHz, elevation angle is 90 degrees, comparison of DF performance of discone antennas (with 120 degree alignment and a 0.5 scaled discone on the center) and dipole antennas having four elements . . . . .	47
Figure 3.34 648 MHz, elevation angle is 108 degrees, comparison of DF performance of discone antennas (with 120 degree alignment and a 0.5 scaled discone on the center) and dipole antennas having four elements . . . . .	47

Figure 3.35 800 MHz, elevation angle is 72 degrees, comparison of DF performance of discone antennas (with 120 degree alignment and a 0.5 scaled discone on the center) and dipole antennas having four elements . . . . .	48
Figure 3.36 800 MHz, elevation angle is 90 degrees, comparison of DF performance of discone antennas (with 120 degree alignment and a 0.5 scaled discone on the center) and dipole antennas having four elements . . . . .	49
Figure 3.37 800 MHz, elevation angle is 108 degrees, comparison of DF performance of discone antennas (with 120 degree alignment and a 0.5 scaled discone on the center) and dipole antennas having four elements . . . . .	49
Figure 3.38 1148 MHz, elevation angle is 72 degrees, comparison of DF performance of discone antennas (with 120 degree alignment and a 0.5 scaled discone on the center) and dipole antennas having four elements . . . . .	50
Figure 3.39 1148 MHz, elevation angle is 90 degrees, comparison of DF performance of discone antennas (with 120 degree alignment and a 0.5 scaled discone on the center) and dipole antennas having four elements . . . . .	51
Figure 3.40 1148 MHz, elevation angle is 108 degrees, comparison of DF performance of discone antennas (with 120 degree alignment and a 0.5 scaled discone on the center) and dipole antennas having four elements . . . . .	52
Figure 3.41 1496 MHz, elevation angle is 72 degrees, comparison of DF performance of discone antennas (with 120 degree alignment and a 0.5 scaled discone on the center) and dipole antennas having four elements . . . . .	52
Figure 3.42 1496 MHz, elevation angle is 90 degrees, comparison of DF performance of discone antennas (with 120 degree alignment and a 0.5 scaled discone on the center) and dipole antennas having four elements . . . . .	53
Figure 3.43 1496 MHz, elevation angle is 108 degrees, comparison of DF performance of discone antennas (with 120 degree alignment and a 0.5 scaled discone on the center) and dipole antennas having four elements . . . . .	54
Figure 4.1 Circular array antenna pattern with antenna interelement distance 35cm . .	58
Figure 4.2 Dipole antenna dimensions . . . . .	59
Figure 4.3 Heron feko model isometric view, with four antennas under main body with antenna interelement distance of 35cm. . . . .	60

Figure 4.4 Heron feko model front view, with four antennas under main body with antenna interelement distance of 35cm. . . . .	60
Figure 4.5 Heron feko model back view, with four antennas under main body with antenna interelement distance of 35cm. . . . .	61
Figure 4.6 Heron feko model including infinite dielectric ground medium , with dielectric medium properties, relative permittivity $\epsilon_r=15$ and conductivity $\sigma=0.04$ , four antenna under main body with antenna interelement distance of 35cm. . . . .	61
Figure 4.7 Heron feko model including infinite perfect electric conductor ground medium, with four antenna under main body with antenna interelement distance of 35cm. . . . .	62
Figure 4.8 Heron feko model isometric view, with eight antennas on rear wing arms with antenna interelement distance of 35cm. . . . .	63
Figure 4.9 Heron feko model detailed antenna view, with eight antennas on rear wing arms with antenna interelement distance of 35cm. . . . .	63
Figure 4.10 Heron feko model back view, with eight antennas on rear wing arms with antenna interelement distance of 35cm. . . . .	64
Figure 4.11 Heron feko model including infinite dielectric ground medium , with dielectric medium properties, relative permittivity $\epsilon_r=15$ and conductivity $\sigma=0.04$ , eight antenna on rear wing arms with antenna interelement distance of 35cm. . . . .	64
Figure 4.12 Heron feko model including infinite perfect electric conductor ground medium, model has 10 meters elevation from ground medium, with eight antennas on rear wing arms with antenna interelement distance of 35cm. . . . .	65
Figure 4.13 Heron feko model including infinite perfect electric conductor ground medium, model has four meters elevation from ground medium, with eight antennas on rear wing arms with antenna interelement distance of 35cm. . . . .	65
Figure 4.14 20 MHz, Perfect Electric Conductor versus Dielectric medium, with relative permittivity $\epsilon_r=15$ and conductivity $\sigma=0.04$ , elevation angle is 92 degree. . . . .	67
Figure 4.15 20 MHz, Perfect Electric Conductor versus Dielectric medium, with relative permittivity $\epsilon_r=15$ and conductivity $\sigma=0.04$ , elevation angle is 98 degree. . . . .	68
Figure 4.16 60 MHz, Perfect Electric Conductor versus Dielectric medium, with relative permittivity $\epsilon_r=15$ and conductivity $\sigma=0.04$ , elevation angle is 92 degree. . . . .	68

Figure 4.17 60 MHz, Perfect Electric Conductor versus Dielectric medium, with relative permittivity $\epsilon_r=15$ and conductivity $\sigma=0.04$ , elevation angle is 98 degree. . .	69
Figure 4.18 100 MHz, Perfect Electric Conductor versus Dielectric medium, with relative permittivity $\epsilon_r=15$ and conductivity $\sigma=0.04$ , elevation angle is 92 degree. . .	70
Figure 4.19 100 MHz, Perfect Electric Conductor versus Dielectric medium, with relative permittivity $\epsilon_r=15$ and conductivity $\sigma=0.04$ , elevation angle is 98 degree. . .	70
Figure 4.20 250 MHz, Perfect Electric Conductor versus Dielectric medium, with relative permittivity $\epsilon_r=15$ and conductivity $\sigma=0.04$ , elevation angle is 92 degree. . .	71
Figure 4.21 250 MHz, Perfect Electric Conductor versus Dielectric medium, with relative permittivity $\epsilon_r=15$ and conductivity $\sigma=0.04$ , elevation angle is 98 degree. . .	71
Figure 4.22 375 MHz, Perfect Electric Conductor versus Dielectric medium, with relative permittivity $\epsilon_r=15$ and conductivity $\sigma=0.04$ , elevation angle is 92 degree. . .	72
Figure 4.23 375 MHz, Perfect Electric Conductor versus Dielectric medium, with relative permittivity $\epsilon_r=15$ and conductivity $\sigma=0.04$ , elevation angle is 98 degree. . .	72
Figure 4.24 500 MHz, Perfect Electric Conductor versus Dielectric medium, with relative permittivity $\epsilon_r=15$ and conductivity $\sigma=0.04$ , elevation angle is 92 degree. . .	73
Figure 4.25 500 MHz, Perfect Electric Conductor versus Dielectric medium, with relative permittivity $\epsilon_r=15$ and conductivity $\sigma=0.04$ , elevation angle is 98 degree. . .	73
Figure 4.26 20 MHz, Perfect Electric Conductor versus Dielectric medium, with relative permittivity $\epsilon_r=15$ and conductivity $\sigma=0.04$ , elevation angle is 92 degree. . .	74
Figure 4.27 20 MHz, Perfect Electric Conductor versus Dielectric medium, with relative permittivity $\epsilon_r=15$ and conductivity $\sigma=0.04$ , elevation angle is 98 degree. . .	75
Figure 4.28 60 MHz, Perfect Electric Conductor versus Dielectric medium, with relative permittivity $\epsilon_r=15$ and conductivity $\sigma=0.04$ , elevation angle is 92 degree. . .	75
Figure 4.29 60 MHz, Perfect Electric Conductor versus Dielectric medium, with relative permittivity $\epsilon_r=15$ and conductivity $\sigma=0.04$ , elevation angle is 98 degree. . .	76
Figure 4.30 100 MHz, Perfect Electric Conductor versus Dielectric medium, with relative permittivity $\epsilon_r=15$ and conductivity $\sigma=0.04$ , elevation angle is 92 degree. . .	77
Figure 4.31 100 MHz, Perfect Electric Conductor versus Dielectric medium, with relative permittivity $\epsilon_r=15$ and conductivity $\sigma=0.04$ , elevation angle is 98 degree. . .	77

Figure 4.32 250 MHz, Perfect Electric Conductor versus Dielectric medium, with relative permittivity $\epsilon_r=15$ and conductivity $\sigma=0.04$ , elevation angle is 92 degree. . .	78
Figure 4.33 250 MHz, Perfect Electric Conductor versus Dielectric medium, with relative permittivity $\epsilon_r=15$ and conductivity $\sigma=0.04$ , elevation angle is 98 degree. . .	79
Figure 4.34 375 MHz, Perfect Electric Conductor versus Dielectric medium, with relative permittivity $\epsilon_r=15$ and conductivity $\sigma=0.04$ , elevation angle is 92 degree . .	79
Figure 4.35 375 MHz, Perfect Electric Conductor versus Dielectric medium, with relative permittivity $\epsilon_r=15$ and conductivity $\sigma=0.04$ , elevation angle is 98 degree . .	80
Figure 4.36 500 MHz, Perfect Electric Conductor versus Dielectric medium, with relative permittivity $\epsilon_r=15$ and conductivity $\sigma=0.04$ , elevation angle is 92 degree . .	81
Figure 4.37 500 MHz, Perfect Electric Conductor versus Dielectric medium, with relative permittivity $\epsilon_r=15$ and conductivity $\sigma=0.04$ , elevation angle is 98 degree . .	81
Figure 4.38 500 MHz, Perfect Electric Conductor versus air, ground 10m vs 4m, elevation angle is 92 degree . . . . .	82
Figure 4.39 500 MHz, Perfect Electric Conductor versus air, ground 10m vs 4m, elevation angle is 98 degree . . . . .	83
Figure 5.1 Monopole antenna dimensions . . . . .	86
Figure 5.2 Circular array antenna pattern with antenna interelement distance 35cm . .	87
Figure 5.3 Hummer feko model isometric view. Monopole antenna interelement distance is 35cm. . . . .	87
Figure 5.4 Hummer feko model detailed antenna view . . . . .	88
Figure 5.5 Hummer feko model front view . . . . .	88
Figure 5.6 Hummer feko model side view . . . . .	89
Figure 5.7 Hummer feko model back view . . . . .	89
Figure 5.8 Hummer feko model bottom view . . . . .	90
Figure 5.9 Hummer feko model above infinite dielectric ground medium . . . . .	90
Figure 5.10 20 MHz, Perfect Electric Conductor versus Dielectric medium, with relative permittivity $\epsilon_r=15, 13$ and $4$ respectively, and conductivity $\sigma=0.04, 0.03$ and $0.06$ respectively, elevation angle is 72 degrees. . . . .	92

Figure 5.11 20 MHz, Perfect Electric Conductor versus Dielectric medium, with relative permittivity $\epsilon_r=15, 13$ and $4$ respectively, and conductivity $\sigma=0.04, 0.03$ and $0.06$ respectively, elevation angle is $88$ degrees. . . . .	93
Figure 5.12 100 MHz, Perfect Electric Conductor versus Dielectric medium, with relative permittivity $\epsilon_r=15, 13$ and $4$ respectively, and conductivity $\sigma=0.04, 0.03$ and $0.06$ respectively, elevation angle is $72$ degrees. . . . .	94
Figure 5.13 100 MHz, Perfect Electric Conductor versus Dielectric medium, with relative permittivity $\epsilon_r=15, 13$ and $4$ respectively, and conductivity $\sigma=0.04, 0.03$ and $0.06$ respectively, elevation angle is $88$ degrees. . . . .	94
Figure 5.14 250 MHz, Perfect Electric Conductor versus Dielectric medium, with relative permittivity $\epsilon_r=15, 13$ and $4$ respectively, and conductivity $\sigma=0.04, 0.03$ and $0.06$ respectively, elevation angle is $72$ degrees. . . . .	95
Figure 5.15 250 MHz, Perfect Electric Conductor versus Dielectric medium, with relative permittivity $\epsilon_r=15, 13$ and $4$ respectively, and conductivity $\sigma=0.04, 0.03$ and $0.06$ respectively, elevation angle is $88$ degrees. . . . .	96
Figure 5.16 375 MHz, Perfect Electric Conductor versus Dielectric medium, with relative permittivity $\epsilon_r=15, 13$ and $4$ respectively, and conductivity $\sigma=0.04, 0.03$ and $0.06$ respectively, elevation angle is $72$ degrees. . . . .	96
Figure 5.17 375 MHz, Perfect Electric Conductor versus Dielectric medium, with relative permittivity $\epsilon_r=15, 13$ and $4$ respectively, and conductivity $\sigma=0.04, 0.03$ and $0.06$ respectively, elevation angle is $88$ degrees. . . . .	97
Figure 5.18 500 MHz, Perfect Electric Conductor versus Dielectric medium, with relative permittivity $\epsilon_r=15, 13$ and $4$ respectively, and conductivity $\sigma=0.04, 0.03$ and $0.06$ respectively, elevation angle is $72$ degrees. . . . .	98
Figure 5.19 500 MHz, Perfect Electric Conductor versus Dielectric medium, with relative permittivity $\epsilon_r=15, 13$ and $4$ respectively, and conductivity $\sigma=0.04, 0.03$ and $0.06$ respectively, elevation angle is $88$ degrees. . . . .	98
Figure 5.20 20 MHz, Perfect Electric Conductor versus Dielectric medium, with relative permittivity $\epsilon_r=13$ , and conductivity $\sigma=0.03$ , elevation angle is $72$ degrees. . . . .	101
Figure 5.21 20 MHz, Perfect Electric Conductor versus Dielectric medium, with relative permittivity $\epsilon_r=13$ , and conductivity $\sigma=0.03$ , elevation angle is $88$ degrees. . . . .	101

Figure 5.22 100 MHz, Perfect Electric Conductor versus Dielectric medium, with relative permittivity $\epsilon_r=13$ , and conductivity $\sigma=0.03$ , elevation angle is 72 degrees. . .	102
Figure 5.23 100 MHz, Perfect Electric Conductor versus Dielectric medium, with relative permittivity $\epsilon_r=13$ , and conductivity $\sigma=0.03$ , elevation angle is 88 degrees. . .	103
Figure 5.24 250 MHz, Perfect Electric Conductor versus Dielectric medium, with relative permittivity $\epsilon_r=13$ , and conductivity $\sigma=0.03$ , elevation angle is 72 degrees. . .	104
Figure 5.25 250 MHz, Perfect Electric Conductor versus Dielectric medium, with relative permittivity $\epsilon_r=13$ , and conductivity $\sigma=0.03$ , elevation angle is 88 degrees. . .	104
Figure 5.26 375 MHz, Perfect Electric Conductor versus Dielectric medium, with relative permittivity $\epsilon_r=13$ , and conductivity $\sigma=0.03$ , elevation angle is 72 degrees. . .	105
Figure 5.27 375 MHz, Perfect Electric Conductor versus Dielectric medium, with relative permittivity $\epsilon_r=13$ , and conductivity $\sigma=0.03$ , elevation angle is 88 degrees. . .	105
Figure 5.28 500 MHz, Perfect Electric Conductor versus Dielectric medium, with relative permittivity $\epsilon_r=13$ , and conductivity $\sigma=0.03$ , elevation angle is 72 degrees. . .	106
Figure 5.29 500 MHz, Perfect Electric Conductor versus Dielectric medium, with relative permittivity $\epsilon_r=13$ , and conductivity $\sigma=0.03$ , elevation angle is 88 degrees. . .	107
Figure 5.30 20 MHz, Perfect Electric Conductor versus Dielectric medium, with relative permittivity $\epsilon_r=4$ , and conductivity $\sigma=0.06$ , elevation angle is 72 degrees. . .	108
Figure 5.31 20 MHz, Perfect Electric Conductor versus Dielectric medium, with relative permittivity $\epsilon_r=4$ , and conductivity $\sigma=0.06$ , elevation angle is 88 degrees. . .	108
Figure 5.32 100 MHz, Perfect Electric Conductor versus Dielectric medium, with relative permittivity $\epsilon_r=4$ , and conductivity $\sigma=0.06$ , elevation angle is 72 degrees. . .	109
Figure 5.33 100 MHz, Perfect Electric Conductor versus Dielectric medium, with relative permittivity $\epsilon_r=4$ , and conductivity $\sigma=0.06$ , elevation angle is 88 degrees. . .	110
Figure 5.34 250 MHz, Perfect Electric Conductor versus Dielectric medium, with relative permittivity $\epsilon_r=4$ , and conductivity $\sigma=0.06$ , elevation angle is 72 degrees. . .	111
Figure 5.35 250 MHz, Perfect Electric Conductor versus Dielectric medium, with relative permittivity $\epsilon_r=4$ , and conductivity $\sigma=0.06$ , elevation angle is 88 degrees. . .	111
Figure 5.36 375 MHz, Perfect Electric Conductor versus Dielectric medium, with relative permittivity $\epsilon_r=4$ , and conductivity $\sigma=0.06$ , elevation angle is 72 degrees. . .	112

Figure 5.37 375 MHz, Perfect Electric Conductor versus Dielectric medium, with relative permittivity  $\epsilon_r=4$ , and conductivity  $\sigma=0.06$ , elevation angle is 88 degrees. . . 113

Figure 5.38 500 MHz, Perfect Electric Conductor versus Dielectric medium, with relative permittivity  $\epsilon_r=4$ , and conductivity  $\sigma=0.06$ , elevation angle is 72 degrees. . . 113

Figure 5.39 500 MHz, Perfect Electric Conductor versus Dielectric medium, with relative permittivity  $\epsilon_r=4$ , and conductivity  $\sigma=0.06$ , elevation angle is 88 degrees. . . 114

# CHAPTER 1

## INTRODUCTION

### 1.1 Direction Finding

Direction Finding (DF) is the process of determining the direction of an emitter. Emitter signal refers to radio signals in case of radio direction finding. Direction finding or direction-of-arrival (DOA) estimation is also an important problem for other kinds of signals such as acoustic, ultrasound and seismic signals [1]. Direction of arrival estimation is important for locating and tracking the signals in military or civilian applications.

Electronic Warfare (EW) and Signal Intelligence (SIGINT) systems demand for location of emitter signals as an important requirement for Electronic Support and Electronic Attack systems [2]. To find location of emitters we need to find Angle of Arrival (AOA) or Direction of Arrival (DOA) of the transmitter signals. Thus accurate DOA estimation is required for accuracy in emitter location.

Radio direction finding finds applications in navigation, military intelligence, mobile communication, wireless 911 emergency call locating, geolocation, sonar, seismology, search and rescue, radio astronomy, public security, environmental monitoring, law enforcement and communication intelligence (COMINT)[1],[3].

#### 1.1.1 History of Direction Finding

Many advances have been made in the field of direction finding since the early 1900s. The first direction finding system is patented in 1902 by John Stone. The first attempts at Direction Finding made use of the directional characteristics of antenna elements by Marconi in 1906

and by Ettore Bellini, Alessandro Tosi in 1909. However the use of multiple antennas and phased antenna arrays did not lag far behind by Frank Adcock in 1919, who proposed an improved direction finding antenna design named Adcock antenna[4].

Radio Direction Finding (RDF) works by comparing the signal strength of a directional antenna pointing in different directions. At first, this system was used by land and marine-based radio operators, using a simple rotatable loop antenna linked to a degree indicator. This system was later adopted for both ships and aircraft, and was widely used in the 1930s and 1940s. On pre-World War II aircraft, RDF antennas are easy to identify as the circular loops mounted above or below the fuselage. Later loop antenna designs were enclosed in an aerodynamic, teardrop-shaped fairing. In ships and small boats, RDF receivers first employed large metal loop antennas, similar to aircraft, but usually mounted on top of a portable battery-powered receiver[64].

After World War II, developments in electronics have extended the capabilities of DF systems. Changing from analog to digital world gives DF systems the ability to monitor and track wide frequency range signals by the use of fast A/D converters and processors at the end of 1970's. However DF techniques do not change much except for superresolution algorithms in 1980's [4],[65]. In the middle of 1990's the field of personal wireless communications has emerged and the applications of array signal processing to communication systems have become a new driving force [65]. In the following section, classical and modern Direction Finding(DF) techniques are discussed.

### **1.1.2 Classical and Modern Direction Finding Techniques**

Direction finding methods can be analyzed in two subsections, namely, classical methods and modern methods(super resolution methods). Classical methods can also be subdivided as amplitude based methods, phase based methods and hybrid methods [5]. Examples of amplitude based methods are directional antenna, Buttlar array, Watson-Watt [2],[5],[6]. Interferometer method and Pseudo-Doppler method are examples of phase based methods. Interferometer method is based on phase comparison of the antenna signals[9]-[26]. Almost all of the classical direction finding methods assume a single emitting source. Therefore when there are multipath signals due to reflections from the environment, these methods generate large errors [5]. On the other hand, if we ignore the multipath case, usually the narrowband signal

is not corrupted by co-channel interference and hence single source assumption is frequently valid especially in a communication scenario. In fact this is the reason for widespread use of classical methods in today's commercial DF systems. One of the most powerful classical DF methods is the correlative interferometer algorithm. This algorithm is based on data collection and comparison. In this respect, correlative interferometer [3],[7],[8] models the array imperfections such as mutual coupling and gain/phase mismatch within the collected data implicitly. It turns out that, classical methods and super resolution algorithms have approximately the same direction finding performance in case of single source. Correlative interferometer algorithm can be implemented in different ways. In this respect, there are phase-only and magnitude and phase correlative interferometer algorithms in the literature. In this thesis, correlative interferometer algorithm, which uses both the magnitude and phase information, is used in order to evaluate the DF performance of different antenna arrays.

Some examples of modern or super resolution methods are MUSIC, Min-Norm, ESPRIT, Maximum Likelihood and Beamforming methods. MUSIC, Min-Norm, ESPRIT are also called subspace based method [1],[5]. When there is only a single source, classical and superresolution techniques perform similarly. However, when there is more than one source, then superresolution techniques perform significantly better than the classical DF methods. In fact, superresolution methods perform beyond the Rayleigh resolution limit that is why these methods are called superresolution methods[5]. Super resolution methods have distinct advantages when there are multiple sources, co-channel interference and multipath signals. Forward backward spatial smoothing [5], can be used to handle the multipath signals where the model covariance matrix is rank deficient. Co-channel interference is observed when two or more source signal bandwidths overlap in frequency. In this thesis, direction finding problem is considered for narrowband signals.

## **1.2 Description of Thesis Work**

In general, direction finding antenna arrays are mounted on a platform. The complex nature of the platform makes it hard if not impossible to find a closed form solution of the electromagnetic equations for the purpose of direction finding. Numerical evaluation is an important step for the evaluation of antenna arrays. In this case, electromagnetic problem is solved numerically and an approximate solution is found. While the approximation error depends on

many factors, it is usually small which makes the numerical electromagnetic evaluation tools valuable assets.

In this thesis, a numeric electromagnetic simulation tool, FEKO, is used to determine the direction finding performance of antenna arrays for different environments. In this respect, a methodology to model and simulate the antenna array performance is presented. This methodology allows finding the antenna currents for incident electromagnetic waves. In addition, this method allows the evaluation of DF performance for complex antenna platforms. The antenna current data is then transformed to MATLAB environment for signal processing. Presented approach has certain advantages in terms of computational complexity compared to alternative methods. This methodology is unique to find the antenna array's DF performances on different platforms. In the literature, such a method does not exist. Although antenna gains, complex currents and electromagnetic characteristics of antennas can be found by numerical electromagnetic simulation tools, comparison of DF performance of different antenna sets can not be done with these simulation tools. As a result, this methodology for finding and comparing the DF performances of antenna arrays is unique in the literature.

Correlative Interferometer algorithm is used for direction finding in this study. This algorithm models certain characteristics of antenna arrays such as mutual coupling through the data. In addition, correlative interferometer algorithm is based on data collection and comparison.

Different platforms and antenna types are used to evaluate the DF performance. In chapter 3, discone and dipole antenna arrays' DF performances are compared. The aim is to cover a large frequency band with discone antennas where the same band is covered by two sets of dipole antenna arrays having different dipole lengths and antenna interelement distances. For this purpose, a set of discone antenna arrays is generated having different antenna alignments. The most appropriate discone antenna array is selected for further comparison with two dipole antenna arrays. In chapter 4, dipole antenna arrays are mounted on a UAV(Unmanned Air Vehicle) platform and the effects of antenna placement and ground reflections are investigated. UAV platform is designed and numeric electromagnetic simulations are performed in FEKO. Two different antenna alignment models are generated with four and eight dipole antenna arrays and DF performances of these two antenna models are compared. Ground mediums are also modeled in FEKO as infinite ground mediums. DF performances of dipole antenna arrays are compared for two different ground medium types. These are perfect electric conductor

(PEC) and dielectric ground mediums. Ground reflection effects can be analyzed by this comparison. UAV is calibrated in the ground and test data is collected in the air. In chapter 5, a different platform and antenna array are used. In this case, a vehicle, SUV (Sport Utility Vehicle), and monopole antenna arrays' DF performance are investigated. For this purpose, SUV platform is generated and numeric electromagnetic simulations are performed in FEKO. In this chapter, three different dielectric ground mediums are designed. DF performance of the SUV model is found by collecting the calibration data on PEC ground medium and correlating this data with the data collected when SUV is on one of the dielectric ground mediums. DF performance comparison is done among these three different dielectric ground mediums. In addition, in this chapter a method is presented to reduce errors due to changes in ground medium characteristics. For this purpose, correction data is generated by using pre-saved error data file. Using this error data file, robustness of the monopole antenna model for changes in the dielectric ground medium is tested. This method is a very useful tool for finding the antenna response due to medium imperfections.

### **1.3 Organization**

In chapter 2, DF system components and numerical electromagnetic computational tools are described and analyzed in detail.

In chapter 3, wideband antenna DF system is studied. In this chapter, comparison of DF performances of discone antenna and dipole antenna is accomplished.

In chapter 4, dipole antenna's DF performance on UAV is tested for different ground mediums.

In chapter 5, monopole antenna's DF performance is tested on SUV for different ground mediums and error reduction performance of a designed method is analyzed.

In chapter 6, conclusion is given. In this chapter, outcomes of the simulations performed are discussed.

## **CHAPTER 2**

### **DF SYSTEM COMPONENTS AND NUMERICAL ELECTROMAGNETIC COMPUTATIONAL TOOLS**

In this thesis work, Direction Finding (DF) performance of antennas are considered under multipath effects of different ground mediums. Overall simulation scheme can be divided into two parts as DF system components and numerical electromagnetic computational tools.

In section 2.1, general block diagram of the simulation steps is given. Then signal model is defined. Correlative Interferometer method which is the method used in DF simulations is analyzed. Cubic spline interpolation method is discussed which is used in interpolation of data points to obtain a better azimuth scan resolution with smaller data steps. Finally multipath effects are studied.

In section 2.2, numerical electromagnetic computational tools' general overview is given, then method of moments, which is the solution method used in experiments is discussed. Finally numerical electromagnetic program FEKO which is used in simulations is described and simulation settings for this program are observed.

#### **2.1 DF System Components**

In this section, components generating the DF system are discussed. Flow chart of simulation pattern is given. Then signal model is described. Correlative interferometer method which is the method used in finding the DF performance is explained. Flow chart of correlative interferometer method is discussed. Cubic spline interpolation method is described which is the method used to obtain smaller azimuth data steps from a large azimuth interval data set.

### 2.1.1 Flow Chart of Simulation Methodology

In this section, flow chart of the simulation steps that constitute the DF system simulations is given. Description of each block in the flow chart is also studied.

In Figure 2.1, flow chart of the overall simulation pattern is given. According to the figure, the first step in the simulation is creating the models of the antennas and the platform. CAD models of antennas and platform are designed in FEKO program using ready geometrical structures such as cylinder, cube, cone, plate and line. Variables are defined for the geometrical structures to change any parameter in the antenna model easily. Then numerical electromagnetic simulation is performed with appropriate selection of operating frequency, ports and loads of antennas. Operating frequency can be a single frequency or a set of frequencies with a constant frequency step. Antenna currents are obtained from ports. Loads are defined on ports, loading can be serial or parallel and load value can be real or complex. In the simulations, plane wave excitation is used as a source to excite antennas. Azimuth, elevation angle span of plane wave excitation, magnitude and phase of plane wave must be determined properly. Vertical linear polarization is used. After the parameters of simulations are determined, the overall model is divided into triangular meshes according to the maximum operating frequency. Numerical electromagnetic analysis is done on the mesh structure of the model not on the original geometrical model. Mesh size is an important parameter which determines the duration of the simulation and quality of simulation. If the model is divided into smaller meshes, better approximation for the model is obtained and hence more exact current data from meshes can be obtained. Numerical electromagnetic simulation is performed on the created mesh model with the parameters defined above.

In this thesis, antenna current outputs of FEKO program are used. Antenna currents are read from .out file of FEKO program. In section 2.1.3, details of usage of these antenna currents' data are described. In .out file, detailed electromagnetic analysis data is included. Since only the antenna current data is used in simulations, the current data and the corresponding frequency, azimuth and elevation angle identities are saved on .mat file to save memory by extracting unnecessary part and for future use in MATLAB.

Two types of data are used in simulations, namely calibration and test data. Details of calibration and test data are explained in section 2.1.3 and in chapters 3, 4 and 5 as well. Correlation

of calibration and test data and calculation of azimuth angle and Root Mean Square Error (RMSE) are explained in section 2.1.3. Finally, RMSE vs. azimuth angle figures are plotted in MATLAB and results of simulations are given in chapters 3, 4 and 5.

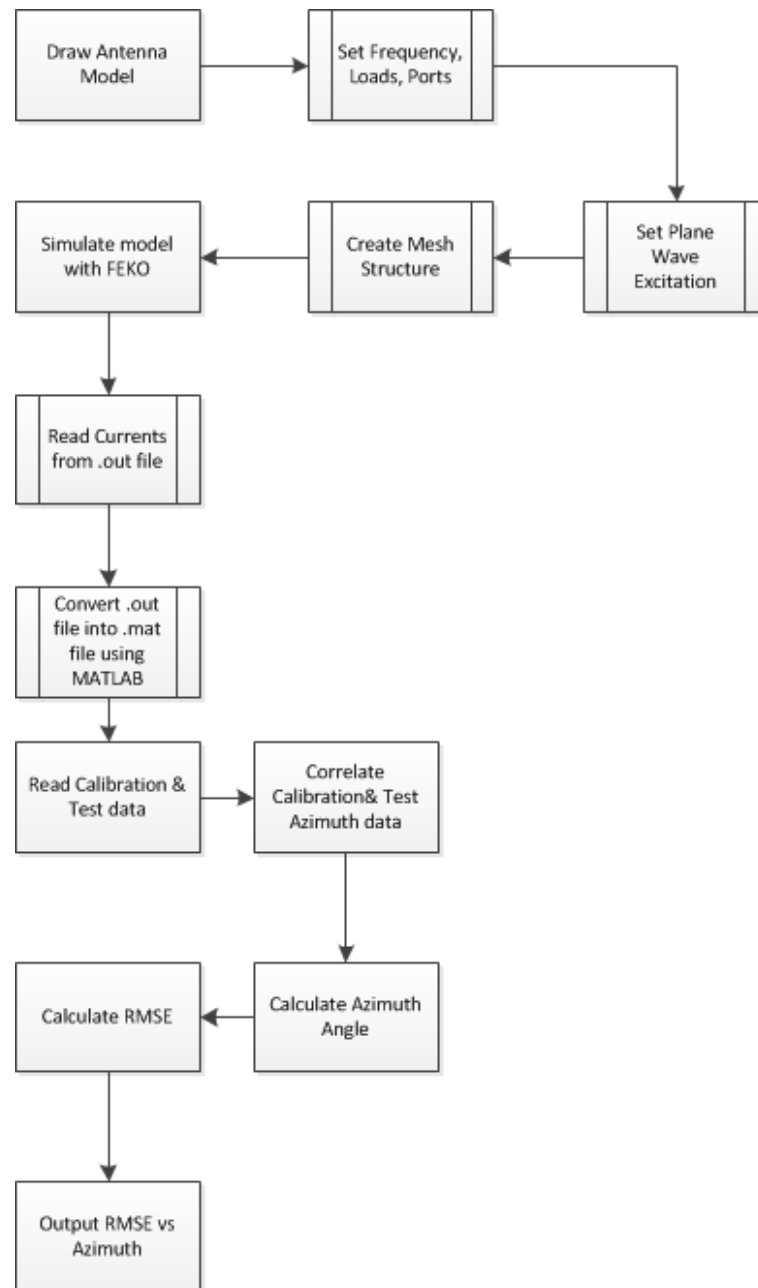


Figure 2.1: Flow Chart of Simulation Pattern

### 2.1.2 Signal Model

There are some assumptions made for the signal model. First assumption is far field assumption. It is assumed that signal sources are far enough from the antenna arrays. In [1], a rule of thumb for this assumption states that when the distance between the sources and antenna arrays is larger than  $2D^2/\lambda$  far field is assumed. Here  $D$  is the dimension of the array,  $\lambda$  is the wavelength of the signal. Far field assumption is also used in FEKO simulations. Plane wave excitation is used as the source signal and simulations are accomplished with this source model. Narrowband assumption is used which requires signal sources to have the same carrier frequencies and frequency content is concentrated around carrier frequency within a small frequency band. Transmission medium is assumed to be linear and isotropic which means that the mediums around signal source and antennas have the same physical properties in all directions and linearity property ensures that signals at any point can be superposed linearly. Additive white Gaussian noise (AWGN) is assumed which has zero mean, spatially uncorrelated random process with variance  $\sigma^2$ . Noise is uncorrelated with signals [1].

Using the assumptions, signal model can be given as [51]:

$$\mathbf{y}(t) = \mathbf{A}\mathbf{s}(t) + \mathbf{e}(t), t = 1, 2, \dots, N \quad (2.1)$$

where  $\mathbf{y}(t)$  is the received signal,

$$\mathbf{A} = \begin{bmatrix} \mathbf{a}(\phi_1, \theta_1) & \dots & \mathbf{a}(\phi_n, \theta_n) \end{bmatrix} \quad (2.2)$$

is the array manifold matrix with elements  $\mathbf{a}(\phi_l, \theta_l)$  which are array steering vectors with unknown azimuth and elevation angles " $\phi_l, \theta_l$ " respectively for the  $l$ 'th source. There are total of " $n$ " sources. Array steering vector has the following form if the first sensor is chosen as the reference point of the array.

$$\mathbf{a}(\phi, \theta) = \begin{bmatrix} 1 & e^{-i\omega_c\tau_2} & \dots & e^{-i\omega_c\tau_K} \end{bmatrix}^T \quad (2.3)$$

where " $K$ " is the total number of array elements,  $\tau_2$  is the 2'nd antennas delay term that carries DOA information and  $\omega_c$  is the carrier frequency. Source signal or input signal  $\mathbf{s}(t)$  is a multiple source signal with elements

$$\mathbf{s}(t) = \begin{bmatrix} s_1(t) & \dots & s_n(t) \end{bmatrix}^T \quad (2.4)$$

Noise term is expressed as  $\mathbf{e}(t)$  which is additive white Gaussian noise [51].

This signal model is a general model. In our case, correlative interferometer algorithm is used. This algorithm can be used appropriately for only a single source. The algorithm generates large errors for multiple source case. Therefore, a single plane wave is used in the simulations. Thus  $n=1$  in our case for single source analysis. However multiple paths caused by ground reflections are present in the simulated data. Received signal reduces to

$$\mathbf{Y} = \mathbf{a}(\phi, \theta)s(t) + \mathbf{E} \quad (2.5)$$

In our study, we are interested in the currents read from antenna arrays and we use these current readings as our received signal and we add noise on this signal and obtain the resulting expression. In the following section, details of direction finding algorithm used in the simulations are explained.

### 2.1.3 Correlative Interferometer Method

In this section, DF method used in simulations is given. This method is called Correlative Interferometer method in the literature [3], [7], [8]. The method is based on finding the correlation of two data sets. These two data sets are called calibration and test data sets. Calibration data is the data saved for calibration of the antenna set. Then any test data which is obtained by changing the simulation environment (ground plane's dielectric properties, height of the platform) of the calibration data is compared with the calibration data. The maximum correlation point is the point of interest in this method. Data sets used in the simulations are the antenna current data sets. DF performances of the antenna sets are determined by the correlation of these antenna current data sets.

As in almost all classical algorithms, correlative interferometer algorithm assumes a single source signal. For noise free case, the received signal model in equation (2.5) becomes as follows:

$$\mathbf{Y} = \mathbf{a}(\phi, \theta)s(t) \quad (2.6)$$

In this expression "t" refers to snapshots. Total number of snapshots is represented by "N". Array steering vector  $\mathbf{a}(\phi, \theta)$  is a  $K \times 1$  column vector. Note that,  $s(t)$  is only a scalar for a single snapshot. In fact, the numerical electromagnetic simulation in FEKO results in the following expression as the output:

$$\mathbf{y} = \mathbf{a}(\phi, \theta)s \quad (2.7)$$

In this expression "s" represents complex scalar constant. Correlative interferometer algorithm is based on observing array output for different azimuth, elevation and frequency values. Then the test data is correlated with the previously observed data to find the true azimuth and elevation angles. Received signal model including additive noise is given as follows:

$$\mathbf{Y}_{test} = \mathbf{a}(\phi, \theta)s + \mathbf{E} \quad (2.8)$$

$\mathbf{E}$  is additive white Gaussian noise weighted according to SNR value and obtained randomly and separately for every antenna element and for each snapshot,  $\mathbf{Y}_{test}$  is the test data's received signal for a specific azimuth, elevation angle and for constant frequency. Received signal is obtained from antenna current measurements and SNR. Noise is added only to test data, calibration data is noise free. Actually  $\mathbf{Y}_{test}$  is a matrix with number of rows equals to number of antennas and number of columns equals to number of snapshots. Calculation of  $\mathbf{Y}_{test}$  is done separately for every antenna element, thus random noise term is different for every antenna.

In this work, calibration or test data is not directly used. Instead, autocorrelation matrix is employed to use the information content of the data more effectively. Autocorrelation matrix for test data is calculated from the following expression:

$$\mathbf{R}_t = \frac{1}{N} \mathbf{Y}_{test} \mathbf{Y}_{test}^H \quad (2.9)$$

In this expression  $(.)^H$  refers to Hermitian operation.  $\mathbf{R}_t$  is  $K \times K$  autocorrelation matrix. Upper-diagonal elements of autocorrelation matrix are ordered to obtain the test column vector of size  $K + (K - 1)! \times 1$  as follows:

$$\mathbf{r}_{test} = \left[ \mathbf{R}_t(1, 1) \quad \mathbf{R}_t(1, 2) \quad \mathbf{R}_t(1, K) \quad \cdots \quad \mathbf{R}_t(K-1, K-1) \quad \mathbf{R}_t(K-1, K) \quad \mathbf{R}_t(K, K) \right]^T \quad (2.10)$$

For calibration data, noise term is not used and received signal for calibration data is expressed as:

$$\mathbf{y}_{cal} = \mathbf{a}(\phi, \theta)s \quad (2.11)$$

where  $\mathbf{y}_{cal}$  is the calibration data's received signal. Total number of antennas is the same for calibration and test data. Since calibration data is noise-free, single snapshot is used. In this expression  $\mathbf{y}_{cal}$  is a column vector of dimension  $K \times 1$ .

Autocorrelation matrix for calibration data is calculated from the following expression:

$$\mathbf{R}_c = \mathbf{y}_{cal} \mathbf{y}_{cal}^H \quad (2.12)$$

$\mathbf{R}_c$  is  $K \times K$  autocorrelation matrix. Upper-diagonal elements of autocorrelation matrix are ordered to obtain the calibration column vector of size  $K + (K - 1) \times 1$  as follows:

$$\mathbf{r}_{cal} = \left[ \mathbf{R}_c(1, 1) \quad \mathbf{R}_c(1, 2) \quad \mathbf{R}_c(1, K) \quad \cdots \quad \mathbf{R}_c(K - 1, K - 1) \quad \mathbf{R}_c(K - 1, K) \quad \mathbf{R}_c(K, K) \right]^T \quad (2.13)$$

Both calibration column vector and test column vector are calculated for every azimuth angle in the azimuth span. Following expression finds the scalar correlation value of the test data and calibration data [3],[7]:

$$c_{corr} = \left| \frac{\mathbf{r}_{test}^H \mathbf{r}_{cal}}{\sqrt{\mathbf{r}_{test}^H \mathbf{r}_{test} \mathbf{r}_{cal}^H \mathbf{r}_{cal}}} \right| \quad (2.14)$$

$c_{corr}$  takes values between 0 and 1. Higher  $c_{corr}$  value means better correlation. During the evaluation of this expression, test column vector is selected for a fixed azimuth angle in the azimuth span and then correlation is found from executing this expression for every azimuth angle in calibration column vector. Azimuth angle value which gives the maximum correlation expression is the calibration data's azimuth angle in respond to test data's azimuth angle. If both azimuth values are equal, then there is zero root mean square error for this test data's azimuth angle. Calculated calibration data's azimuth angle can be different from the test data's azimuth angle due to interfering sources such as low SNR and multipath reflection. Source of error might be changes in the simulation environment such as different dielectric medium properties. Test data is noisy while calibration data is noise-free, in low SNR simulations this may result in erroneous correlation between calibration and test data. Thus high RMSE's occur for these low SNR simulations.

#### 2.1.4 Flow Chart of Correlative Interferometer Methodology

In this section, flow chart of correlative interferometer method is given. Detailed signal model and analysis in the method are explained in sections 2.1.2 and 2.1.3, respectively. In this section, general operation of the method is discussed.

In the azimuth scan simulations, current values are obtained for every azimuth, elevation angles, frequency set and for every antenna. That means we have a single current value for the antenna we are interested and for a specified frequency, azimuth and elevation angle settings. In this study Direction Finding (DF) performance of any antenna set is obtained by calculating Root Mean Square Error (RMSE) value for each azimuth angle in the azimuth set

and for a fixed elevation angle.

In Figure 2.2, flow chart of correlative interferometer method is given. Details of the elements of flow chart will be explained in this section.

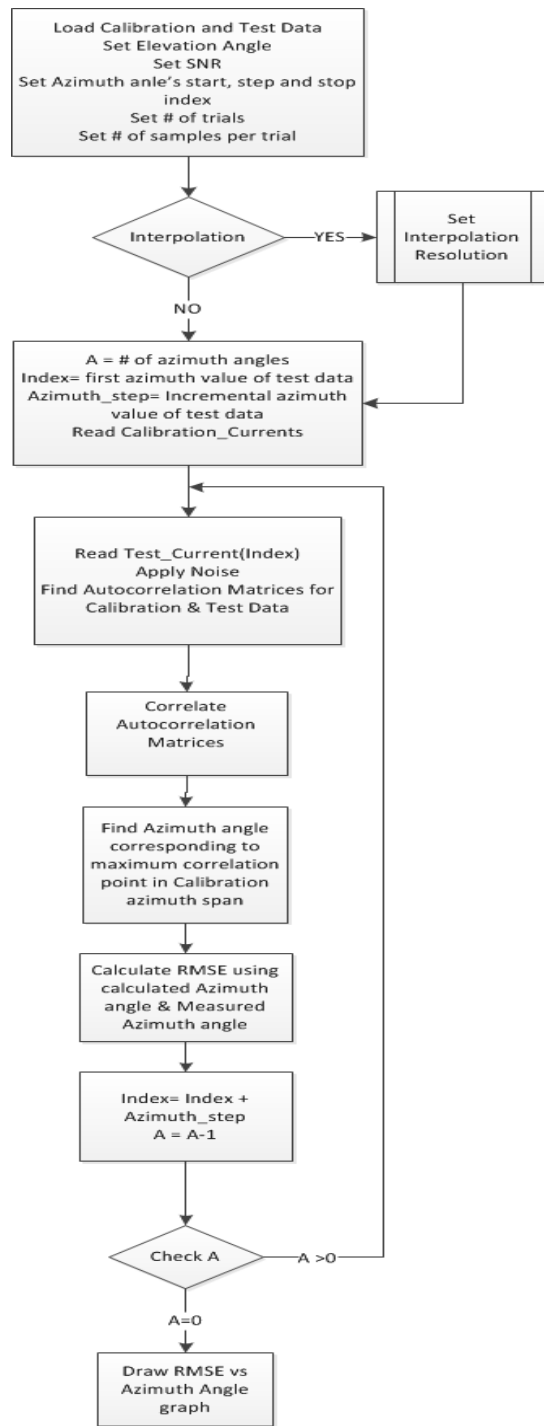


Figure 2.2: Flow Chart of Correlative Interferometer Method

Simulation system is composed of two parts. First part is numerical electromagnetics simulation part. In this part current values are obtained for the predefined settings of frequency, azimuth and elevation angles. These currents are written in a text file by the numerical electromagnetic program, namely, FEKO. Text file is read by MATLAB program to extract only current values and discard irrelevant data to make up the data set. Data set composed of gain and phase of the current values for each azimuth, elevation and frequency set. Data set is saved in .mat file for later use in DF performance evaluation in MATLAB.

In the second part of the simulation, current values are used to obtain RMSE's. This is accomplished by correlating two different data sets and finding the highest correlation using correlative interferometer algorithm which was explained in section 2.1.3. If the effect of any differences in the simulation model is to be tested, two different sets of data should be used for calibration and test data. Calibration data must consist of original data which is collected during calibration process and test data includes the changes in the simulation environment. These data sets are used to find the correlation among themselves.

DF performance of an antenna set is tested in noisy environment with a constant Signal to Noise Ratio (SNR). RMSE values are calculated separately for each azimuth angle. Finally, RMSE vs azimuth angle graph is obtained for the selected calibration and test data.

### **2.1.5 Cubic Spline Interpolation Method**

In simulations of chapter-3, azimuth data is collected with 1 degree of resolution, so the minimum RMSE error term is 1 degree if we use this azimuth resolution. This means, if higher correlation is obtained for neighboring calibration data other than the actual data for every iteration, then RMSE becomes 1 degree. Smaller data steps result in smaller RMSE. Data interval can be decreased by data interpolation. Azimuth resolution of the data is increased by interpolating the 2 end points which are the existing data points. By interpolation we obtain the desired resolution. In this study, cubic spline interpolation is used to obtain 0.1 degree of azimuth resolution for the calibration data. Interpolation is only applied to calibration data. Test data is not interpolated.

Splines are defined as piecewise polynomials with smoothly joined parts [52]. Degree  $p$  spline is defined with a polynomial of  $p$ 'th degree which requires  $(p+1)$  coefficients to resolve. End

points of spline polynomials are called knots. For smooth splines we need additional limits which require the continuity of the spline as well as its derivatives up to the order of (p-1) at the end points. As a result, only one degree of freedom is left to consider. In this thesis work we use B-splines with equal spacing and uniform knots. These kind of splines can be formulated with the following expression:

$$s(x) = \sum_{k \in \mathbb{Z}} c(k) \beta^p(x - k) \quad (2.15)$$

In this equation,  $\beta^p(x)$  refers to the basis function for the B-spline. The term "k" represents integer shift for basis function of amount k. Coefficients of basis functions are mapped to integer shifts and given by c(k). The primary basis function which is the zero degree basis function is defined as follows:

$$\beta^0(x) = \begin{cases} 1, & \text{if } -\frac{1}{2} < x < \frac{1}{2} \\ \frac{1}{2}, & \text{if } |x| = \frac{1}{2} \\ 0, & \text{otherwise} \end{cases} \quad (2.16)$$

Primary basis function is a rectangular pulse, any p'th degree of polynomial can be derived from this basis function by convolving this function (p+1) times [52] as shown in the following equation.

$$\beta^p(x) = \beta^0(x) * \beta^0(x) * \dots * \beta^0(x) \quad (2.17)$$

In this equation, "\*" refers to convolution. If we apply convolution of (p+1) times creates triangular shape for 1'st degree basis and as we increase the degree smoother curves obtained which are continuous as well as their (p-1) degree derivatives.

In spline polynomials, the most widely used one is the cubic spline [53],[54]. Cubic spline basis function can be represented with  $\beta^3(x)$  and expression for the cubic spline is given as follows:

$$\beta^3(x) = \begin{cases} \frac{2}{3} - |x|^2 + \frac{|x|^3}{2}, & \text{if } 0 \leq |x| < 1 \\ \frac{(2-|x|)^3}{6}, & \text{if } 1 \leq |x| < 2 \\ 0, & \text{if } 2 \leq |x| \end{cases} \quad (2.18)$$

In thesis work, cubic B-spline polynomials are used as interpolation method with two points. MATLAB ready function interp1 is used with piecewise cubic spline interpolation method.

### 2.1.6 Multipath Effects

In this study, we develop simulation environment for ground calibration of models. Here the term model refers to the antennas and the platform on which the antennas are mounted. In this environment, models are placed above an infinite ground medium. Properties of infinite ground medium are defined by the relative permittivity and conductivity of the medium.

In the simulations performed, two types of infinite ground medium are used. First type is the perfect electric conductor (PEC) infinite ground medium. Second type is the dielectric infinite ground medium. Properties of ground mediums are defined in related chapters where they are used.

The importance of ground mediums comes from the fact that they reflect the planar waves such that antennas observe two different sources of signal. However there exists only one source. The main source of the signal comes from direct path, which is the source we want to find the direction. The secondary source of signal is created from the reflection of the signal of the main source from ground plane which is called reflected wave.

In Figure 2.3, direct wave and ground reflected wave can be observed. Here there are two paths for waves to travel from transmitter to receiver.

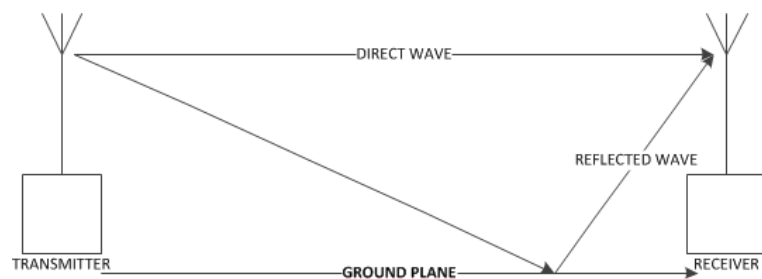


Figure 2.3: Reflection from smooth and conducting surface

In our simulations, as a single source, plane wave is used instead of transmitter and current values which read from antenna elements include the effects of both direct and reflected waves.

In Figure 2.4, plane wave is reflected from smooth and conducting surface. In our simulations this surface can be perfect electric conductor (PEC) or dielectric medium. In this case direct

wave is the plane wave with incident elevation angle and reflected wave is the plane wave with attenuated amplitude and phase. In addition, elevation angle of the reflected wave is mirror image of the direct wave's elevation angle.

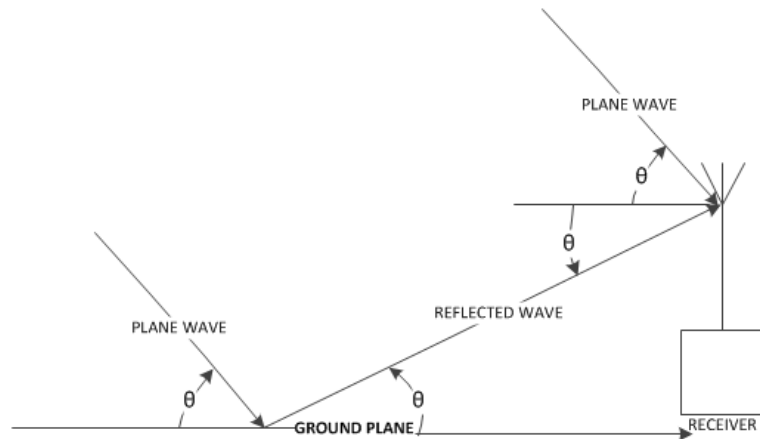


Figure 2.4: Plane Waves reflection from smooth and conducting surface

In RF communications, reflected waves can be used to transfer the Electromagnetic (EM) waves in a distance which can not be reached with direct waves. Actually earth reflections are sources of signal propagation for HF band. However, reflected waves arrive at the receiving antenna with a different phase and amplitude from the direct wave. In specific distances, phase difference can be 180 degrees which causes fading depending on the magnitude of the reflected wave [55],[56]. Numerical electromagnetic simulation tool ignores propagation losses and only line of sight propagation applies. In [57],[58] and [59] multipath effects on interferometer method accuracy are analyzed and errors due to multipath are formulated for specific scenarios. Multipath effects are very important in DF performance of antennas. In the literature multipath effects and ground reflections are analyzed in detail [41]-[50].

In our models, effects of reflected waves can be observed on the currents read from the receiving antennas. When the ground medium is selected as PEC medium, magnitude and phase values change significantly. In the simulations, path losses are ignored since the simulation environment is free space [60]. Thus attenuation is not applicable to the plane wave after reflection from ground medium.

During simulations, calibration data is collected when the model is above the ground with an elevation whose value is model dependent. However test data is collected with a different

ground medium or in free space. As a result calibration and test data have different multipath effects and currents read from the antennas are different both in magnitude and phase. This difference is the main point in our analysis.

In chapter-3, antennas are placed in free space. So both calibration and test data are collected in the same ground medium. In this chapter, Direction Finding (DF) performances of antennas are analyzed in noisy environment. Antennas' resistance to noise are tested and compared.

In chapter-4, antennas are placed on a UAV and calibration data is collected 10 meters above the ground medium. PEC and dielectric infinite ground mediums are used. However test data is collected when the model is in free space. As a result multipath effects on the DF performance are observed clearly. In this chapter Signal to Noise Ratio (SNR) is taken as 150 dB, so we ignore noise effects on DF performance, only multipath effects are analyzed.

In chapter-5, antennas are placed on a vehicle and both calibration and test data are collected 2 meters above the ground medium. However, calibration data is collected on PEC ground medium, while test data is collected on dielectric ground medium. In this chapter, we observe the effects of different ground mediums on DF performance. SNR is taken as 150 dB similar to chapter-4 and different mediums' multipath effects are analyzed.

## **2.2 Numerical Electromagnetic Computational Tools**

Theoretical and closed form solutions for complex structures are hard if not impossible. Therefore in order to analyze some complex structures numerical electromagnetic computational tools are extremely valuable for the analysis of such structures. Various solution methods exist for different sizes of electromagnetic problems. In our analysis, Method of Moments (MoM) is used as the solution method.

In this part, general definitions and overview for the numerical electromagnetics are given and then method of moments will be discussed. Finally FEKO simulation environment is defined and simulation settings for our analyses are developed.

### 2.2.1 FEKO Tools and Simulation Settings

FEKO models can be built and simulations can be done easily on an environment which is called the CADFEKO. CADFEKO is a widely used 3 dimensional numerical electromagnetic simulation environment in which user can be able to create CAD drawing of the model and test its electromagnetic features.

CADFEKO uses different solution methods for calculation of electromagnetic fields. The core method of the CADFEKO program is MoM [60]. In this method, currents are calculated from linear combinations of basis functions and the coefficients are found by the solution of linear algebraic equations also called matrix equations[60]. The basic idea is to transform an integral equation into a set of simultaneous linear algebraic equations[61]. Conversion of a continuous domain integral equation into a linear system of equations requires a discretization process known as Method of Moments.

Storage requirement of MoM is formulated as  $O(L^3)$  where  $O(.)$  represents Big-O notation which is a measure of complexity,  $L$  is the number of unknowns. So if the number of elements in the problem doubles, MoM needs to solve four times more linear set of equations to find unknowns. Applying this increase to 3-dimensions for volume integrals, sixth power of  $L$  becomes the complexity. If we double the frequency, we need storage of 64 times more memory for matrix coefficients[62]. As a result solution of electrically large problems, where model is too large in terms of wavelength or equivalently in high frequency applications, Method of Moments is not appropriate. However in our case volume equivalence principle is not used, only surface equivalence principle is used and objects are divided into triangular mesh elements, FEKO uses these mesh elements to find currents induced on them. In our simulations, Method of Moments (MoM) is used as the solution method due to its accuracy and speed for electrically small models.

In electrically large problems, Physical Optics (PO) Method or Uniform Theory of Diffraction (UTD) method yields faster solutions which require less memory and CPU time. However, these methods can only be used if the model to be analyzed is too large in terms of wavelengths or in other terms operating frequency is too high. In addition UTD and PO can only be used for perfectly conducting well shaped structures like rectangles, cylinders or cubes. They can not be used in solution of complex and asymmetric structures [60].

In [63], considerations and applications of above mentioned solution methods are discussed. Especially, modeling of dielectric materials in FEKO is considered. Dielectric structures are solved with various techniques in MoM, namely surface equivalence principle, volume equivalence principle and special Green's functions for planar multilayer media [60],[63]. Numerical methods for solving the Maxwell's equations are carried out in computer simulations such that faster electromagnetic analysis with a desired precision can be achieved. Numerical electromagnetic computational program FEKO is widely used in the literature [27]-[40].

In chapters 4 and 5, FEKO simulations are performed with the platforms lying above the infinite ground mediums. The materials used in these mediums are perfect electric conductor (PEC) and dielectric medium defined by relative permittivity and conductivity in constant frequency. In [63], there is a table (Table 1, page 146) which compares memory requirements and CPU times between finite dielectric ground medium and infinite dielectric ground medium. According to this table, finite ground medium requires nearly 6 times more memory space and CPU time to complete simulations as compared to infinite ground medium. This situation occurs because FEKO creates meshes for finite ground medium while for infinite ground medium FEKO uses special Green's function which models the infinite dielectric ground medium implicitly without creating meshes. Using special Green's function is computer resource efficient [63]. For that reason, in chapters 4 and 5, ground mediums are modeled as infinite ground mediums.

## CHAPTER 3

### WIDEBAND ANTENNA DF SYSTEM

Commercial Direction Finding (DF) systems usually use more than one antenna array to cover VHF and UHF frequency bands. Such systems require mounting space and increase system cost and complexity. There is a clear motivation to cover a large frequency band with a single antenna array. In this chapter, a discone antenna array is used for this purpose. It is compared with an alternative DF system where the same frequency band is covered with two dipole antenna arrays. While such a comparison can not be seen as an objective process, it gives valuable insight on the advantages and disadvantages of such an attempt.

Direction finding performances of antennas are tested using FEKO simulation results and MATLAB analysis. Root mean square error (RMSE) values are determined for the azimuth span from 0 degree to 360 degrees. Thus, comparison of DF performance for any azimuth angle can be done by using the same parameters for two different antenna array simulations.

In this work, several different discone antenna arrays are designed and tested while only a subset is presented in the thesis. The main reason is discone antenna has a large volume and building an array with no spatial aliasing is a challenge for the frequency band under investigation.

Discone antenna is consisted of a cone and a disc on top of it. Shape of the discone is the limiting factor in our analysis. Cone part of the antenna prevents us to obtain an interelement distance which avoids spatial aliasing. For this reason, different discone antenna models are simulated having better DF performance with smaller interelement distance. The best DF performance among different discone antenna models is achieved in a model having 120 degrees aligned 3 discone antennas and 0.5 scaled, reversed and elevated discone antenna on the center of 3 antennas. This model has a stable RMSE vs azimuth angle characteristics with

Table 3.1: Discone antenna design parameters

Parameter Name	Value (cm)
Discone Length	26.75
Disc Radius	10.72
Cone Base Radius	15.3
Cone Top Radius	0.62

low RMSE values and azimuth independent characteristic, which is observable in section 3.2. In addition, the lowest interelement distance value among discone antenna models is obtained by this model.

### 3.1 Antenna Models

Two types of antennas' Direction Finding (DF) performance are compared in this chapter, namely discone and dipole antennas. Antenna dimensions and FEKO models of these antennas are given in the following two sections.

#### 3.1.1 Discone Antenna Model

In this section, various discone antenna models are given. All of the models are tested in terms of their DF performance. Performances are limited by spatial aliasing which is primarily affected by the antenna interelement distance. Different models are created to obtain the lowest antenna interelement distance, but non-symmetric antenna models having lower antenna interelement distance give angle dependent DF characteristics which means in some azimuth sectors, RMSE is much lower than the average RMSE and in some azimuth sectors RMSE is higher. Thus non-symmetric discone antenna models are eliminated. From the remaining discone antenna models, antenna model giving the best DF performance is selected which is a four discone antenna model with three antennas 120 degrees aligned and one antenna 0.5 scaled, reversed and elevated from the center of the discs of three discone antennas. This model is given in Figure 3.4 and used in discone antenna simulations in the following sections. Dimensions of discone antenna are given in Figure 3.1. In Table 3.1, values of the discone antenna design parameters are given.

In Figure 3.2, circular array structure of the discone antenna placements is given. Antenna

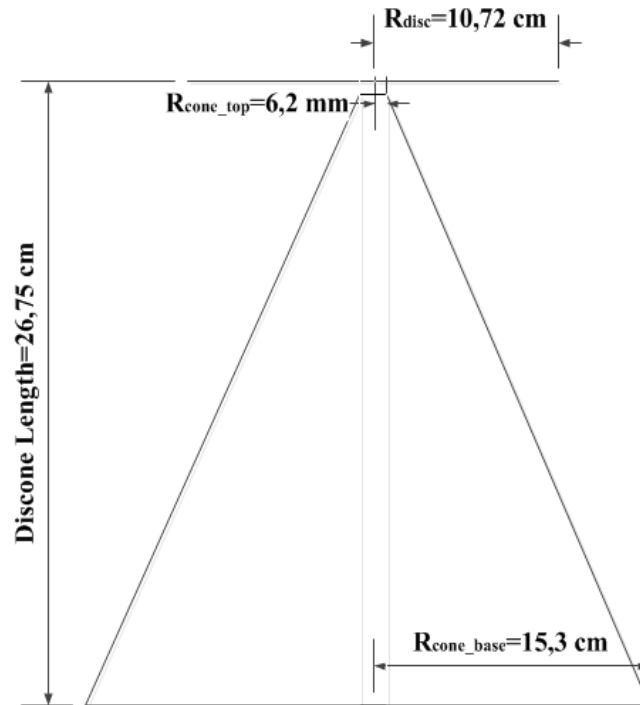


Figure 3.1: Discone antenna dimensions

interelement distance is 18.4 centimeters and radius of the circular array is the same as the antenna interelement distance and 18.4 centimeters.

In Figure 3.3, four antenna discone model can be seen. In this model, antenna interelement distance of each antenna pair is the same. All the antennas have the same size. The main problem in this case is the array elements can not be placed closer to avoid spatial aliasing at high frequencies.

In Figure 3.4, another four antenna structure is used. In this figure three antennas having the same size are placed with 120 degrees spacing with respect to the reference antenna placed in +x axis. The fourth antenna is reversed, elevated, scaled and centered between three antennas. Scale factor for the fourth antenna is 0.5, which means that the fourth antenna has half the dimensions of other three antennas. This model is the one used in discone antenna DF simulations. Since there is an elevation difference for the fourth antenna, other three antennas can be placed closer as compared to Figure 3.3. The antenna array structure is more robust to the spatial aliasing.

In Figure 3.5, reversed antenna has a scale factor of one, which means the fourth antenna has

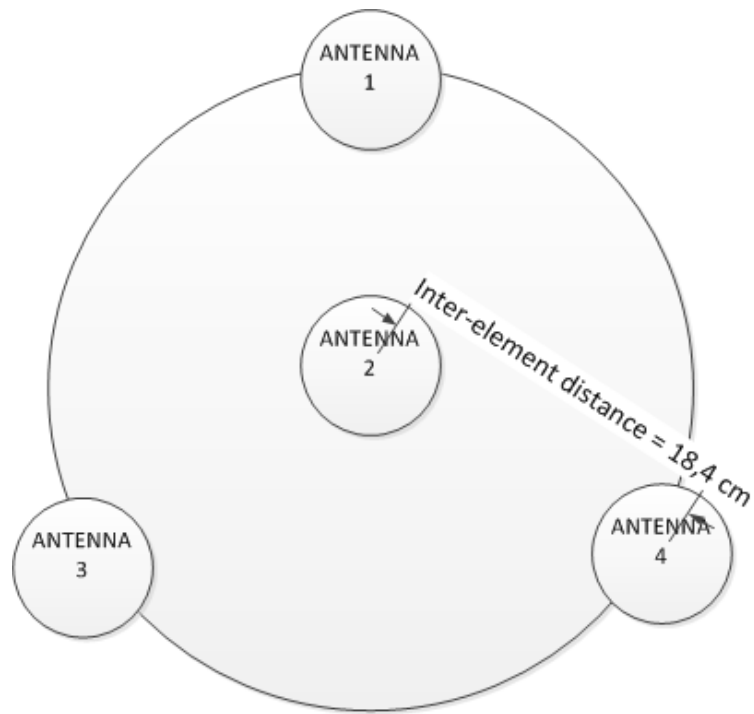


Figure 3.2: Discone antenna array structure

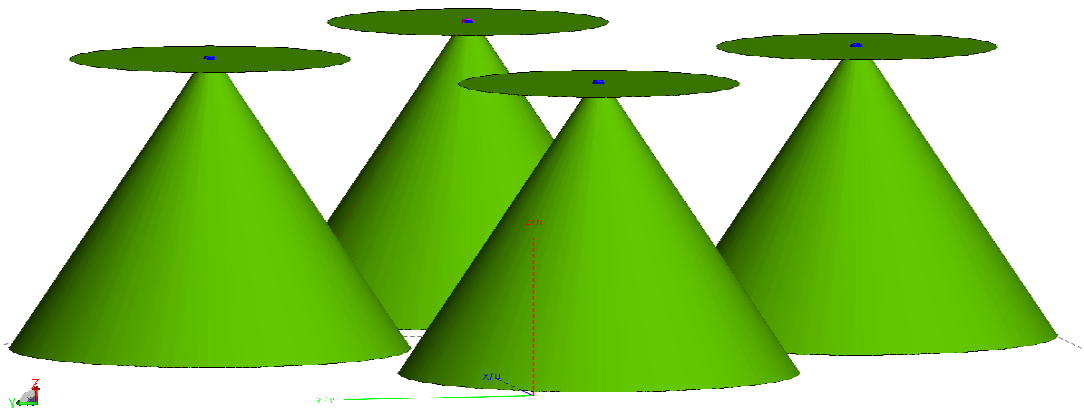


Figure 3.3: CADFEKO model of discone with four antennas

the same size with the other three antennas. In this figure, fourth antenna is again reversed, elevated and centered. In addition, other three discone antennas are separated by 120 degrees. DF performance of this antenna structure varies significantly in azimuth compared to that of

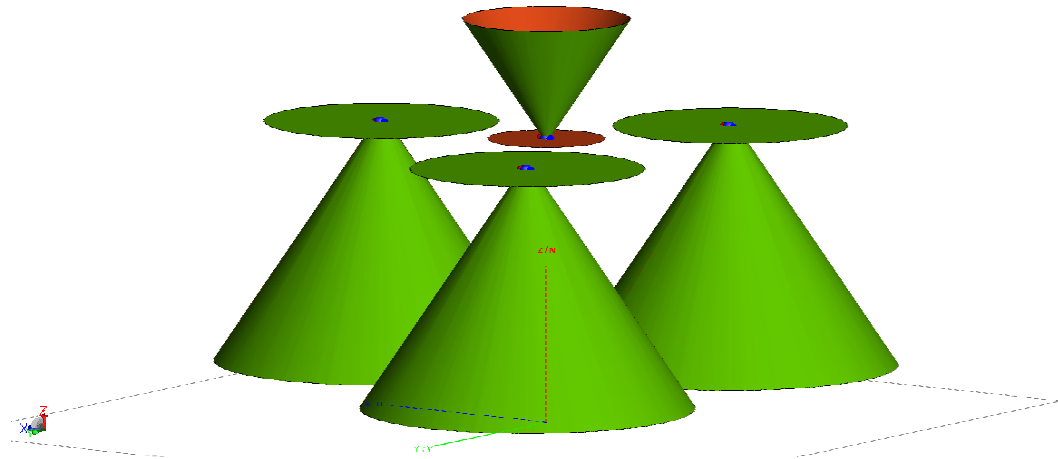


Figure 3.4: CADFEKO model of discone with four antennas, three antennas separated by 120 degree, one antenna reversed, scaled by 0.5 and centered between three antennas

the structure in Figure 3.4, also RMSE levels for this antenna structure is higher.

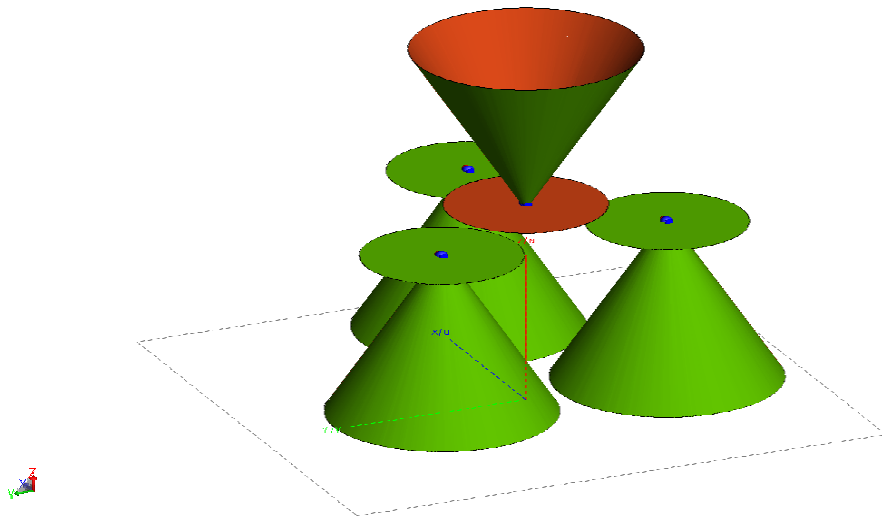


Figure 3.5: CADFEKO model of discone with four antennas, three antennas separated by 120 degree, one antenna reversed and centered between three antennas

In Figure 3.6, antennas are separated by 135 degrees. In this figure, reference antenna is placed in +x direction and other two antennas are positioned 135 degrees away wrt +x axis. Fourth antenna is reversed and has the same size with other three antennas. However DF performance of this antenna structure is worse than that of the antenna structure in Figure 3.5.

Separating the antennas increases the RMSE levels.

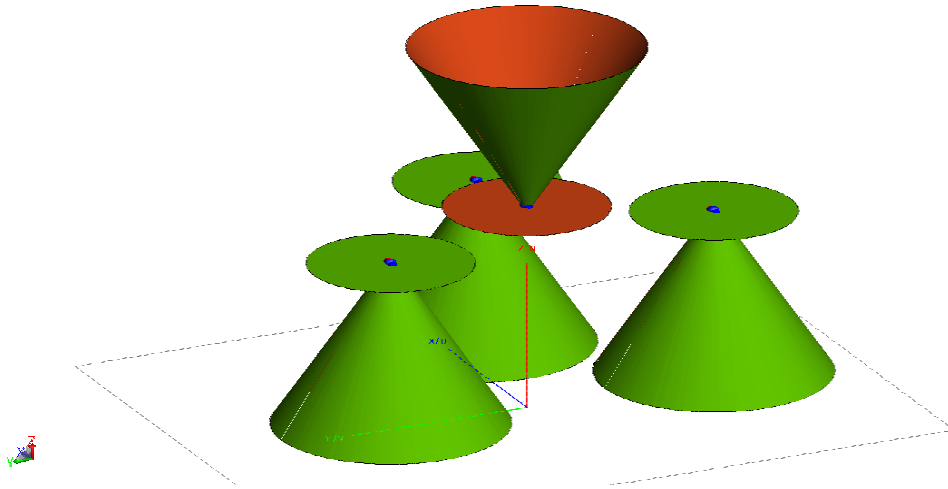


Figure 3.6: CADFEKO model of discone with four antennas, three antennas separated by 135 degree, one antenna reversed and centered between three antennas

In Figure 3.7, four antennas are used such that two antennas are reversed, and both antennas elevated with the same elevation value such that discs of the antennas are on the same elevation level. Antennas lying on  $+y$  and  $-y$  axes are reversed because if both discone antennas have the same alignment there is a limitation in the antenna interelement distance, such that interelement distance is limited with the discone antennas base radius. We do not want to observe spatial aliasing effects which result in huge RMSE on the order of 100 degrees. If we do not decrease the antenna interelement distance, we observe spatial aliasing around 400 MHz. Reversing two antennas helps us to decrease antenna interelement distance, but still interelement distance is not small enough to prevent spatial aliasing. In addition, DF performance of this antenna structure is azimuth dependent which means, RMSE levels fluctuate in azimuth.

In Figure 3.8, two antennas are reversed, but with different elevations. By changing elevations of the antennas we can decrease the interelement distance with respect to the model having same elevation values with reversed antennas. Elevation is applied such that the antenna in  $-x$  axis has the lowest elevation. Antenna in  $+y$  axis is elevated from  $-x$  axis antenna.  $+x$  axis antenna is also elevated from  $+y$  axis antenna with the same elevation value. Thus  $+x$  axis antenna has twice the elevation value from the  $-x$  axis antenna.  $-y$  axis antenna is elevated

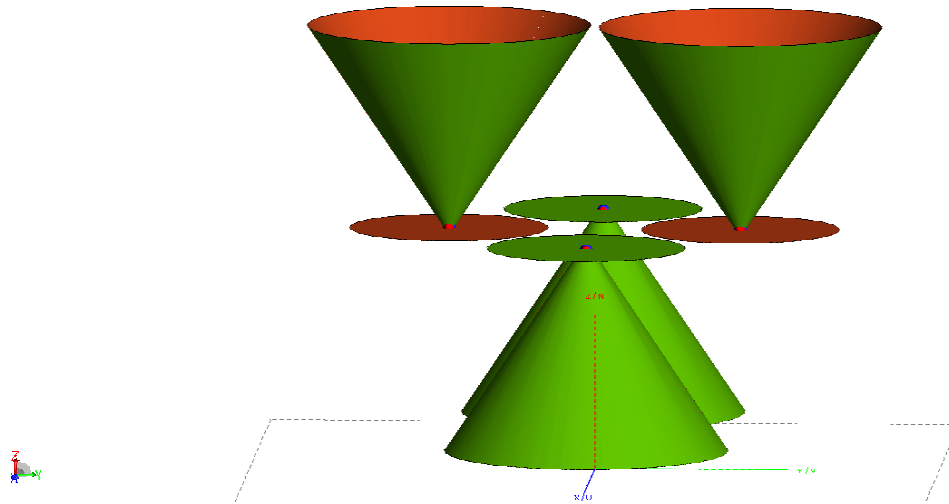


Figure 3.7: CADFEKO model of discone with four antennas, antennas are reversed and have the same z-axis coordinates

from +x axis antenna with the same elevation value. As a result, -y axis antenna has three times elevated from -x axis antenna. In this model, each pair of neighboring antennas has the same elevation value. This model is developed to decrease the antenna interelement distance with respect to the model which contains reversed antennas having same elevation values. Since the antennas are discone antennas and cone part of the antenna prevents to decrease the interelement distance, stair-like structure having different elevation values is required. Two of the antennas lying on +y and -y axis are reversed also to decrease the antenna interelement distance. In this antenna structure, the lowest antenna interelement distance is obtained among all of the discone antenna models. However, RMSE characteristic of this antenna structure has high fluctuations that prevent this antenna structure to be used in simulations.

In Figure 3.9, five antennas are used. Four antennas have the same alignment and one of the antennas is reversed and placed on top of +x axis antenna. This model improves the DF performance, but it has a directional performance such that, DF performance is better around azimuth angles which correspond to +x axis and worsens in other azimuth directions. Also from the comparison of DF performances of five dipole antenna array with this model, we find that five dipole antenna array has a better DF performance.

In Figure 3.10, four discone antennas and one dipole antenna are used. Dipole antenna is placed on the center of four discone antennas. With the addition of a dipole antenna, antenna

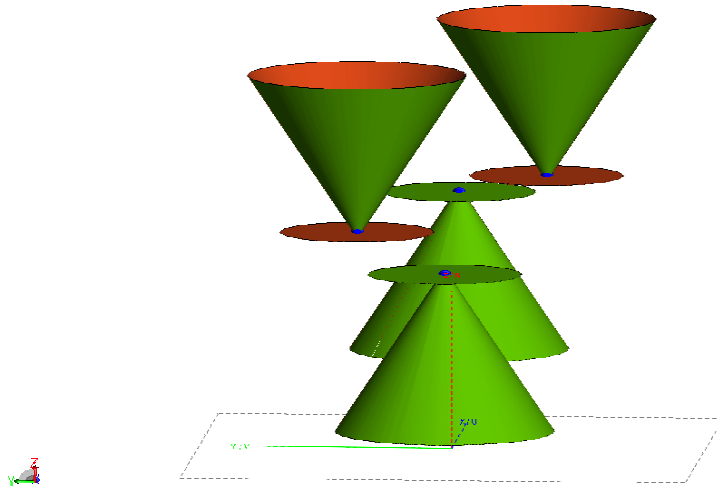


Figure 3.8: CADFEKO model of discone with four antennas, antennas are reversed and have different z-axis coordinates

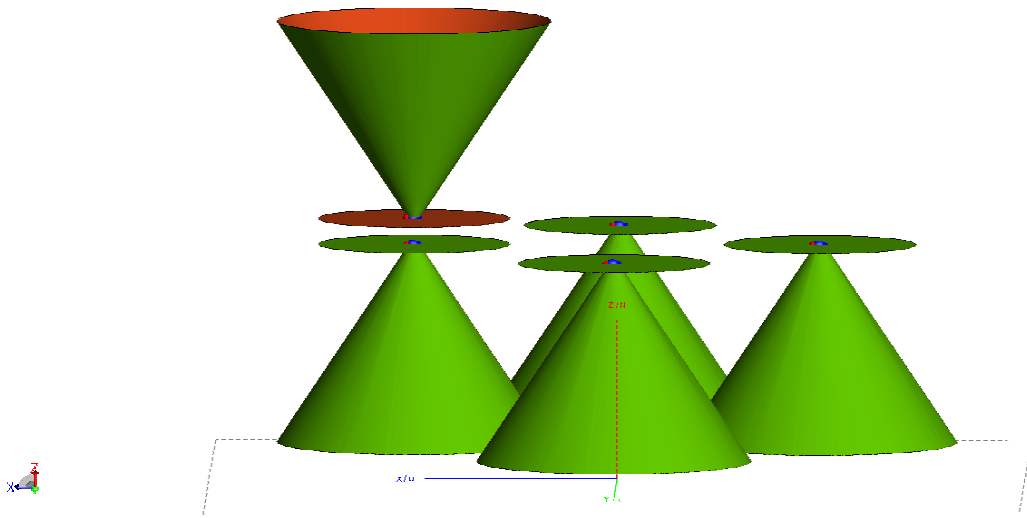


Figure 3.9: CADFEKO model of discone with five antennas, four of the antennas are on the same plane, one antenna is reversed and placed on top of x-axis antenna with a gap

interelement distance is decreased with respect to four discone antennas. But DF simulations with this model and five dipole antennas show that, DF performance of five dipole antennas is better than that of this model.

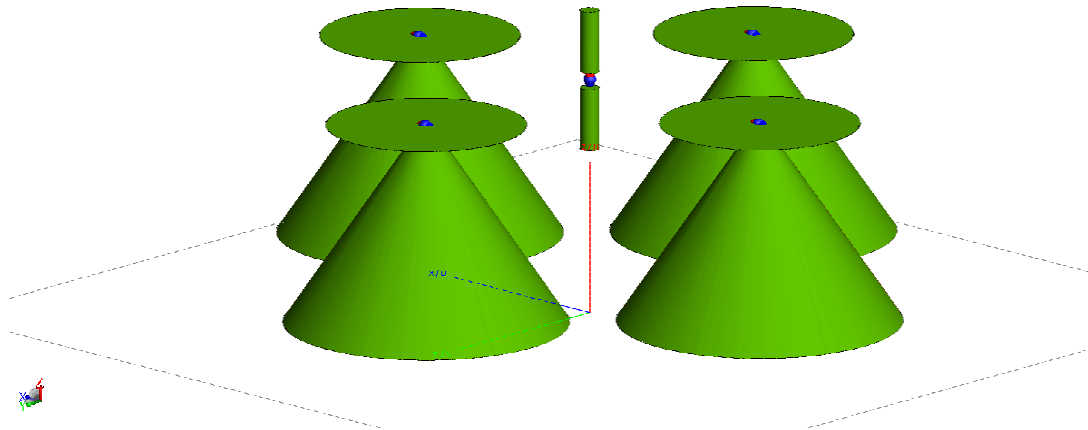


Figure 3.10: CADFEKO model of discone with five antennas with one dipole on the center of the four discone antennas lying on the same plane

### 3.1.2 Dipole Antenna Model

Two sets of dipole antennas are used to cover the frequency band used in simulations. Frequency band of 104-1496 MHz is divided into two parts of 104-648 MHz and 648-1496 MHz. These frequency bands are called band-1 and band-2, respectively. For each frequency band, a different set of dipole antennas is used. Dipole antenna arrays for band-1 and band-2 are given in the following sections.

#### 3.1.2.1 Band-1 Dipole Antenna Model

Dimensions of band-1 dipole antenna are given in Figure 3.11. In Table 3.2, values of the band-1 dipole antenna design parameters are given. Dipole antenna has a length of 40 centimeters which is designed to give the best DF performance for frequency 375 MHz. This frequency is in the middle of band-1. The dipole length is half the wavelength value for frequency 375 MHz. Dipole antenna has a radius of one centimeter. There is a two centimeter gap between the poles of the antenna. In the FEKO model, there is a wire line constructing a port within the gap touching the two poles of the dipole and currents are measured from these ports.

Table 3.2: Band-1 dipole antenna design parameters

Parameter Name	Value (cm)
Dipole Length	40
Dipole Radius	1
Dipole Gap	2

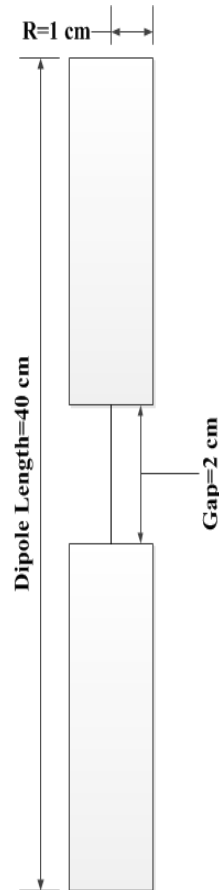


Figure 3.11: Band-1 dipole antenna dimensions

In Figure 3.12, circular array structure of the band-1 dipole antenna placements is given. Antenna interelement distance is 23 centimeters and radius of the circular array is 16 centimeters.

In Figure 3.13, FEKO model of band-1 dipole antenna can be seen. In this figure, dipole antennas are placed on axes.

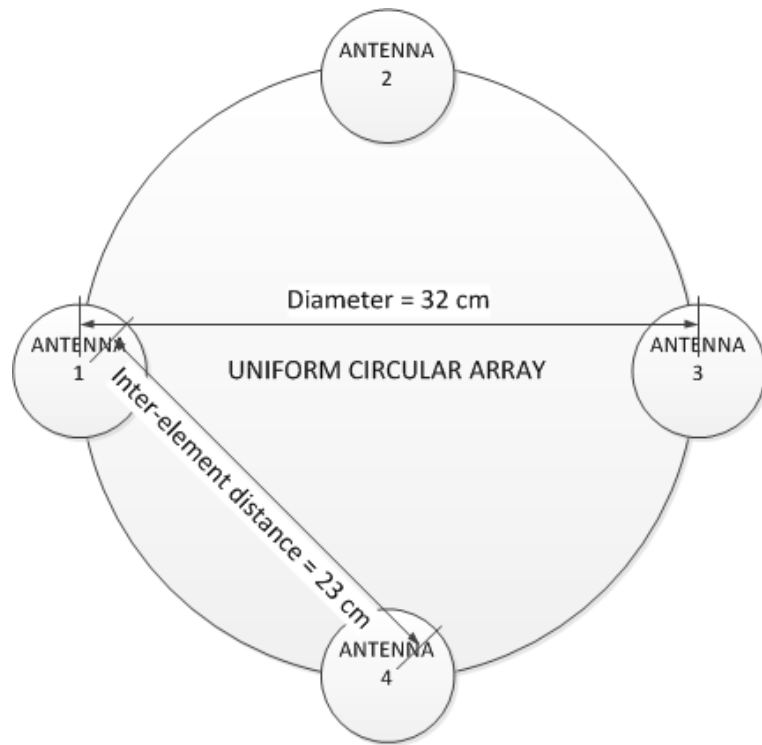


Figure 3.12: Band-1 dipole antenna array structure

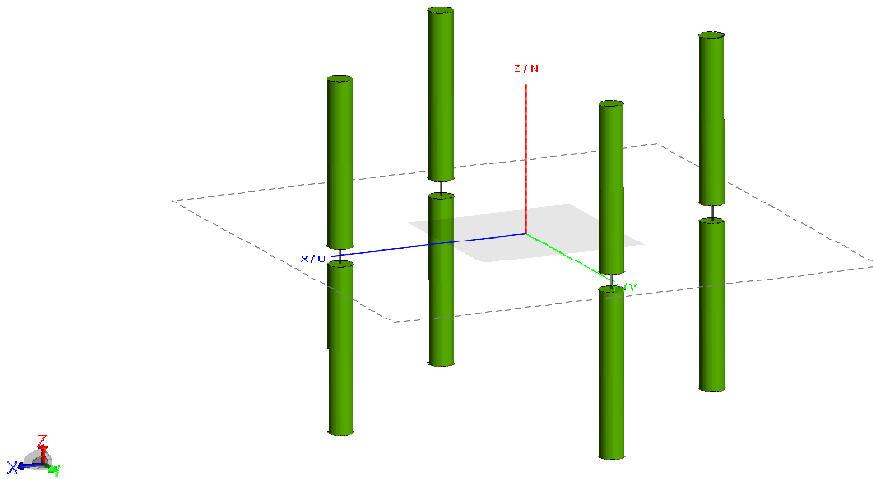


Figure 3.13: CADFEKO model of band-1 dipole antenna

### 3.1.2.2 Band-2 Dipole Antenna Model

Dimensions of band-2 dipole antenna are given in Figure 3.14. In Table 3.3, values of the band-1 dipole antenna design parameters are given. Dipole antenna has a length of 14 cen-

Table 3.3: Band-2 dipole antenna design parameters

Parameter Name	Value (cm)
Dipole Length	14
Dipole Radius	1
Dipole Gap	2

timeters which is designed to give the best DF performance for frequency 1075 MHz. This frequency is in the middle of band-2. The dipole length is half the wavelength value for frequency 1075 MHz. Dipole antenna has a radius of one centimeter. There is a two centimeter gap between the poles of the antenna.

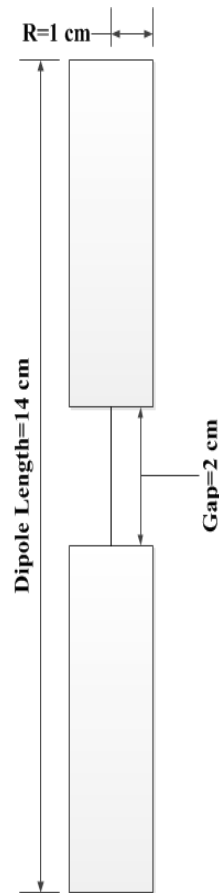


Figure 3.14: Band-2 dipole antenna dimensions

In Figure 3.15, circular array structure of the band-2 dipole antenna placements is given. Antenna interelement distance is 10 centimeters and radius of the circular array is 7 centimeters.

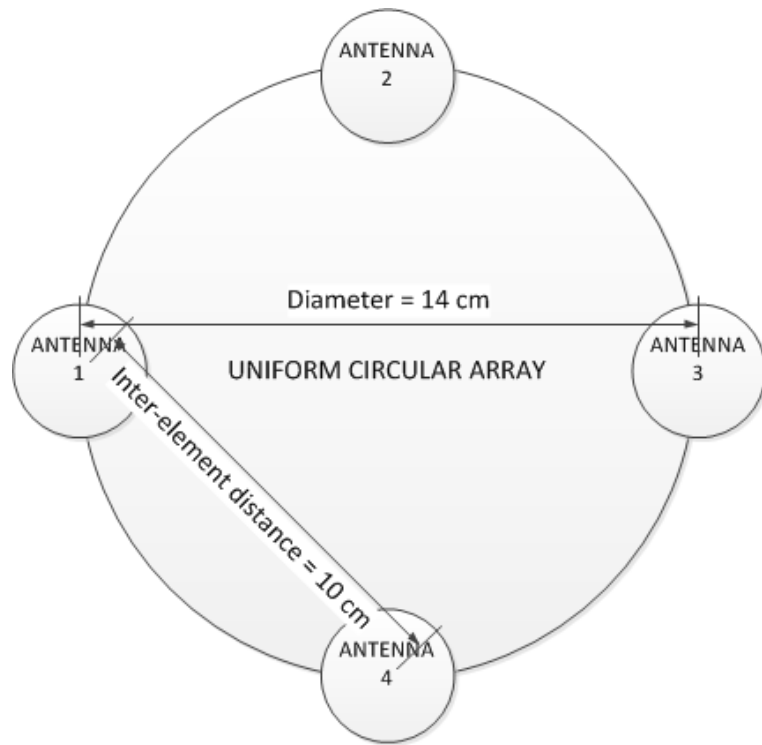


Figure 3.15: Band-2 dipole antenna array structure

In Figure 3.16, FEKO model of band-2 dipole antenna can be observed. If we compare this figure with Figure3.13, we can notice that the length of the dipole is shortened, as expected.

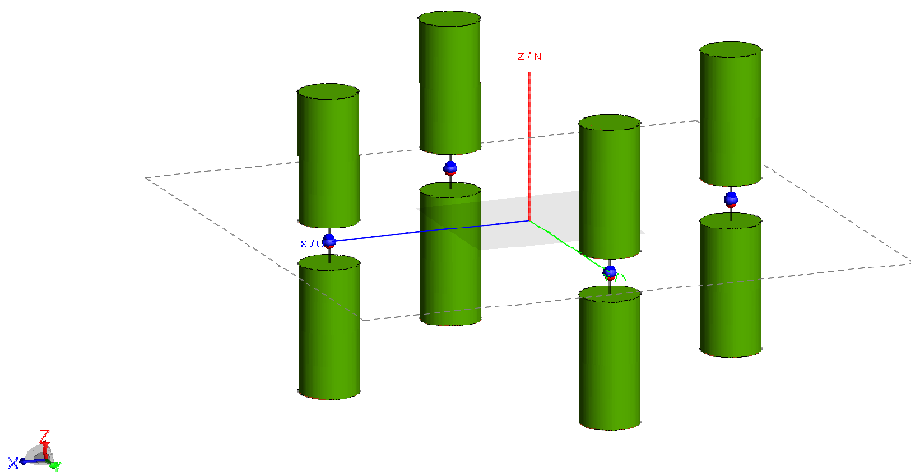


Figure 3.16: CADFEKO model of band-2 dipole antenna

## 3.2 Wideband Antenna Simulation Results

In the following analysis, we compare the DF performances of two different antenna models. One of the model is discone antenna model which is shown in Figure 3.4. Second model is dipole antenna model. In both models four antennas are used.

A frequency band of 104-1496 MHz is used in the simulations. This frequency band is divided into two parts. Band-1 is composed of the frequency band 104-648 MHz and band-2 is composed of the frequency band 648-1496 MHz. Two sets of dipole antennas are used in implementation of these two frequency bands as stated in the dipole antenna model part. However, there is only one set of discone antenna used in both frequency bands.

For band-1, azimuth scan simulations are realized for discrete frequency values in this band, namely, at 104 MHz, 312 MHz, 452 MHz, 504 MHz and 648 MHz. Discrete frequency values are used because FEKO simulation durations get too large on the order of few days if we use continuous band of frequencies covering the total band in numerical electromagnetic simulations of these antenna models. In frequency band-1 analysis, first set of dipole antennas is used which contains band-1 dipoles.

For band-2, simulations are accomplished in the discrete frequency values of 648 MHz, 800 MHz, 1148 MHz and 1496 MHz. In band-2 analysis, frequency 648 MHz is repeated, however DF simulations for dipole antenna is done for band-2 dipoles which are smaller in length and having lower antenna interelement distance. The same discone antennas are used in band-1 and band-2.

Three elevation angle values are used in the following simulations ,namely, 72, 90 and 108 degrees. 90 degrees of elevation corresponds to the horizontal plane including x and y axes. 72 degrees of elevation is defined to be 18 degrees tilted upwards from the horizontal plane. Similarly 108 degrees is by definition 18 degrees tilted downwards from the horizontal plane.

In the azimuth scan simulations, both calibration and test data are loaded with the same data. Thus DF performances of the antenna models are tested with respect to noise only. Noise is added to the test data to simulate realistic scenario. Test data can be thought as observation or measurement data while calibration data is obtained by calibration in noise free environment. Signal to Noise Ratio (SNR) is 15dB in the following analysis. Average of 30 trials is taken

with 500 snapshots collected per trial.

Azimuth data is collected with one degree intervals in FEKO simulations. In addition, cubic spline interpolation is used to obtain calibration data with 0.1 degree interval from the original one degree interval data.

### 3.2.1 Band-1 Simulations

In this section, Root Mean Square Error (RMSE) versus azimuth angle simulation results for frequencies 104 MHz, 312 MHz, 452 MHz, 504 MHz and 648 MHz are given. In each frequency, results are given for three elevation angle values namely 72, 90 and 108 degrees.

In Figure 3.17, DF performance comparison between discone antennas and dipole antennas are done for frequency 104 MHz at an elevation angle of 72 degrees. In this figure, DF performances of discone antennas are better than that of dipole antennas over all azimuth angles of interest. Average RMSE of dipole antennas is three times higher than average RMSE of discone antennas.

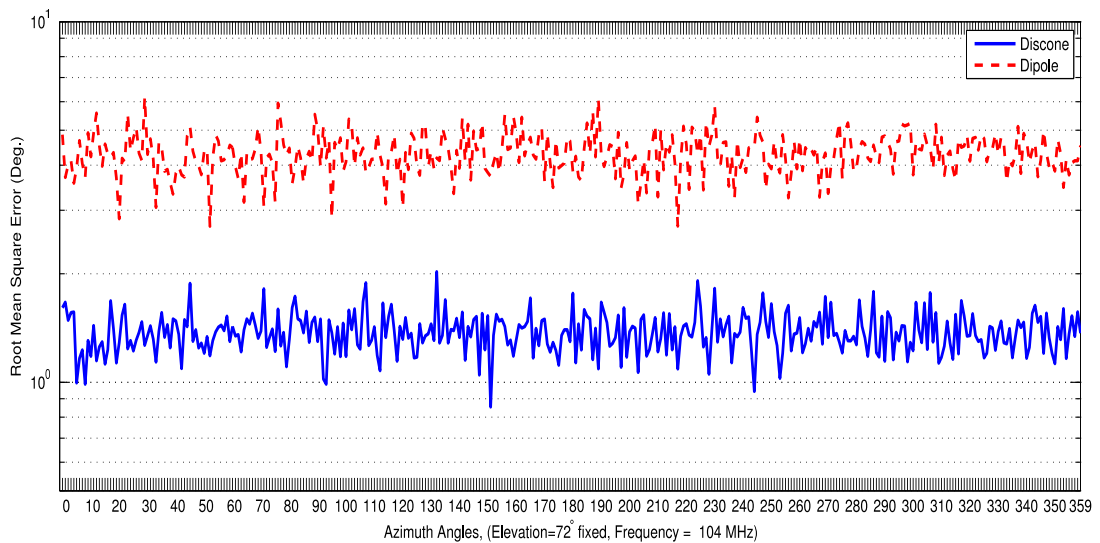


Figure 3.17: 104 MHz, elevation angle is 72 degrees, comparison of DF performance of discone antennas (with 120 degree alignment and a 0.5 scaled discone on the center) and dipole antennas having four elements

In Figure 3.18, DF performance comparison between discone antennas and dipole antennas are done for frequency 104 MHz at an elevation angle of 90 degrees. In this figure, DF

performance of discone antenna is still better. If we compare this figure with Figure 3.17, average root mean square errors (RMSE) for both models are decreased for elevation angle 90 degrees.

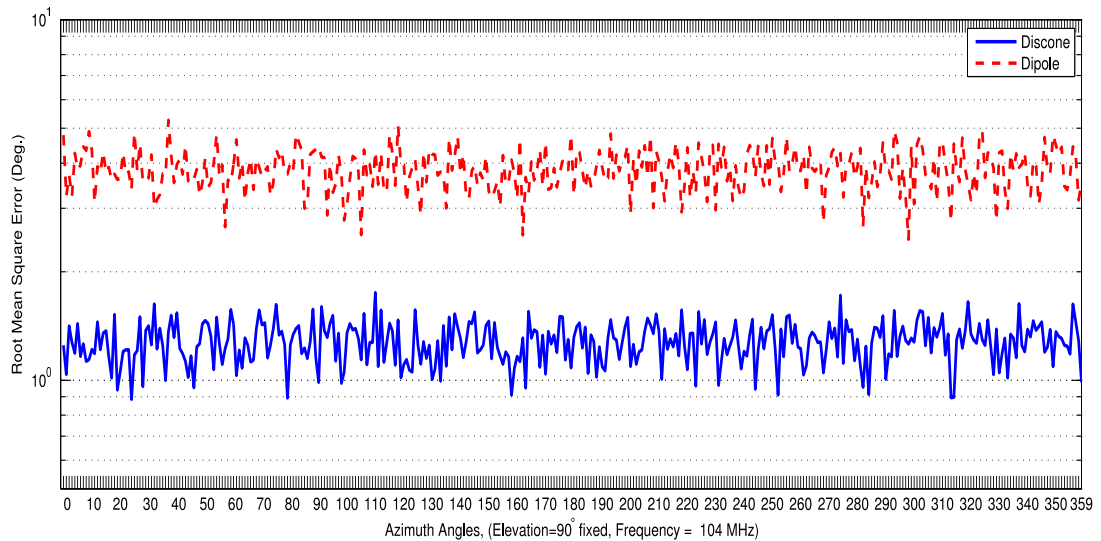


Figure 3.18: 104 MHz, elevation angle is 90 degrees, comparison of DF performance of discone antennas (with 120 degree alignment and a 0.5 scaled discone on the center) and dipole antennas having four elements

In Figure 3.19, DF performance comparison between discone antennas and dipole antennas are done for frequency 104 MHz at an elevation angle of 108 degrees. In this figure, DF performance of discone antenna is still better. As a result, for frequency 104 MHz, discone antennas have lower RMSE independent of the elevation angles of interest. Around 90 degrees of elevation angle, the best DF performances occur in the analyzed elevation angles. Departing from 90 degrees of elevation angle increases the average RMSE level for both antenna models.

In Figure 3.20, DF performance comparison between discone antennas and dipole antennas are done for frequency 312 MHz at an elevation angle of 72 degrees. In this figure, DF performances of discone antenna and dipole antenna are similar. Keeping elevation angles constant, if we compare the simulation results for frequency 312 MHz and 104 MHz, average RMSE is lower for frequency 312 MHz for both antenna models. In 104 MHz, average RMSE is around one degree for discone antennas, however for 312 MHz average RMSE is approximately 0.2 degree for discone antennas. As a result DF performance is improved by

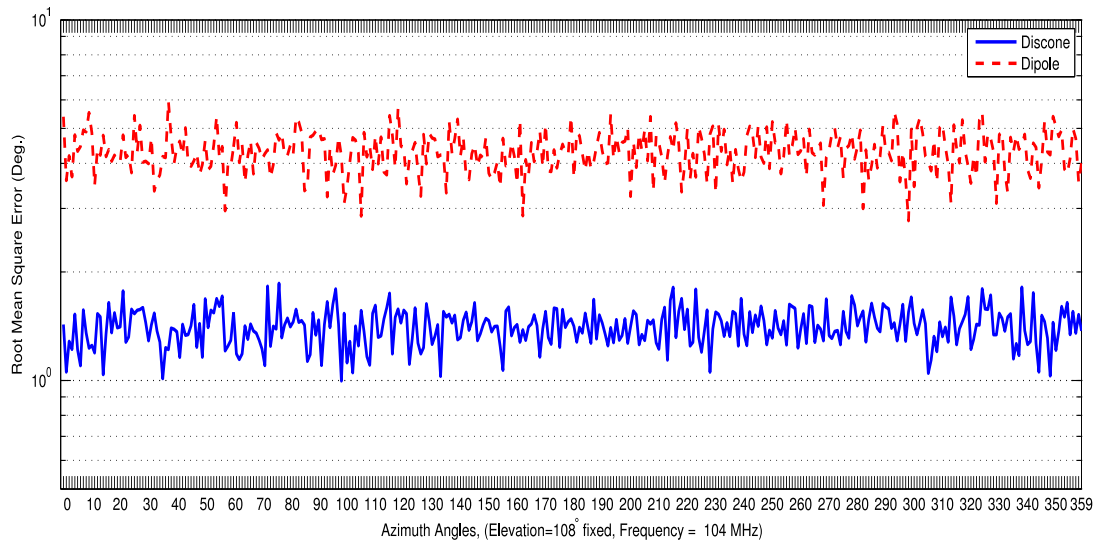


Figure 3.19: 104 MHz, elevation angle is 108 degrees, comparison of DF performance of discone antennas (with 120 degree alignment and a 0.5 scaled discone on the center) and dipole antennas having four elements

five times in 312 MHz as compared to 104 MHz for discone antennas. For dipole antennas average RMSE is four degrees in frequency 104 MHz, whereas average RMSE drops to 0.2 degree in frequency 312 MHz. Thus DF performance of dipole antenna is 20 times better in frequency 312 MHz compared to 104 MHz results.

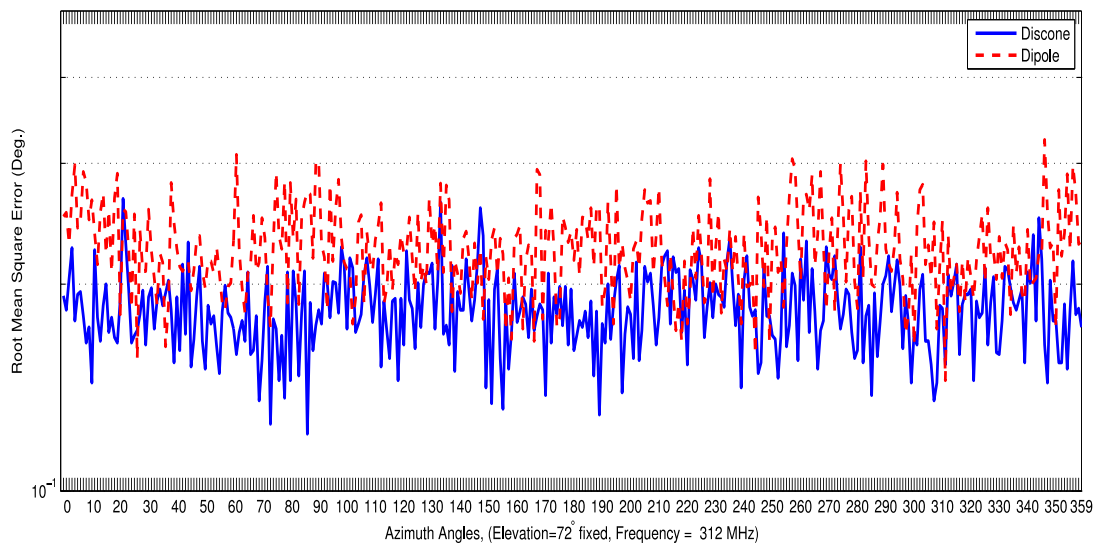


Figure 3.20: 312 MHz, elevation angle is 72 degrees, comparison of DF performance of discone antennas (with 120 degree alignment and a 0.5 scaled discone on the center) and dipole antennas having four elements

In Figure 3.21, DF performance comparison between the discone antennas and dipole antennas are done for frequency 312 MHz at an elevation angle of 90 degrees. In this figure, average RMSE's of discone and dipole antennas are the same. Compared to the 72 degrees of elevation angle results; in elevation angle 90 degrees, average RMSE of dipole antennas is reduced.

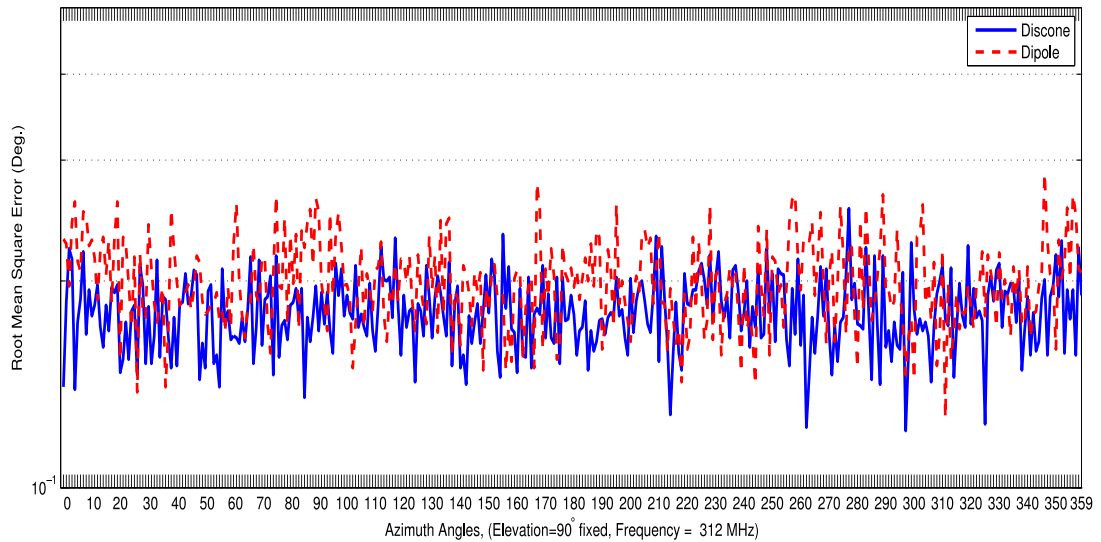


Figure 3.21: 312 MHz, elevation angle is 90 degrees, comparison of DF performance of discone antennas (with 120 degree alignment and a 0.5 scaled discone on the center) and dipole antennas having four elements

In Figure 3.22, DF performance comparison between discone antennas and dipole antennas are done for frequency 312 MHz at an elevation angle of 108 degrees. In this figure, average RMSE levels of antenna models are similar. If we compare the simulation results for frequency 312 MHz, azimuth scan result for elevation angle 90 degrees still has the best DF performance, with the lowest average RMSE values for both antenna models.

In Figure 3.23, DF performance comparison between discone antennas and dipole antennas are done for frequency 452 MHz at an elevation angle of 72 degrees. In this figure, DF performance of discone antenna is better. However, average RMSE of dipole antennas gets closer to the average RMSE of discone antennas compared to 312MHz.

In Figure 3.24, DF performance comparison between discone antennas and dipole antennas are done for frequency 452 MHz at an elevation angle of 90 degrees. In this figure, DF performance of discone antenna is better. Average RMSE level is decreased for both discone

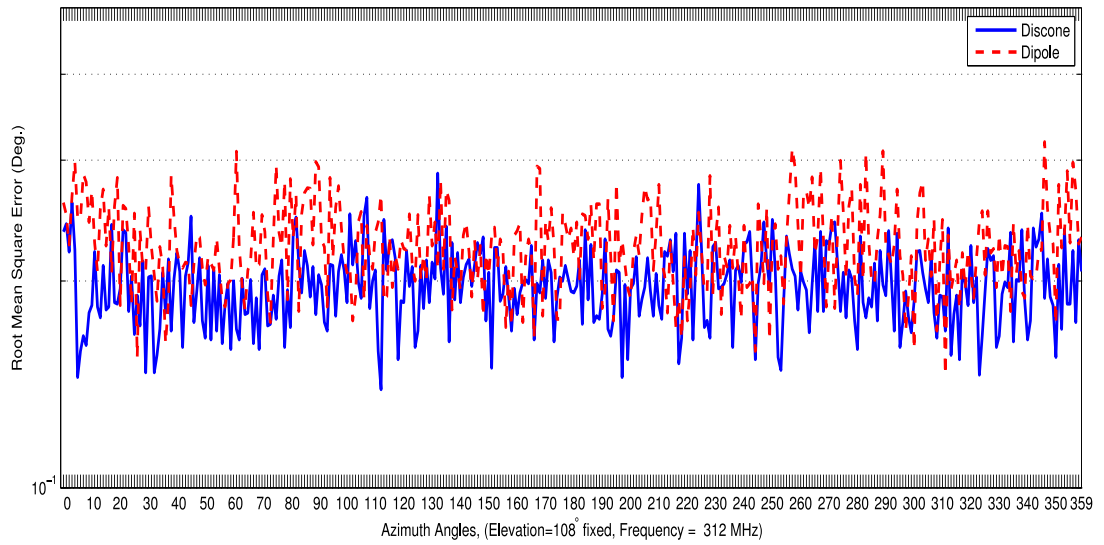


Figure 3.22: 312 MHz, elevation angle is 108 degrees, comparison of DF performance of discone antennas (with 120 degree alignment and a 0.5 scaled discone on the center) and dipole antennas having four elements

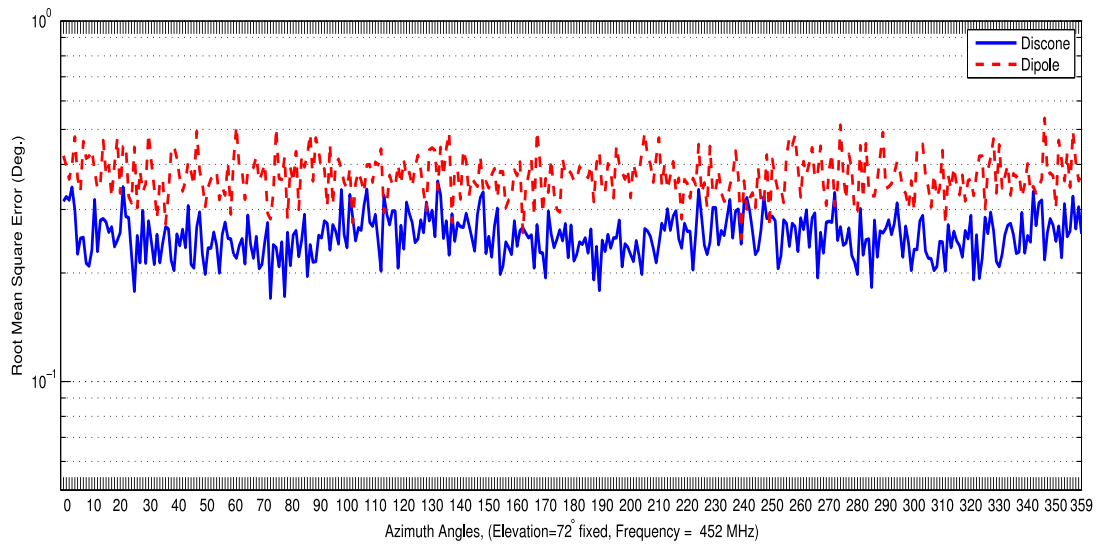


Figure 3.23: 452 MHz, elevation angle is 72 degrees, comparison of DF performance of discone antennas (with 120 degree alignment and a 0.5 scaled discone on the center) and dipole antennas having four elements

and dipole antennas compared to elevation angle 72 degrees.

In Figure 3.25, DF performance comparison between discone antennas and dipole antennas are done for frequency 452 MHz at an elevation angle of 108 degrees. In this figure, DF performance of discone antennas is better. In this elevation value, average RMSE for dipole

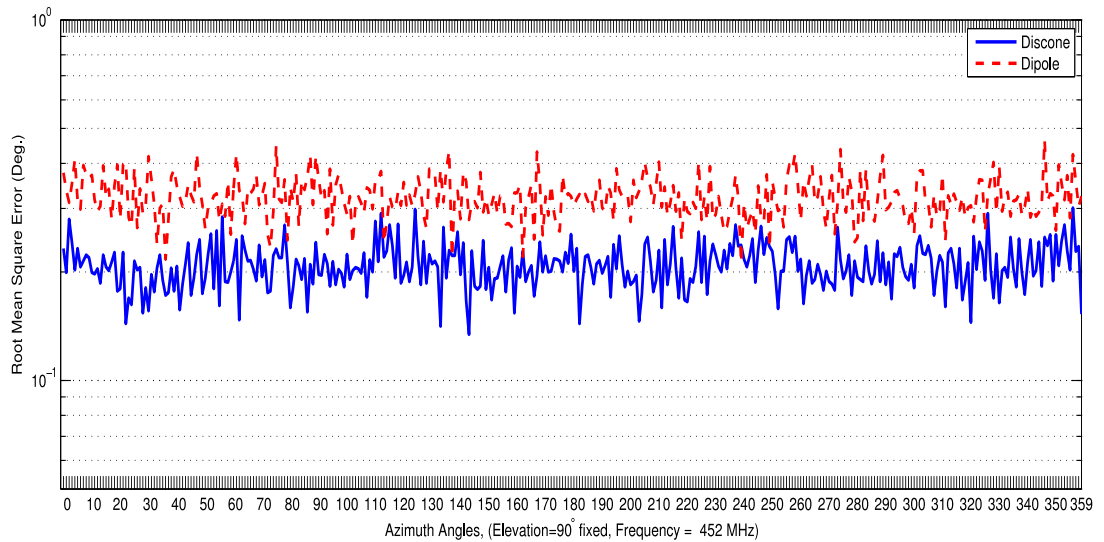


Figure 3.24: 452 MHz, elevation angle is 90 degrees, comparison of DF performance of discone antennas (with 120 degree alignment and a 0.5 scaled discone on the center) and dipole antennas having four elements

antenna is increased while the average RMSE for discone antennas is nearly constant compared to elevation angle 90 degrees results.

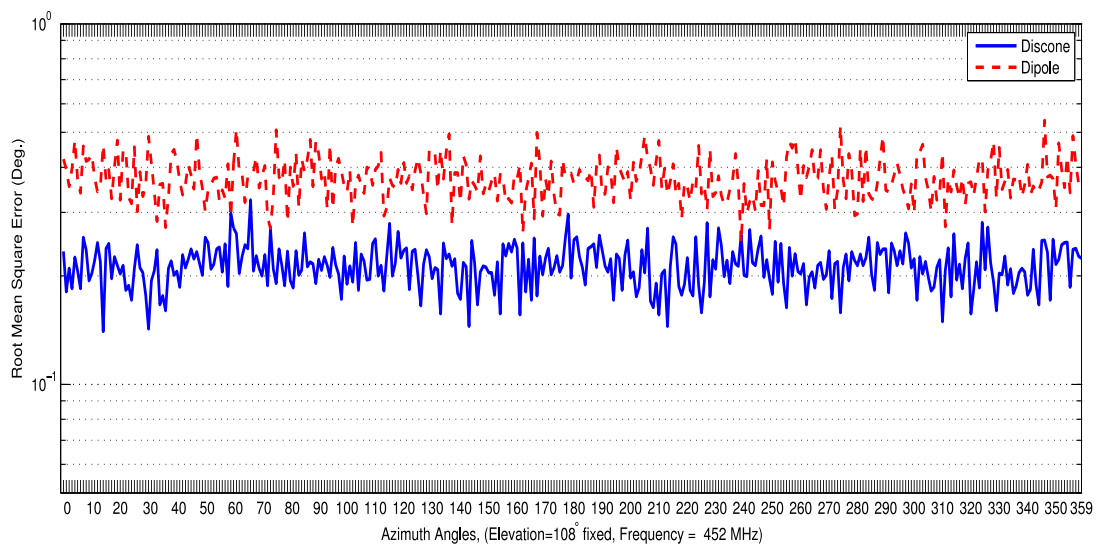


Figure 3.25: 452 MHz, elevation angle is 108 degrees, comparison of DF performance of discone antennas (with 120 degree alignment and a 0.5 scaled discone on the center) and dipole antennas having four elements

In Figure 3.26, DF performance comparison between discone antennas and dipole antennas

are done for frequency 504 MHz at an elevation angle of 72 degrees. In this figure, average RMSE of discone antenna is increased as compared to the average RMSE for frequency 452 MHz. DF performances of dipole and discone antennas are very similar.

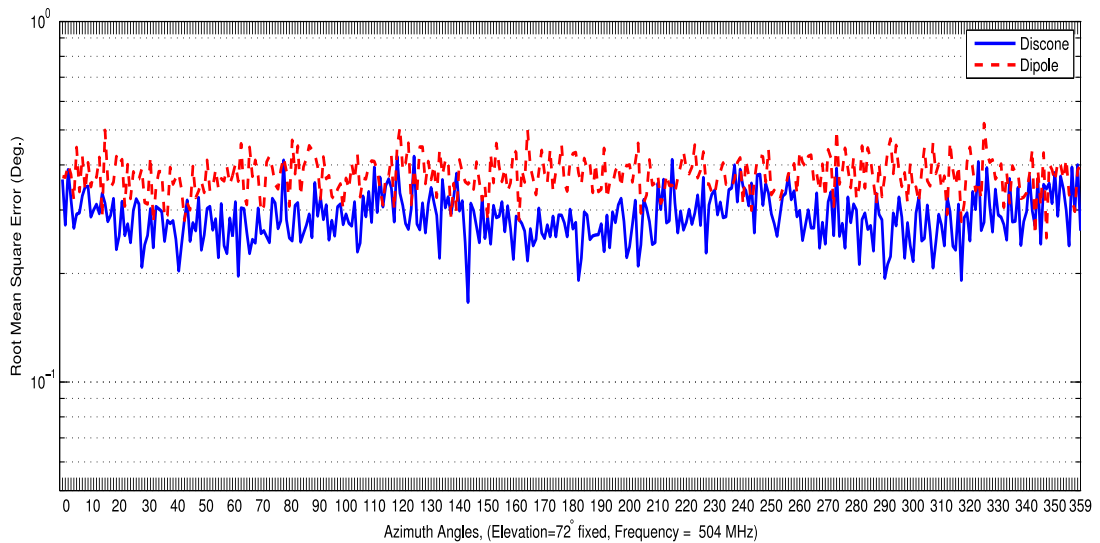


Figure 3.26: 504 MHz, elevation angle is 72 degrees, comparison of DF performance of discone antennas (with 120 degree alignment and a 0.5 scaled discone on the center) and dipole antennas having four elements

In Figure 3.27, DF performance comparison between discone antennas and dipole antennas are done for frequency 504 MHz at an elevation angle of 90 degrees. In this figure, DF performance of discone antenna is better as compared to that of dipole antenna. Average RMSEs are decreased for both models as compared to the results for elevation angle 72 degrees.

In Figure 3.28, DF performance comparison between discone antennas and dipole antennas are done for frequency 504 MHz at an elevation angle of 108 degrees. In this figure, average RMSE of dipole antennas increases noticeably while average RMSE of discone antennas remains constant as compared to the results for elevation angle 90 degrees. Thus average RMSE of dipole antennas is twice the average RMSE of discone antennas.

In Figure 3.29, DF performance comparison between discone antennas and dipole antennas are done for frequency 648 MHz at an elevation angle of 72 degrees. This frequency is used in both band-1 and band-2. However in band-1, band-1 dipole antenna set is used while in band-2, band-2 dipole antenna set is used. Dipole lengths and antenna interelement distance of two dipole sets are different. In this figure, average RMSEs of discone antennas and dipole

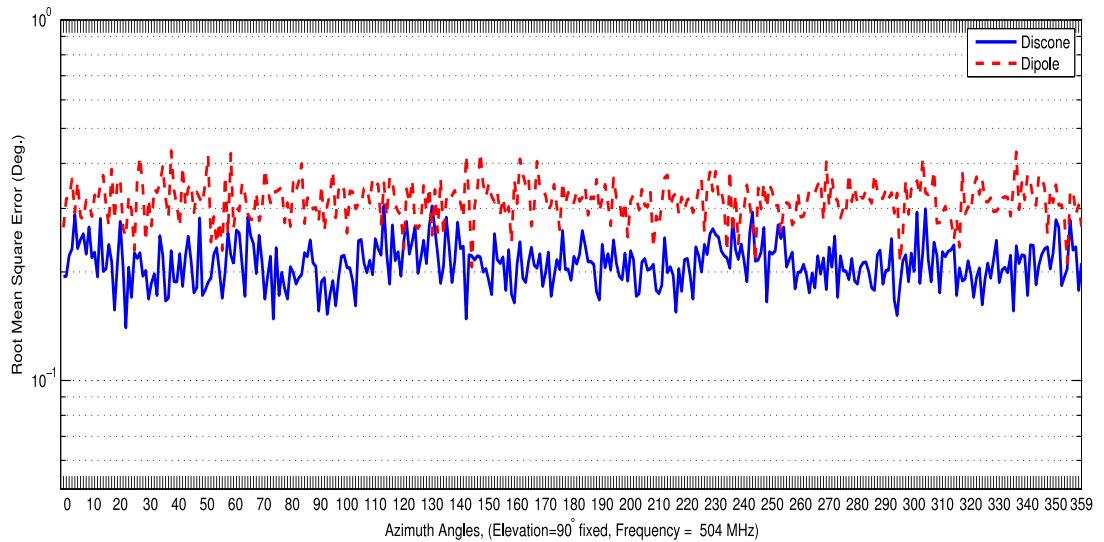


Figure 3.27: 504 MHz, elevation angle is 90 degrees, comparison of DF performance of discone antennas (with 120 degree alignment and a 0.5 scaled discone on the center) and dipole antennas having four elements

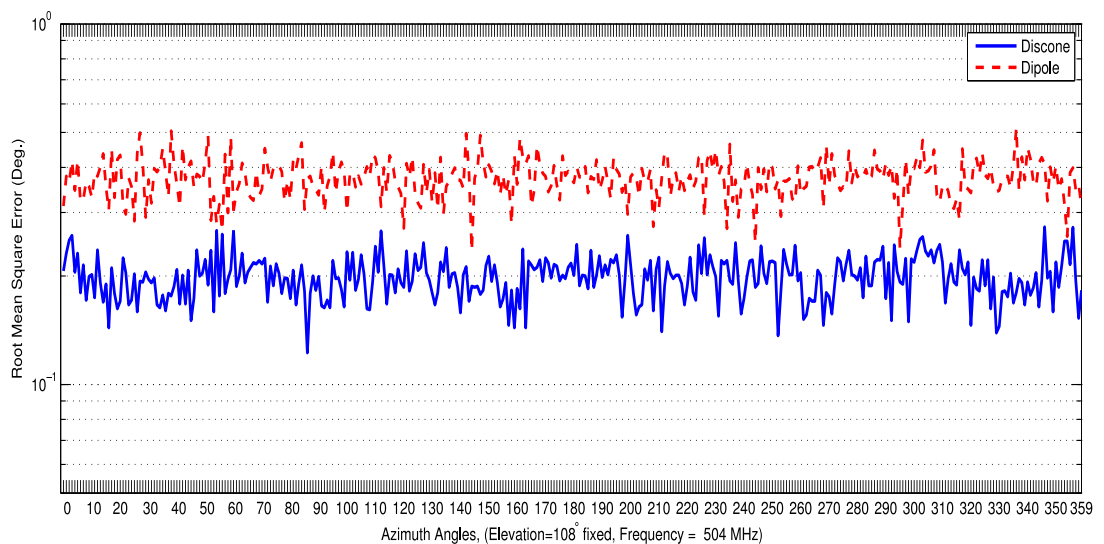


Figure 3.28: 504 MHz, elevation angle is 108 degrees, comparison of DF performance of discone antennas (with 120 degree alignment and a 0.5 scaled discone on the center) and dipole antennas having four elements

antennas are very similar. RMSE fluctuations of discone antennas are much higher.

In Figure 3.30, DF performance comparison between discone antennas and dipole antennas are done for frequency 648 MHz at an elevation angle of 90 degrees. In this figure, DF performances of discone antenna and dipole antenna are similar. Average RMSEs are decreased by

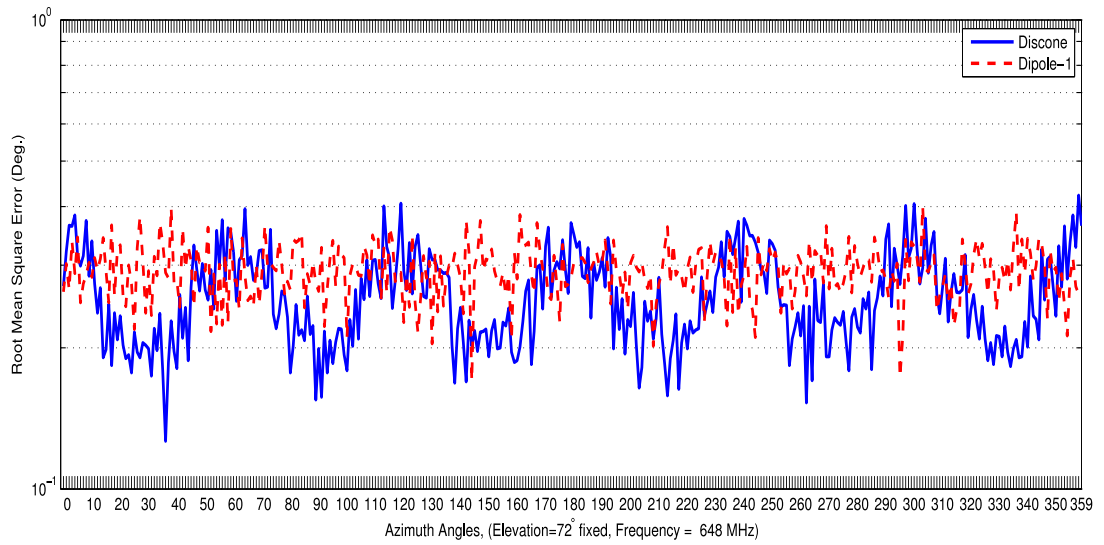


Figure 3.29: 648 MHz, elevation angle is 72 degrees, comparison of DF performance of discone antennas (with 120 degree alignment and a 0.5 scaled discone on the center) and dipole antennas having four elements

0.1 degree for both antenna models as compared to the results for elevation angle 72 degrees. Fluctuations in RMSE of discone antennas are disappeared.

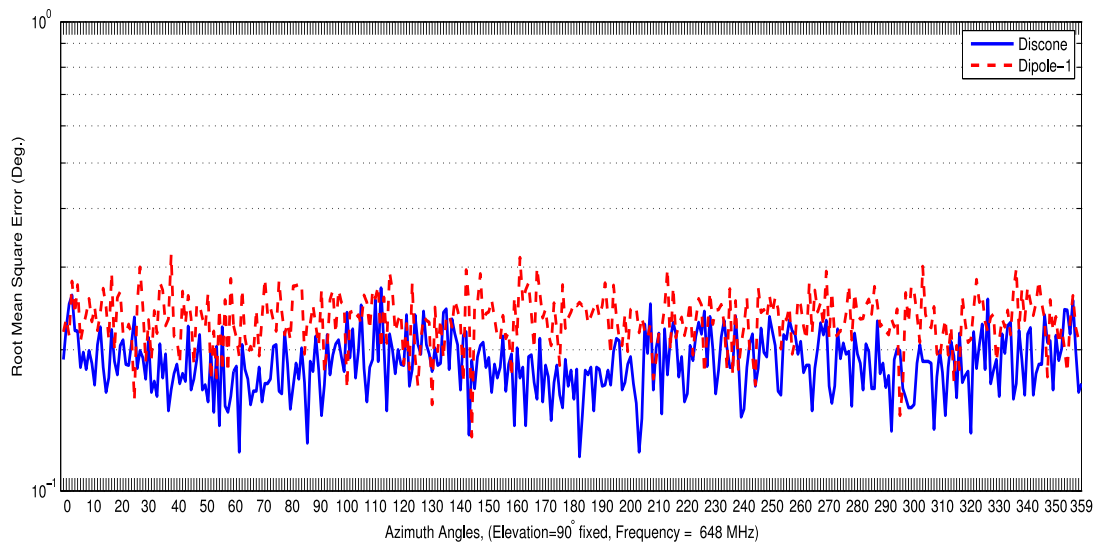


Figure 3.30: 648 MHz, elevation angle is 90 degrees, comparison of DF performance of discone antennas (with 120 degree alignment and a 0.5 scaled discone on the center) and dipole antennas having four elements

In Figure 3.31, DF performance comparison between discone antennas and dipole antennas

are done for frequency 648 MHz at an elevation angle of 108 degrees. In this figure, average RMSE of dipole antennas increases while average RMSE of discone antennas decreases as compared to the results for elevation angle 90 degrees. Average RMSE of dipole antenna is twice the average RMSE of discone antenna.

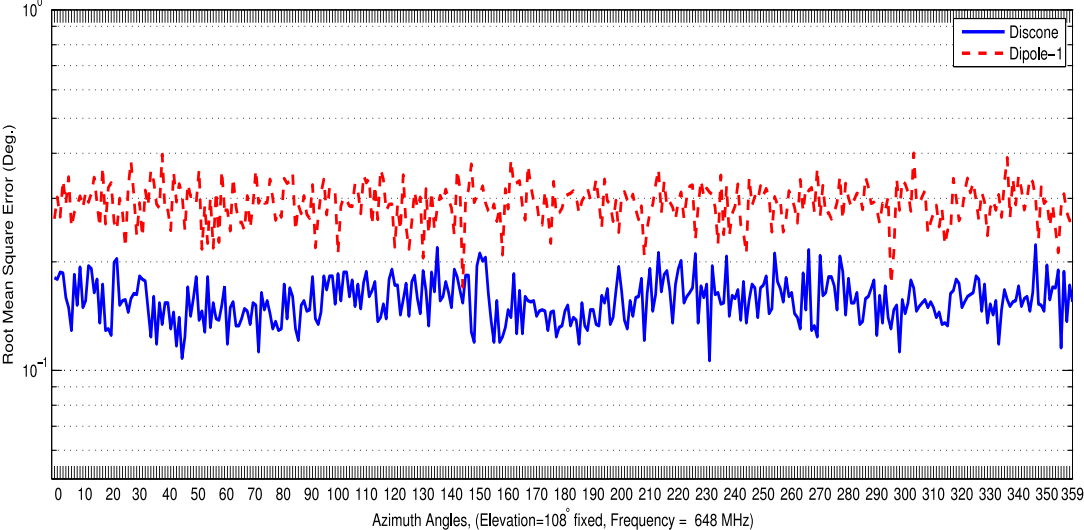


Figure 3.31: 648 MHz, elevation angle is 108 degrees, comparison of DF performance of discone antennas (with 120 degree alignment and a 0.5 scaled discone on the center) and dipole antennas having four elements

**3.2.2 Band-2 Simulations**

In this section, Root Mean Square Error (RMSE) versus azimuth angle simulation results for frequencies 648 MHz, 800 MHz, 1148 MHz and 1496 MHz are given. In each frequency, results are given for three elevation angle values namely 72, 90 and 108 degrees. In band-2 simulations, band-2 dipole antennas are used. Antenna interelement distance for these dipole antennas is much smaller as compared to discone antenna’s antenna interelement distance. Hence DF performances of discone antennas are much better for all frequencies and elevation angles in band-2.

In Figure 3.32, DF performance comparison between discone antennas and dipole antennas are done for frequency 648 MHz at an elevation angle of 72 degrees. In this figure, average RMSE of dipole antennas is increased to 0.7 degree which is more than twice the value in band-1 dipole antenna results. The main reason is that antenna interelement distance for

band-2 dipole antennas is less than half the antenna interelement distance of band-1 dipole antennas. However, the average RMSE of discone antennas is 0.25 degree which is unchanged in band-2 simulations because the same antenna interelement distance is used in band-1 and band-2 for discone antennas.

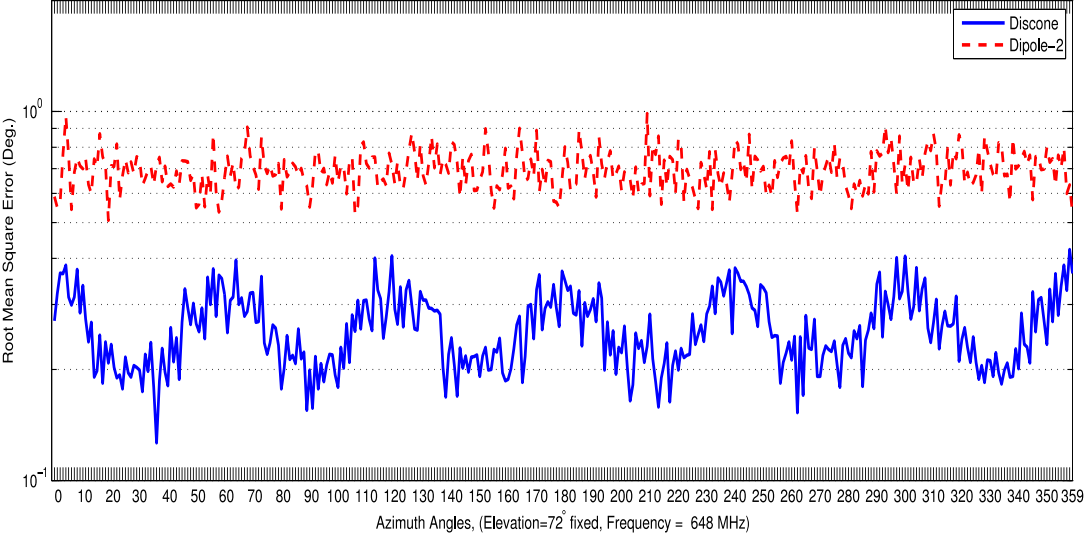


Figure 3.32: 648 MHz, elevation angle is 72 degrees, comparison of DF performance of discone antennas (with 120 degree alignment and a 0.5 scaled discone on the center) and dipole antennas having four elements

In Figure 3.33, DF performance comparison between discone antennas and dipole antennas are done for frequency 648 MHz at an elevation angle of 90 degrees. In this figure, average RMSE of dipole antenna is three times higher than the average RMSE of discone antenna. Average RMSEs are decreased nearly 0.1 degree for both antenna models as compared to the results for elevation angle 72 degrees.

In Figure 3.34, DF performance comparison between discone antennas and dipole antennas are done for frequency 648 MHz at an elevation angle of 108 degrees. In this figure, average RMSE of dipole antenna increases 0.1 degree while average RMSE of discone antennas decreases 0.5 degree as compared to the results for elevation angle 90 degrees.

In Figure 3.35, DF performance comparison between discone antennas and dipole antennas are done for frequency 800 MHz at an elevation angle of 72 degrees. In this figure, DF performance of discone antenna is nearly six times better than that of dipole antennas. Average RMSE for dipole antennas is increased to 0.9 degree, which is more than twice the value as

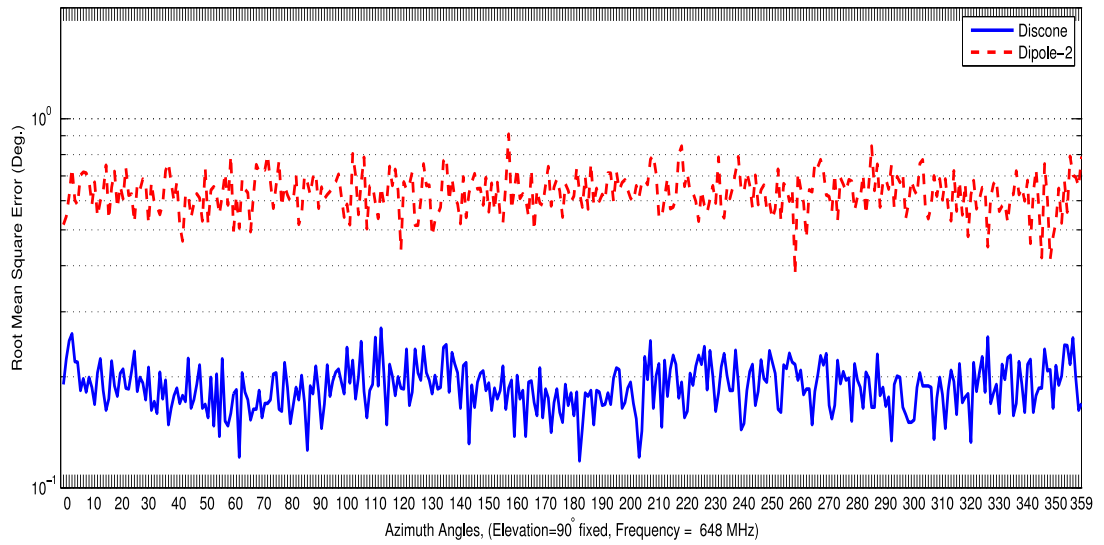


Figure 3.33: 648 MHz, elevation angle is 90 degrees, comparison of DF performance of discone antennas (with 120 degree alignment and a 0.5 scaled discone on the center) and dipole antennas having four elements

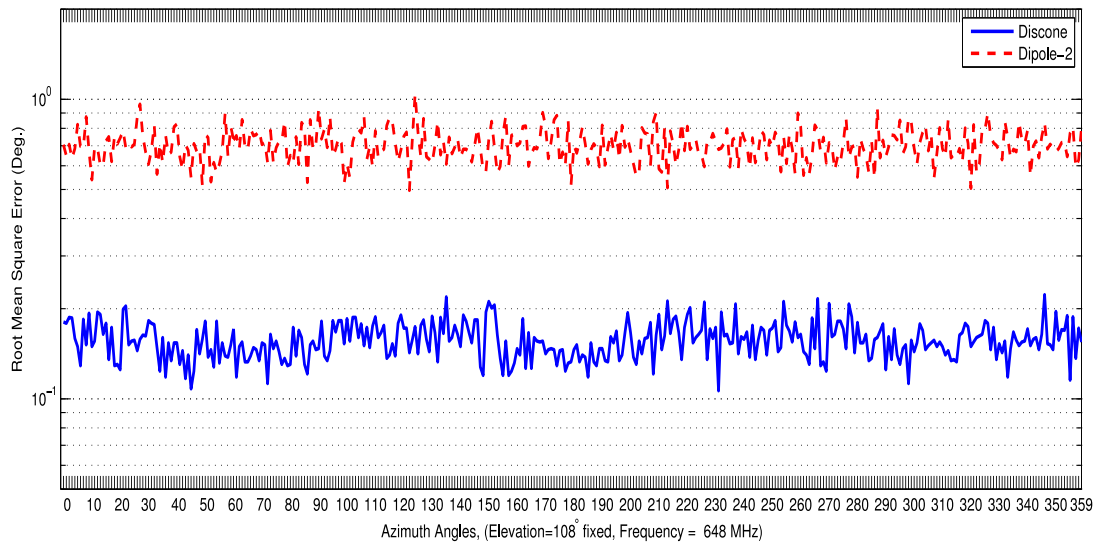


Figure 3.34: 648 MHz, elevation angle is 108 degrees, comparison of DF performance of discone antennas (with 120 degree alignment and a 0.5 scaled discone on the center) and dipole antennas having four elements

compared to the frequency of 504 MHz in frequency band-1. However average RMSE for discone antennas is decreased to 0.1 degree around most of azimuth angles of interest. If we concentrate on the RMSE curve for discone antennas, we will observe that RMSE values tend to increase around 0, 120 and 240 degrees of azimuth angles. This can be explained with the

alignment of discone antennas. Discone antennas are placed in these azimuth angle sectors such that, the first antenna is placed in +x axis, which corresponds to 0 degree of azimuth. The other two antennas are placed in 120 degree neighborhood of this antenna. As a result high RMSE values are due to the antennas placed at that azimuth sector.

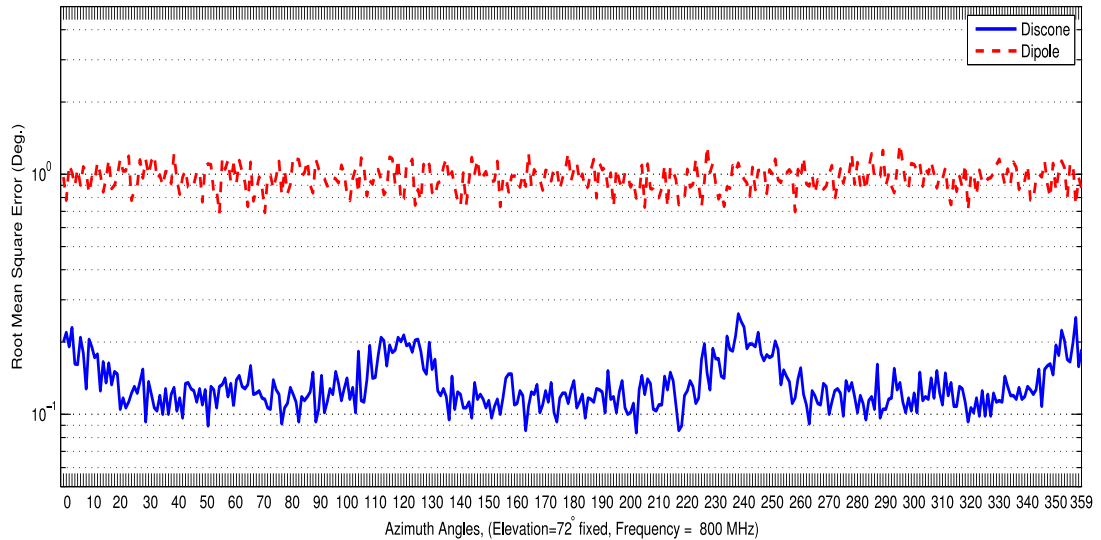


Figure 3.35: 800 MHz, elevation angle is 72 degrees, comparison of DF performance of discone antennas (with 120 degree alignment and a 0.5 scaled discone on the center) and dipole antennas having four elements

In Figure 3.36, DF performance comparison between discone antennas and dipole antennas are done for frequency 800 MHz at an elevation angle of 90 degrees. In this figure, DF performance of discone antenna is still better. Average RMSE value for discone antenna decreased slightly, especially at 0, 120 and 240 degrees of azimuth angles forming nearly uniform characteristics around all azimuth sectors. In addition, average RMSE for dipole antennas is 0.1 degree decreased, as compared to results for elevation angle 72 degrees.

In Figure 3.37, DF performance comparison between discone antennas and dipole antennas are done for frequency 800 MHz at an elevation angle of 108 degrees. In this figure, DF performance of discone antenna is better. Average RMSE of discone antenna is decreased while average RMSE of dipole antenna is increased for elevation angle 108 degrees as compared to elevation angle 90 degrees result. RMSE curve for discone antenna becomes more uniform such that no difference in RMSE can be observed around any azimuth angle.

In Figure 3.38, DF performance comparison between discone antennas and dipole antennas

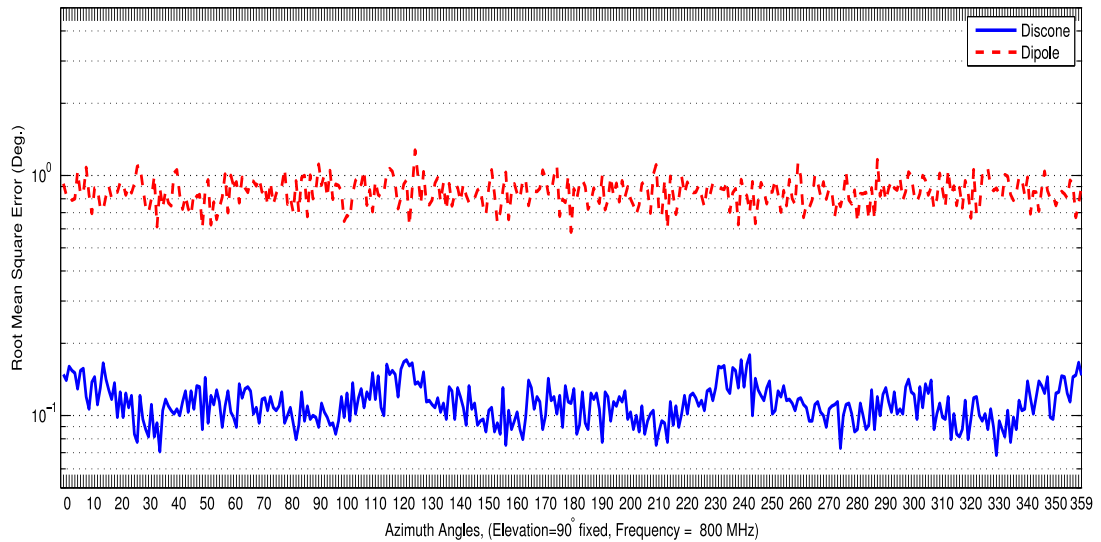


Figure 3.36: 800 MHz, elevation angle is 90 degrees, comparison of DF performance of discone antennas (with 120 degree alignment and a 0.5 scaled discone on the center) and dipole antennas having four elements

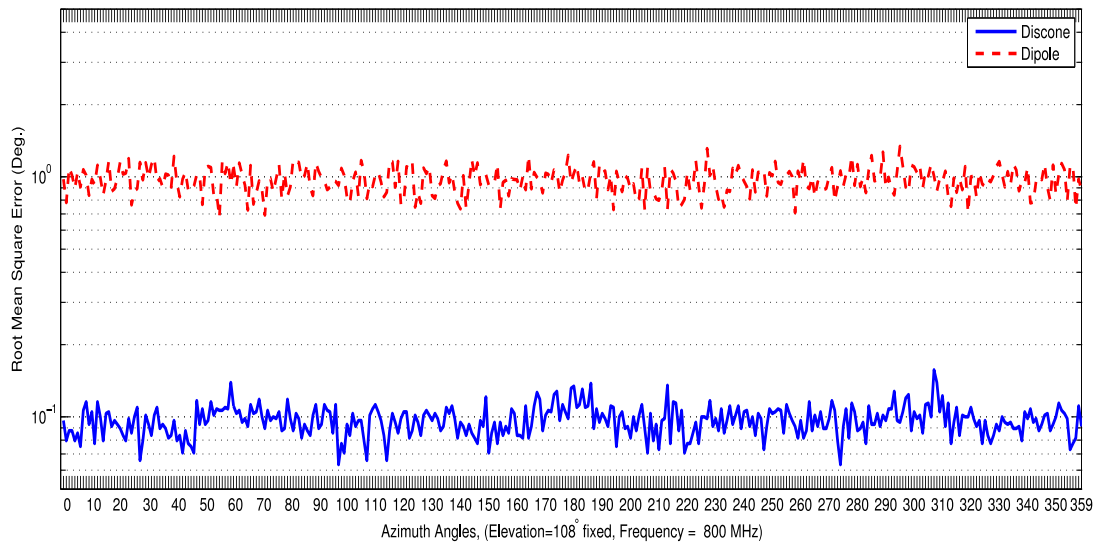


Figure 3.37: 800 MHz, elevation angle is 108 degrees, comparison of DF performance of discone antennas (with 120 degree alignment and a 0.5 scaled discone on the center) and dipole antennas having four elements

are done for frequency 1148 MHz at an elevation angle of 72 degrees. In this figure, discone antennas show fluctuations in RMSE curve. Around 60, 180 and 300 degrees; RMSE levels increase up to one degree RMSE for a band of 60 degrees for discone antennas. These high error bands have the center azimuth angles of 60, 180 and 300 degrees. In these high

error azimuth regions RMSE levels of dipole antennas and discone antennas are similar. We can say that, in azimuth regions corresponding to discone antenna positions (0, 120 and 240 degrees azimuth) RMSE levels decrease, however in other regions RMSE levels increase. If we compare these results with the results for frequency 800 MHz we can conclude that, average RMSE level for discone antennas changed from 0.1 degree for 800 MHz to 0.6 degree for 1148 MHz. However for dipole antennas, average RMSE level does not change noticeably for frequencies of 800 MHz and 1148 MHz. DF performances of discone antennas are affected from elevation angle, especially when the plane wave excitation is coming from elevation angles smaller than 90 degrees.

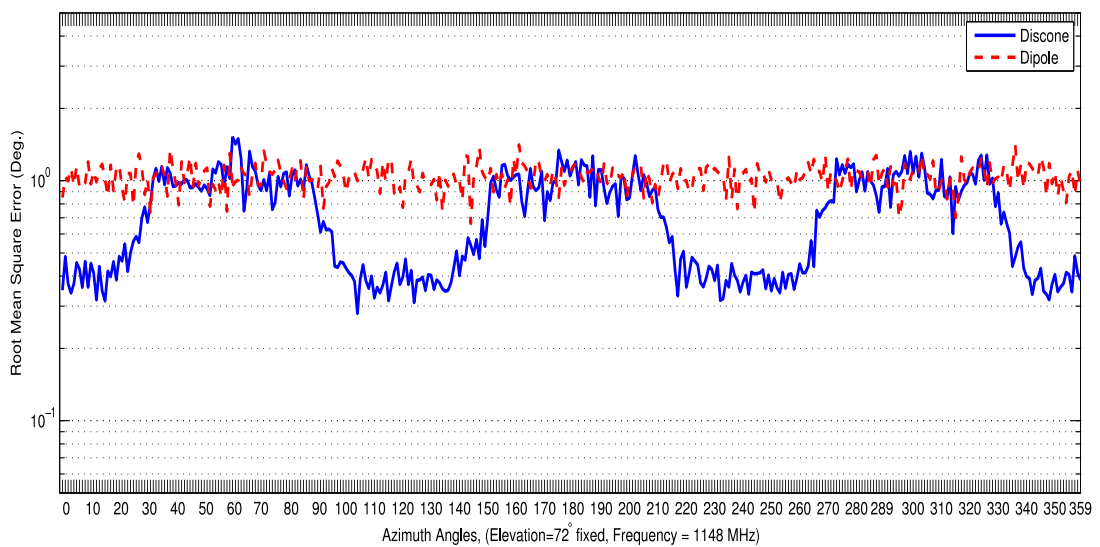


Figure 3.38: 1148 MHz, elevation angle is 72 degrees, comparison of DF performance of discone antennas (with 120 degree alignment and a 0.5 scaled discone on the center) and dipole antennas having four elements

In Figure 3.39, DF performance comparison between discone antennas and dipole antennas are done for frequency 1148 MHz at an elevation angle of 90 degrees. In this figure, DF performance of discone antenna is better. In addition, average RMSE level for discone antennas decreases as compared to elevation angle 72 degrees. But if we compare these RMSE values with the RMSE levels for frequency 800 MHz and elevation angle 90 degrees, we can say that RMSE levels have higher fluctuation for frequency 1148 MHz. For dipole antennas, average RMSE levels are near for frequency 800 and 1148 MHz.

In Figure 3.40, DF performance comparison between discone antennas and dipole antennas

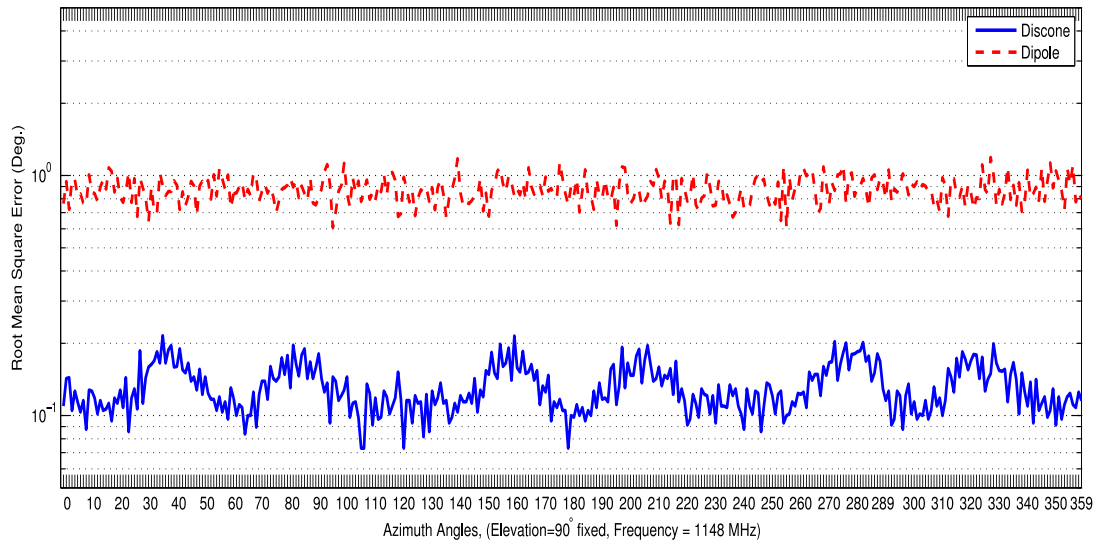


Figure 3.39: 1148 MHz, elevation angle is 90 degrees, comparison of DF performance of discone antennas (with 120 degree alignment and a 0.5 scaled discone on the center) and dipole antennas having four elements

are done for frequency 1148 MHz at an elevation angle of 108 degrees. In this figure, DF performance of discone antenna is nearly 10 times better than that of dipole antenna. Dipole antennas' average RMSE level is nearly one degree. For discone antenna, average RMSE level is decreased as compared to RMSE level for elevation angle 90 degrees. In addition, RMSE fluctuations are lower in elevation angle 108 degrees as compared to fluctuations for elevation angle 72 degrees. Even though the same elevation changes from horizontal plane happen for elevation angle 72 and 108 degrees, DF performance is better for elevation angle 108 degrees. This can be explained with nonsymmetrical shape of discone antennas.

In Figure3.41, DF performance comparison between discone antennas and dipole antennas are done for frequency 1496 MHz at an elevation angle of 72 degrees. In this figure, DF performance of discone antenna is nearly three times better as compared to that of dipole antennas. Discone antenna's RMSE curve shows fluctuations over all azimuth angles. Average RMSE value for discone antennas is 0.3 degree, which is half the average RMSE for frequency 1148 MHz and elevation angle 72 degrees. Average RMSE for dipole antennas is 0.9 degree, which is 0.1 degree lower than the average RMSE for frequency 1148 MHz.

In Figure3.42, DF performance comparison between discone antennas and dipole antennas are done for frequency 1496 MHz at an elevation angle of 90 degrees. In this figure, RMSE curve

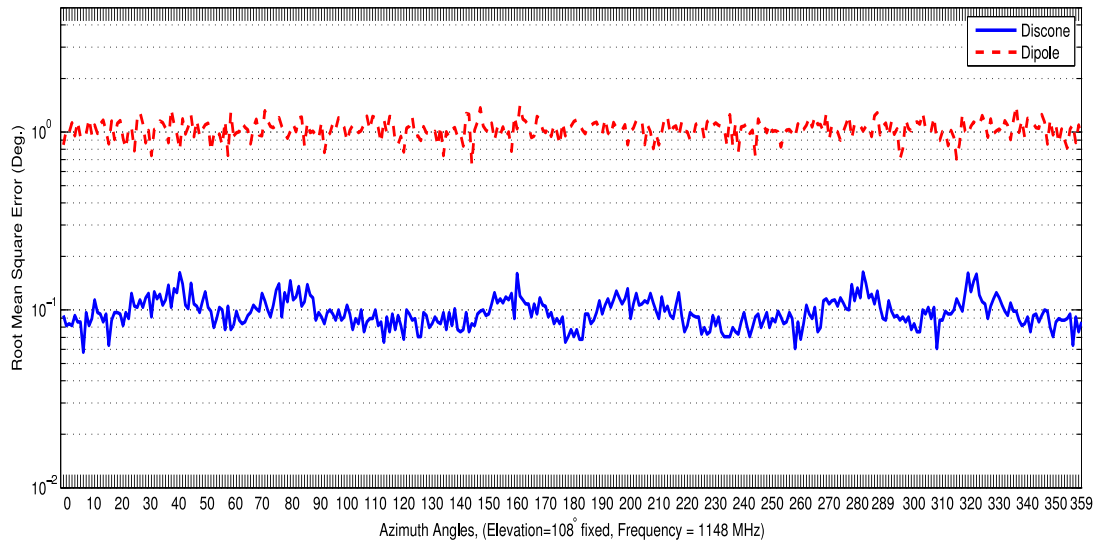


Figure 3.40: 1148 MHz, elevation angle is 108 degrees, comparison of DF performance of discone antennas (with 120 degree alignment and a 0.5 scaled discone on the center) and dipole antennas having four elements

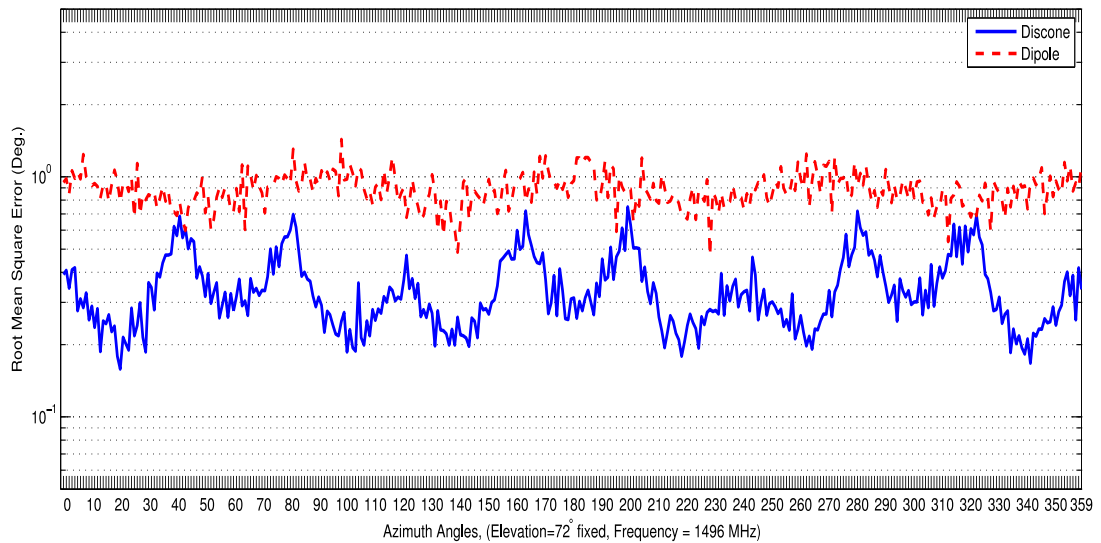


Figure 3.41: 1496 MHz, elevation angle is 72 degrees, comparison of DF performance of discone antennas (with 120 degree alignment and a 0.5 scaled discone on the center) and dipole antennas having four elements

for dipole antenna has peaks at 45, 135, 225 and 315 degrees which correspond to azimuth values between dipole antenna pairs. Dipole antennas are positioned at 0, 90, 180 and 270 degrees of azimuth. Large RMSEs occur when the plane wave is applied at the middle of two dipole antennas. 70 degrees RMSE occurs in these azimuth angles. This high error is due to

the spatial aliasing effect on dipole antenna. However, for discone antenna average RMSE is 0.3 degree and no peaks occur. Spatial aliasing effects are not observed for discone antennas.

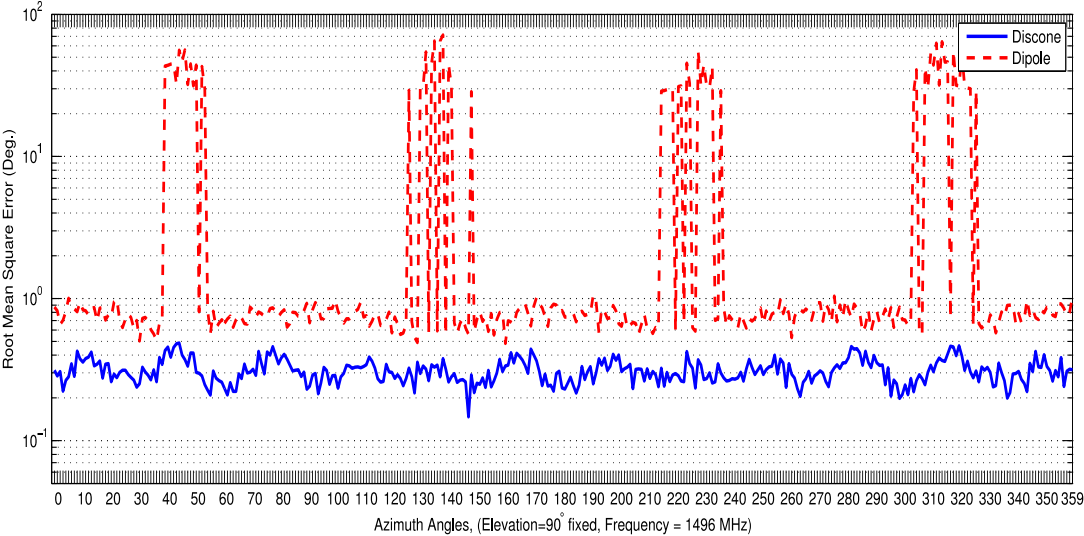


Figure 3.42: 1496 MHz, elevation angle is 90 degrees, comparison of DF performance of discone antennas (with 120 degree alignment and a 0.5 scaled discone on the center) and dipole antennas having four elements

In Figure 3.43, DF performance comparison between discone antennas and dipole antennas are done for frequency 1496 MHz at an elevation angle of 108 degrees. In this figure, DF performance of discone antenna is nearly six times better than the DF performance of dipole antenna. Average RMSE values are 0.15 degree and 0.9 degree for discone and dipole antennas, respectively. Average RMSE level is decreased 0.15 degree for discone antenna as compared to the level for elevation angle 90 degrees. This is the result of the discone antenna's nonsymmetrical structure and similar situation occurs for frequency 1148 MHz. In addition RMSE peaks of 70 degrees can not be observable for dipole antenna in elevation angle 108 degrees.

### 3.3 Discussions

In this chapter, wideband antenna models are created and tested for the DF performance. Among various discone antenna models, one having the lowest antenna interelement distance

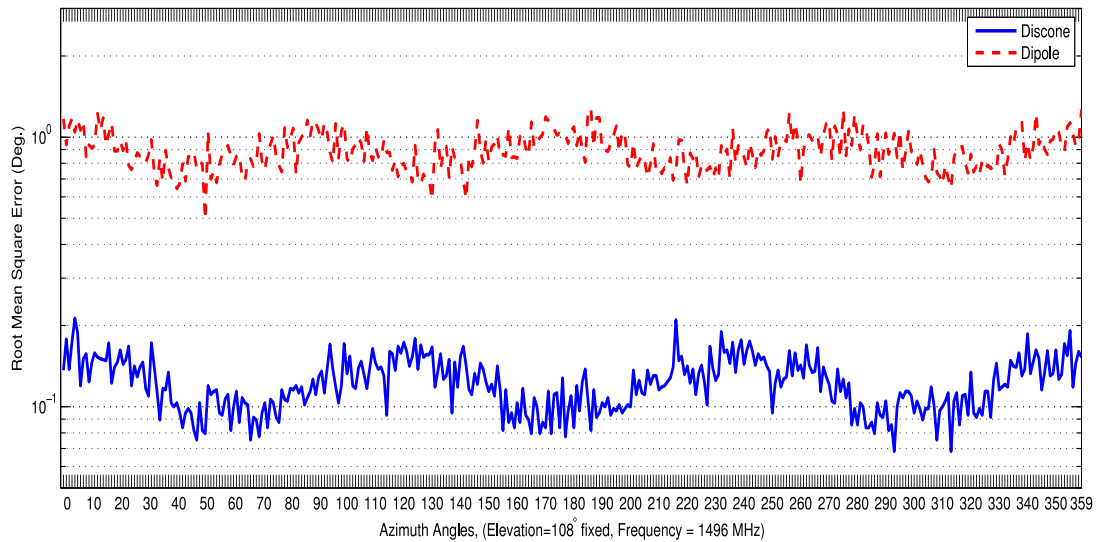


Figure 3.43: 1496 MHz, elevation angle is 108 degrees, comparison of DF performance of discone antennas (with 120 degree alignment and a 0.5 scaled discone on the center) and dipole antennas having four elements

and having small RMSE variance is selected. Wideband antenna is used to cover large frequency bands with a single antenna set that cannot be covered with a single set of narrowband antennas. 104-648 MHz and 648-1496 MHz frequency bands are covered by a single set of discone antennas and the same analyses are carried out by two different sets of dipole antennas. Two dipole antenna sets are different by their length and antenna interelement distance.

If we analyze the results of simulations, we can observe that discone antenna performs better in both frequency bands. However, the maximum frequency which we can use this discone antenna model is limited by the interelement distance of the discone antenna. Discone antennas have a cone base which limits the interelement distance to two times the base radius of the cone. Different antenna models are derived to overcome this limitation but RMSE curves for these models show high fluctuations at some specific azimuth angles.

Discone antenna's DF performance is much better than dipole antennas DF performance especially in band-2. Band-2 dipole antenna's interelement distance is lower than that of band-1 dipole antennas. Hence DF performance of band-1 antenna is better than DF performance of band-2 antenna in frequency 648 MHz where both models have DF simulations. When the dipole antennas get closer, DF performance worsens due to mutual coupling between antennas. However, antenna interelement distance is limited by half the wavelength of the

maximum frequency to prevent spatial aliasing. Spatial aliasing effects are observable for dipole antennas in the case of frequency 1496 MHz and elevation angle 90 degrees.

High variances in RMSE curve occur for disccone antenna due to the shape and interelement distance of the antennas. Interelement distance is limited by the base radius of the cone part in the disccone antenna. This is not the case for dipole antennas, antenna interelement distance is limited to radius of dipole which is much lower than disccone antenna's base radius.

Disccone antenna's RMSE curves show that in band-1, average RMSE is lower in elevation angle 90 degrees compared to average RMSE in elevation angle 108 degrees. However in band-2, the reverse is true. Indeed, as the frequency increases, RMSE level in elevation angle 108 degrees decreases compared to elevation angle 90 degrees results. This can be explained with the shape of the disccone antenna. The plane wave encounters higher radius part in elevation angle 108 degrees and interelement distance is lower from that perspective. Thus DF performance gets better as frequency increases.

## **CHAPTER 4**

### **DF SYSTEM ON UAV WITH DIPOLE ANTENNAS**

In this chapter, Direction Finding (DF) performances of dipole antenna arrays are evaluated on a platform. DF antennas are usually mounted on a mobile platform. The behavior and DF performance of DF antennas change significantly when they are mounted on a complex platform. The evaluation of DF antenna characteristics for such environments has critical value before the system implementation. This evaluation step eliminates several trial and error implementation processes by discarding certain unacceptable configurations.

In this chapter, DF performance of dipole antenna is tested on a UAV model. FEKO model of UAV is designed to have the general shape of the Heron UAV, which is a popular UAV. Heron model is designed in FEKO program using the fundamental geometrical objects in the program. Dimension information about Heron UAV is limited in the literature so approximate values are used in the design. These approximate values are calculated from the pictures of the Heron UAV which can be found in the internet. Antenna models are mounted in two different alignment. In the first model, four dipole antennas are placed under the belly of the UAV. In the second model, two groups of four dipole antennas are mounted at right and left arms carrying the rear wings of UAV. The details of the antenna placements can be found in section 4.1.

Direction finding performances of the dipole antennas are tested with a special set up. UAV is assumed to be calibrated in the ground and test data is assumed to be taken in the air. During the calibration process, UAV model rotated 180 degrees and elevated 10 meters from the ground to prevent multipath effects caused by ground reflections of plane waves. After 180 degrees of rotation, antennas lying under the main body of the UAV stay above the main body with respect to the coordinate axis for four antenna model. Calibration and test data are cor-

related and calculated azimuth angle value in the calibration azimuth table is obtained. Root Mean Square Error (RMSE) is obtained for every azimuth angle separately and RMSE versus azimuth angle plots are obtained. Since the calibration and test data are taken in different environments, only the effect of the ground medium is to be observed. Thus high SNR values are used in the simulations to prevent errors due to noise overshadow the platform effects. In the Heron simulation results section, RMSE versus azimuth angle plots can be seen for different antenna models and ground mediums.

In the following section, dipole antenna and UAV model are given in two subsections. In the first part, dipole antenna model with antenna dimensions are given. In the second part, four antenna and eight antenna model figures can be seen together with the UAV model. Simulation results also analyzed in two subsections following section 4.1. Four antenna and eight antenna simulation results are compared.

In Figure 4.1, circular array structure of the dipole antenna placements can be observed. This structure is used in both four and eight antenna models. However, in eight antenna model, circular array is rotated by 45 degrees as compared to four antenna model. The radius of the array is 25.5 centimeters. The antenna interelement distance is 35 centimeters. These parameters are selected to design an array to cover 20 MHz-500 MHz band. While 35 centimeters correspond to approximately 430 MHz maximum frequency for no spatial aliasing, the evaluations are done up to 500 MHz due to the fact that correlative interferometer and circular array are somewhat more resistant to spatial aliasing.

#### **4.1 Dipole Antenna and UAV Model**

In this section, dipole antenna model dimensions and UAV's FEKO model are given. Two different antenna alignments are used in UAV FEKO model. First model includes four dipole antennas mounted under the belly of the UAV. Second model has eight dipole antennas which are mounted at left and right sides in four dipole antenna groups. Dipole antenna dimensions used in these two different models are the same.

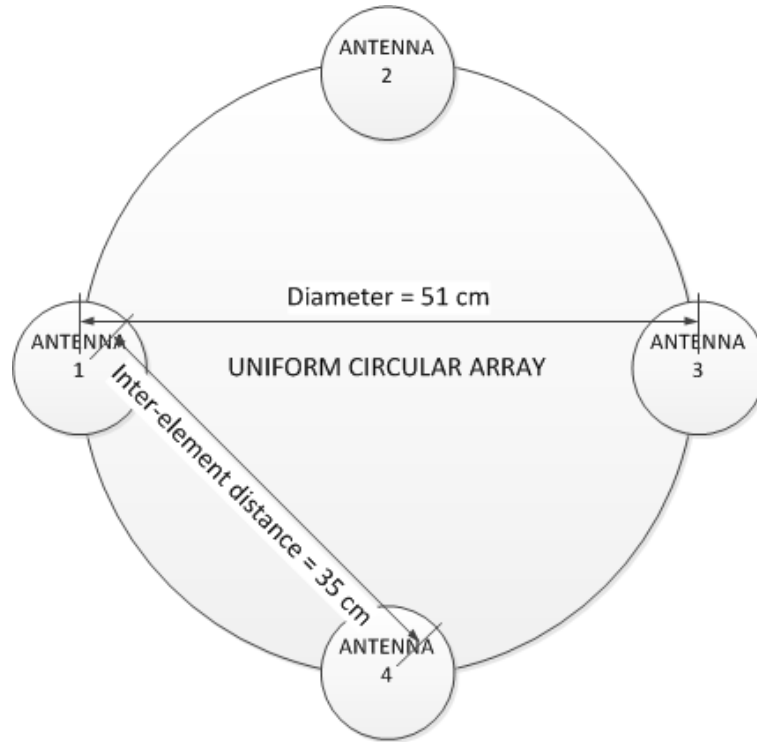


Figure 4.1: Circular array antenna pattern with antenna interelement distance 35cm

Table 4.1: Dipole antenna design parameters

Parameter Name	Value (cm)
Dipole Length	30
Dipole Radius	1.25
Dipole Gap	2.5

#### 4.1.1 Dipole Antenna Model

In Figure 4.2, dimensions of dipole antenna are given. In Table 4.1, values of the dipole antenna design parameters are given. Dipole antenna has a length of 30 centimeters which is designed to give the best DF performance for frequency 500 MHz. This is the maximum frequency in the simulations. The dipole length is half the wavelength value for frequency 500 MHz. Dipole antenna has a radius of 1.25 centimeters. There is a gap of 2.5 centimeters between the poles of the antenna. In the FEKO model, there is a wire line constructing a port within the gap touching the two poles of the dipole and currents are measured from these ports.

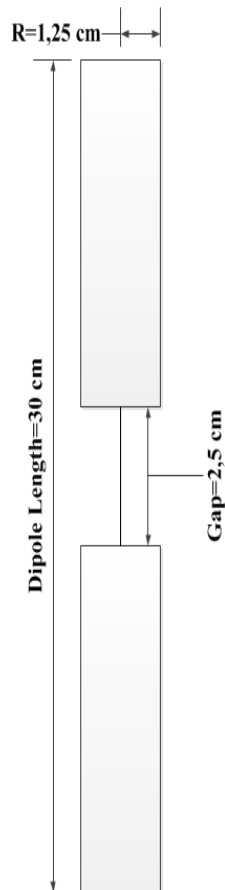


Figure 4.2: Dipole antenna dimensions

#### 4.1.2 UAV Feko Model with Four Antenna

In this section, CADFEKO models of UAV and antennas are given for four antenna case.

In Figure 4.3, Heron cadfeko model with four antennas can be observed. Antennas are placed under the belly of the UAV. In this figure the full coverage of the model is given.

In Figure 4.4, antennas can be observed more clearly. In this model, four dipole antennas are placed as shown in Figure 4.1. Two of the dipoles are on the x axis, nose of the UAV is pointing the positive x direction. The other two dipoles are orthogonal to other two dipoles, placed on the y axis. Left part of the wing is pointing the y axis.

In Figure 4.5 we can see the back of the model. The propeller and the back wings can be observed more clearly.

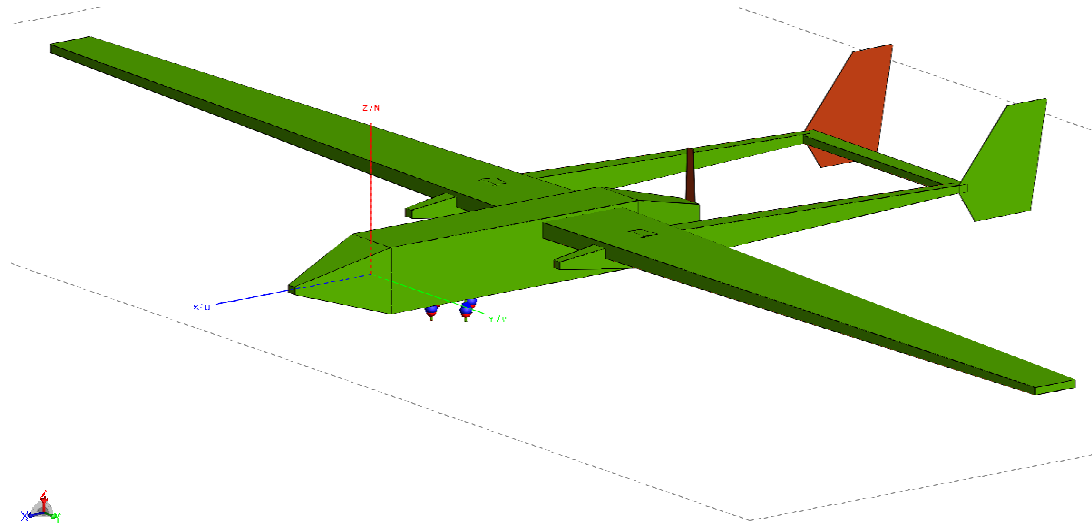


Figure 4.3: Heron feko model isometric view, with four antennas under main body with antenna interelement distance of 35cm.

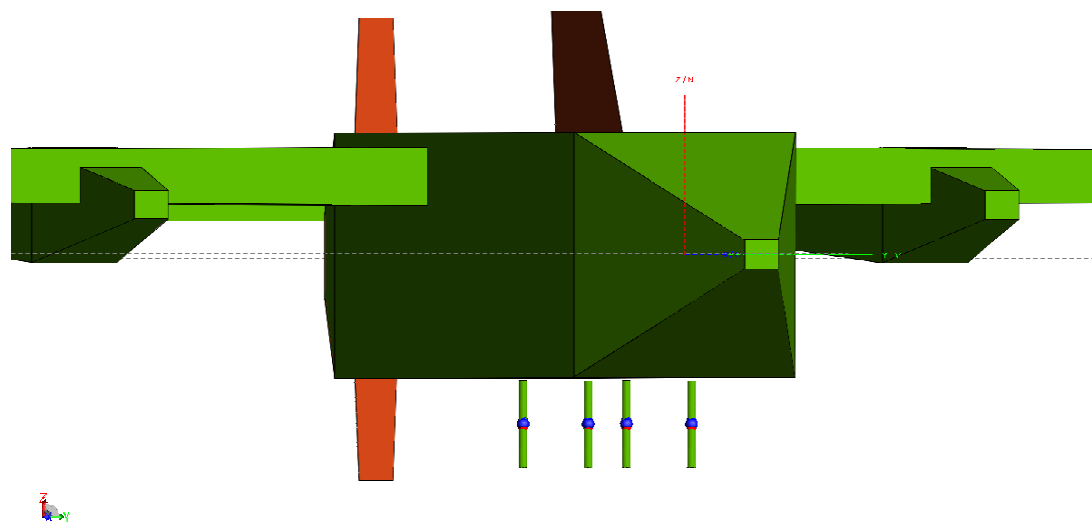


Figure 4.4: Heron feko model front view, with four antennas under main body with antenna interelement distance of 35cm.

In Figure 4.6, the UAV and dipole antennas are rotated 180 degrees and positioned 10 meter above the infinite ground medium to collect the calibration data. This medium is defined as frequency independent medium with relative permittivity  $\epsilon_r=15$  and conductivity  $\sigma=0.04$  Siemens per meter.

In Figure 4.7 the infinite ground medium is selected as perfect electric conductor. In this

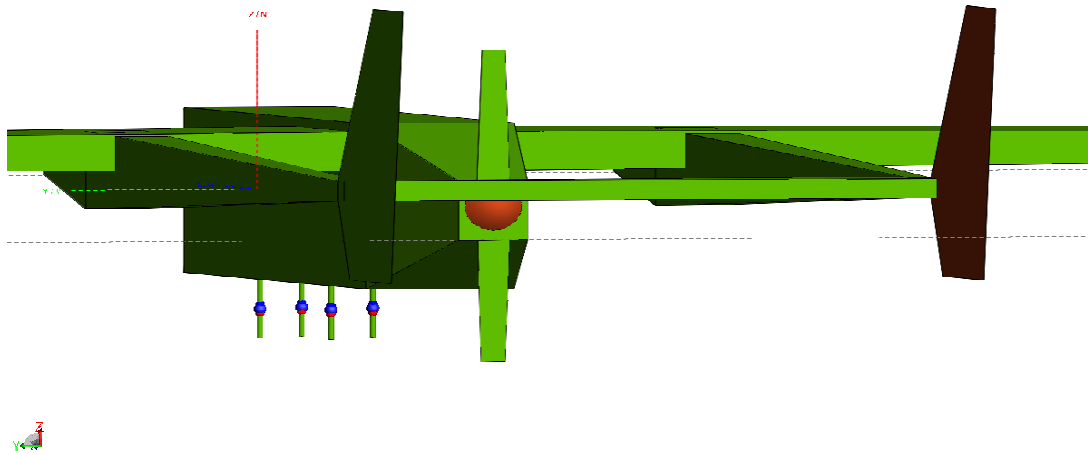


Figure 4.5: Heron feko model back view, with four antennas under main body with antenna interelement distance of 35cm.

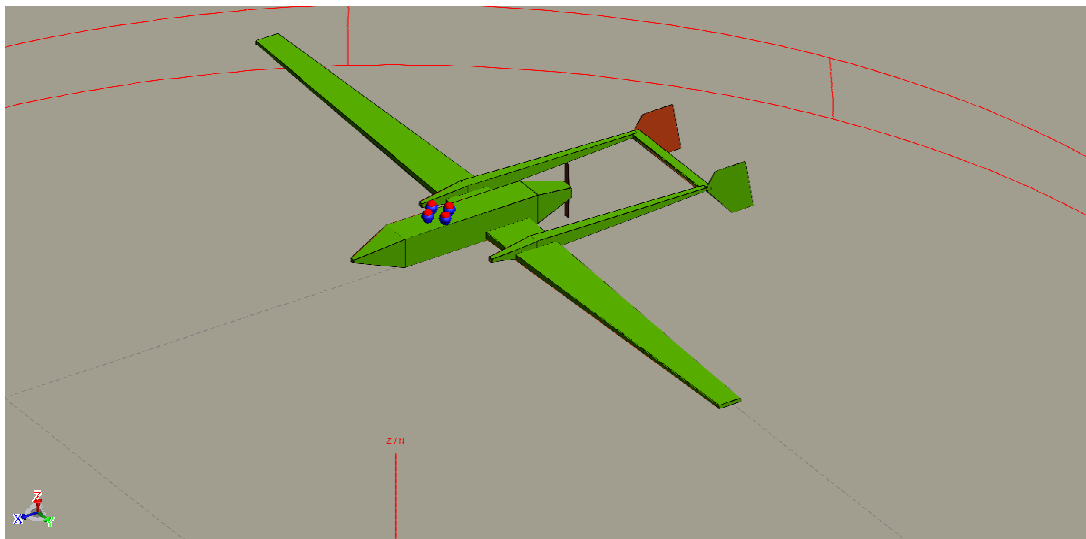


Figure 4.6: Heron feko model including infinite dielectric ground medium , with dielectric medium properties, relative permittivity  $\epsilon_r=15$  and conductivity  $\sigma=0.04$ , four antenna under main body with antenna interelement distance of 35cm.

ground medium, ground reflection effects are clearly observable and used in the simulations to compare the DF performance with the case where the dielectric medium is used as the ground medium.

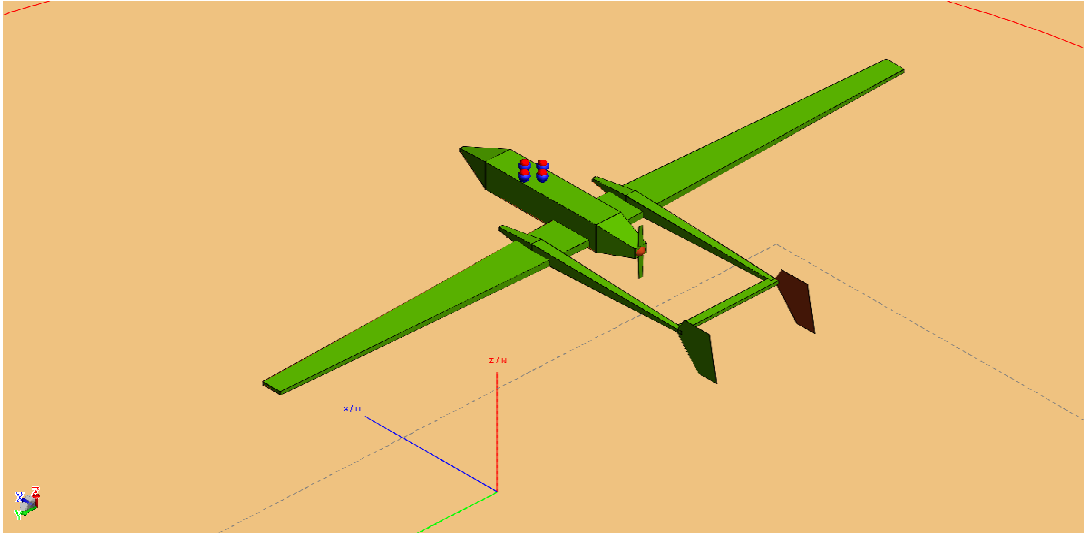


Figure 4.7: Heron feko model including infinite perfect electric conductor ground medium, with four antenna under main body with antenna interelement distance of 35cm.

#### 4.1.3 UAV Feko Model with Eight Antenna

In this section, CADFEKO models of UAV and antennas are given for eight antenna case. In certain cases, the belly of the UAV can not be used since it is reserved for other instruments and devices. Alternative places for antenna placement are usually limited. In this thesis, an alternative place is selected. This is the end of right and left arms carrying the rear wings of UAV. Note that eight antennas are used to cover 360 degrees azimuth almost isotropic.

In Figure 4.8, Heron cadfeko model with eight antennas can be observed. In this model the number of antennas and the positions of the antennas are changed. The antennas are close to the rear wings and are separated as right and left four antenna pairs.

In Figure 4.9, eight dipole antennas can be seen in detail. Dipole antennas are placed such that reflections from rear wings or propeller are minimized.

In Figure 4.10 back view of the model can be observed. In this model, antenna arms can be seen. Antenna arms are placed in order to keep the interelement distance of the dipole antennas constant in addition to carrying the antennas.

In Figure 4.11, the infinite ground medium is selected as dielectric medium. This medium is defined as frequency independent medium with relative permittivity  $\epsilon_r=15$  and conductivity

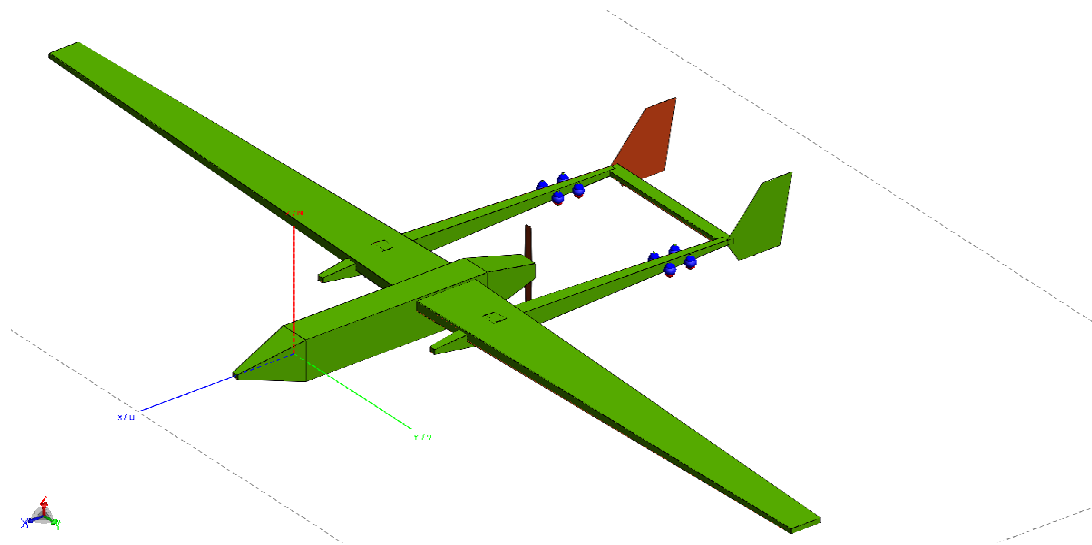


Figure 4.8: Heron feko model isometric view, with eight antennas on rear wing arms with antenna interelement distance of 35cm.

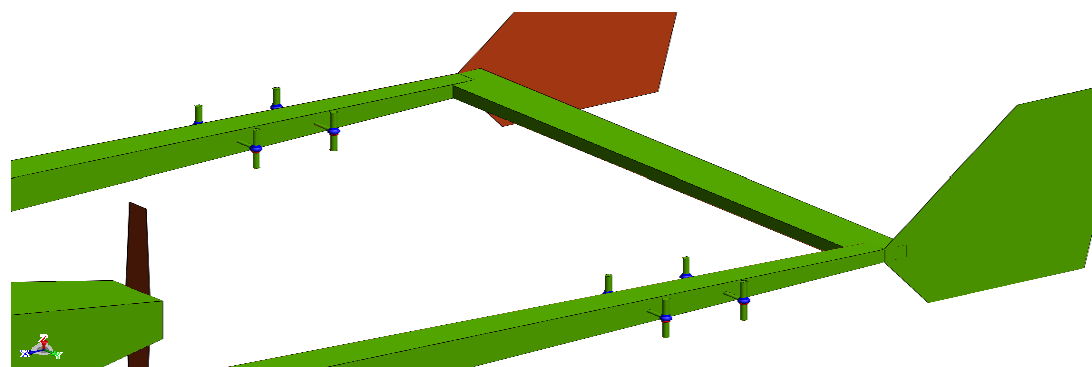


Figure 4.9: Heron feko model detailed antenna view, with eight antennas on rear wing arms with antenna interelement distance of 35cm.

$\sigma=0.04$  Siemens per meter. UAV model is rotated 180 degrees and elevated 10 meters from ground. Antenna positions are unchanged but after rotation, antennas on +y axis relocated on -y axis and vice versa.

In Figure 4.12, the infinite ground medium is selected as perfect electric conductor. The model is 10 meters elevated from the ground. This model is used in two different DF performance comparisons. First comparison is between PEC ground medium with the dielectric ground medium. Second comparison is performed between two differently elevated UAV models. Ten meters and four meters ground elevation values are used for comparison.

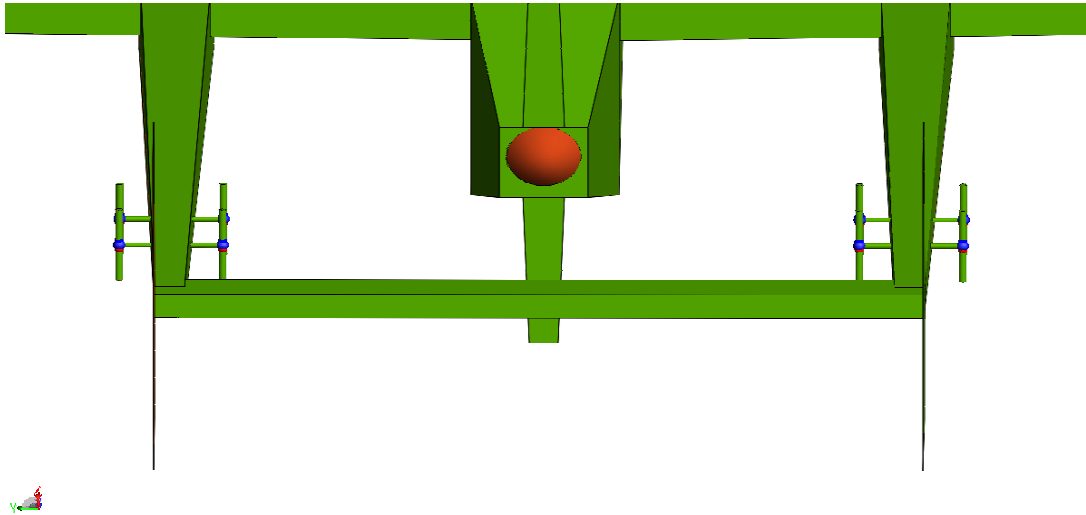


Figure 4.10: Heron feko model back view, with eight antennas on rear wing arms with antenna interelement distance of 35cm.

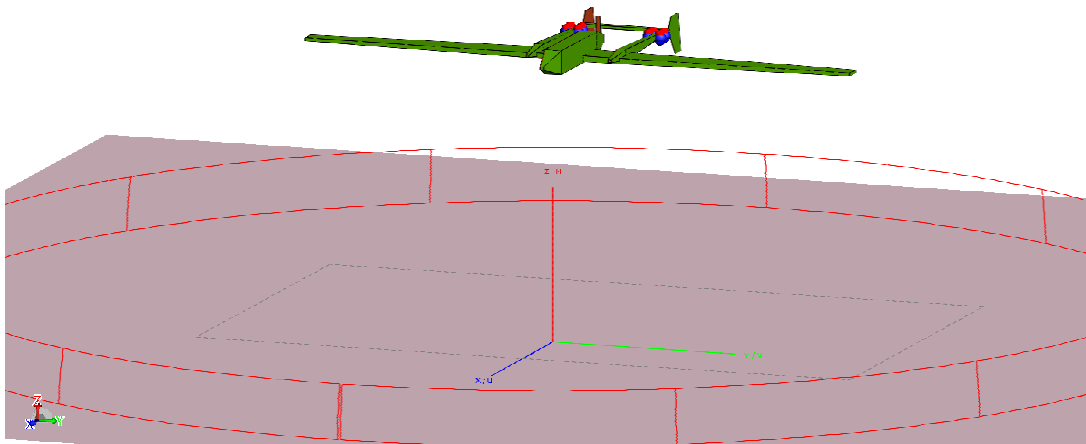


Figure 4.11: Heron feko model including infinite dielectric ground medium , with dielectric medium properties, relative permittivity  $\epsilon_r=15$  and conductivity  $\sigma=0.04$ , eight antenna on rear wing arms with antenna interelement distance of 35cm.

In Figure 4.13, the infinite ground medium is selected as perfect electric conductor(PEC). The model is four meters elevated from the ground. DF performance comparison is performed between four meters and ten meters elevated UAV models above PEC ground medium. The main reason for this DF comparison is to observe the effects of platform elevation on the ground reflections. When RMSE levels increase, it is concluded that ground reflections increase too.

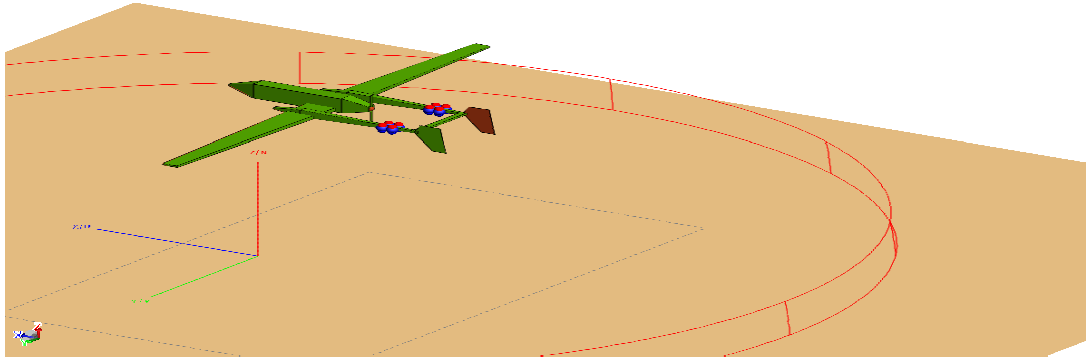


Figure 4.12: Heron feko model including infinite perfect electric conductor ground medium, model has 10 meters elevation from ground medium, with eight antennas on rear wing arms with antenna interelement distance of 35cm.

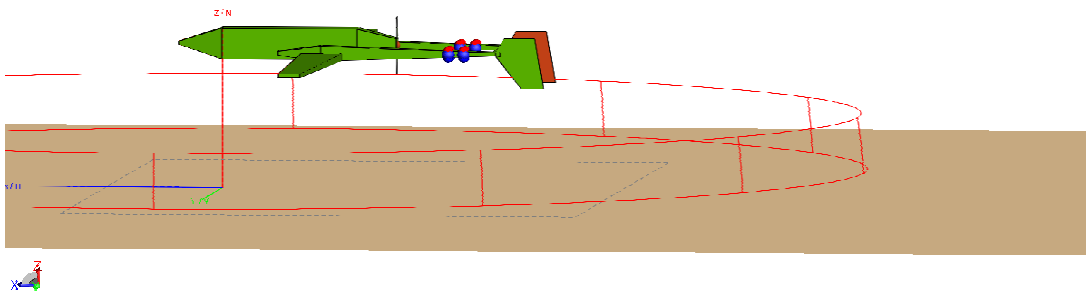


Figure 4.13: Heron feko model including infinite perfect electric conductor ground medium, model has four meters elevation from ground medium, with eight antennas on rear wing arms with antenna interelement distance of 35cm.

## 4.2 Simulation Results for the UAV

In this section, simulation results of the Heron model are given. There are general parameters for the simulations of this part. SNR (Signal to Noise Ratio) is set to be 150dB, 500 snapshots are taken. A single trial is done since we have approximately noise free case. Interpolation

is not performed in these simulations because azimuth data used is dense enough. Azimuth scan is done over 360 degrees with 0.25 degree interval.

Comparison of several different parameters results in various analysis. The effect of ground medium type in DF performance is analyzed by using PEC and dielectric ground mediums. Two different antenna alignments are used, namely, four and eight antenna models. The effect of number of antennas and antenna placement is analyzed with these antenna models. For PEC medium and for 500 MHz, effects of ground elevation level are discussed by putting the UAV platform to 4 and 10 meters from ground. Finally elevation angle effects are mentioned for elevation angles 92 degrees and 98 degrees.

Two models are analyzed in the following subsections. In the first subsection, four antenna model's azimuth scan simulation results are given. In the second subsection eight antenna model's azimuth scan simulation results can be found.

In the first step, 20-100 MHz frequency band is simulated with the mesh sizes determined according to 100 MHz's wavelength. Actually, mesh sizes are taken as 10 percent of the wavelength for the maximum frequency in the band. CADFEKO simulations are done in the specific frequencies given as 20, 60 and 100 MHz. In the second step, individual frequency values are selected and simulated in CADFEKO with mesh sizes determined by the selected frequencies wavelength's 12.5 percent. In this step, frequencies of 250, 375 and 500 MHz are used. Two different elevation angles, namely, 92 degrees and 98 degrees are used, respectively, for obtaining the test data which correspond to 2 degrees and 8 degrees below the x-y plane. During calibrations, UAV is 180 degrees rotated and to match the direction of the elevation angles with the test data, 88 and 82 degrees of elevation angles are used, respectively. The main reason for these elevation values is that test data is collected when the UAV is flying without any rotation. Plane wave excitation is used with vertical linear polarization. Azimuth angles are swept with 0.25 degree of azimuth step over 360 degrees.

#### **4.2.1 Four Antenna Model Simulation Results**

In this section, four antenna model RMSE vs azimuth angle simulation results for the frequency band 20-500 MHz are given.

In Figure 4.14, azimuth scan simulation results for frequency 20 MHz and elevation angle

92 degrees are given. In this figure, dielectric ground medium's DF performance is generally worse than that of perfect electric conductor (PEC) medium in all 360 degrees range. On the average, PEC medium's DF performance is three times better. Around 0 degree and 180 degrees, DF performance of dielectric medium is improved.

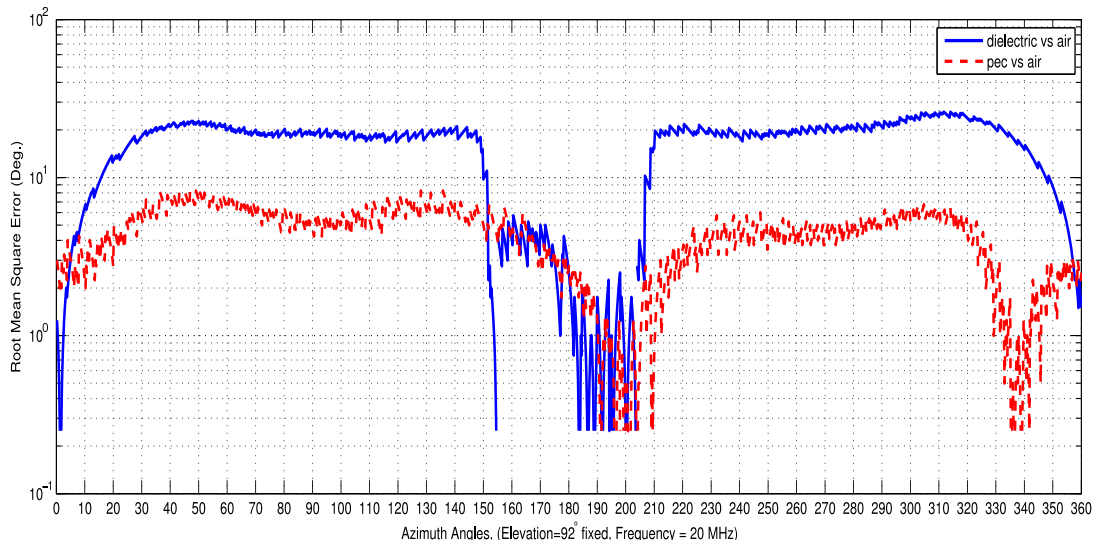


Figure 4.14: 20 MHz, Perfect Electric Conductor versus Dielectric medium, with relative permittivity  $\epsilon_r=15$  and conductivity  $\sigma=0.04$ , elevation angle is 92 degree.

In Figure 4.15 , azimuth scan simulation results for frequency 20 MHz and elevation angle 98 degrees are given. In this figure, dielectric medium's DF performance is generally two times better than DF performance of PEC medium. If we compare the results of this figure with the results for elevation angle 92 degrees, we observe that when elevation angle is increased, reflections from the ground are increased too. Since the average RMSE level for elevation angle 98 degrees is higher than the average RMSE level for the elevation angle 92 degrees, we can say that increasing the elevation angle worsens the DF performance. DF performance in this chapter is measured by comparison of calibration and test data, which simulates ground calibration and test measurement during flight. Thus the effect of ground medium is analyzed. Increasing the elevation angle changes the magnitude and phase of the current read from antennas which results in increased RMSE. As a result, we can say that for frequency 20 MHz, increasing the elevation angle causes higher reflections from ground especially for perfect electric conductor ground medium. If perfect electric conductor is selected as the ground medium, reflections from ground are much more than the reflections for the same elevation

angle in dielectric medium.

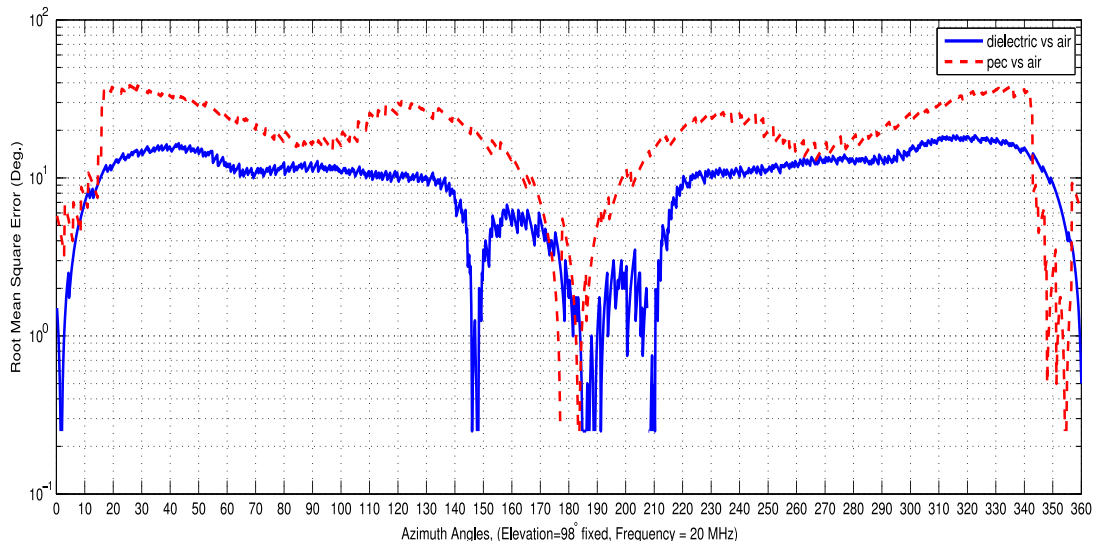


Figure 4.15: 20 MHz, Perfect Electric Conductor versus Dielectric medium, with relative permittivity  $\epsilon_r=15$  and conductivity  $\sigma=0.04$ , elevation angle is 98 degree.

In Figure 4.16, azimuth scan simulation results for frequency 60 MHz and elevation angle 92 degrees are given. In this figure, PEC medium's DF performance is better than dielectric medium's DF performance. Compared to the results for frequency 20 MHz and elevation angle 92 degrees, dielectric medium's DF performance is improved.

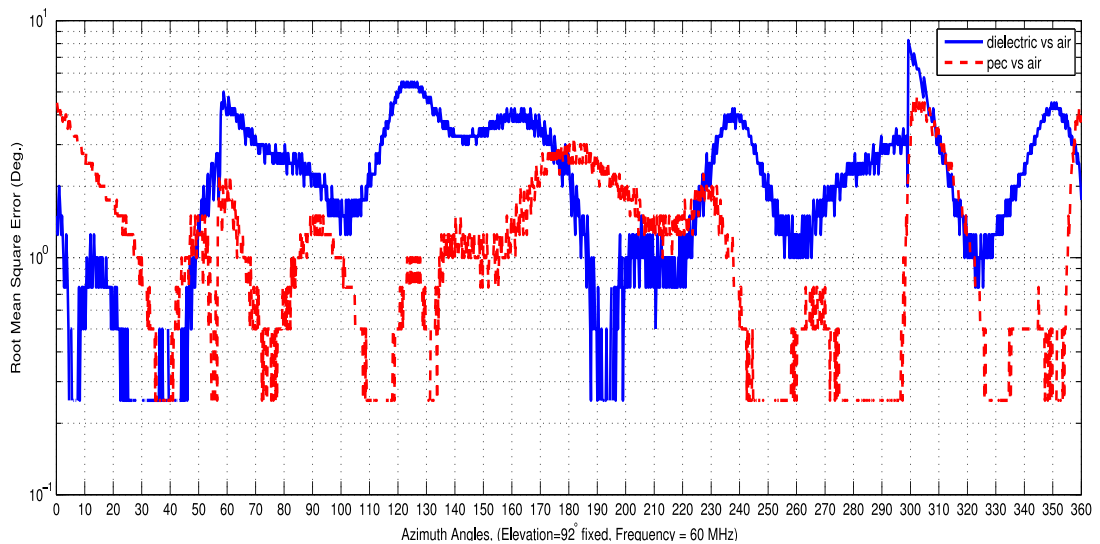


Figure 4.16: 60 MHz, Perfect Electric Conductor versus Dielectric medium, with relative permittivity  $\epsilon_r=15$  and conductivity  $\sigma=0.04$ , elevation angle is 92 degree.

In Figure 4.17, azimuth scan simulation results for frequency 60 MHz and elevation angle 98 degrees are given. In this figure, dielectric medium's DF performance is 10 times better than DF performance of PEC medium.

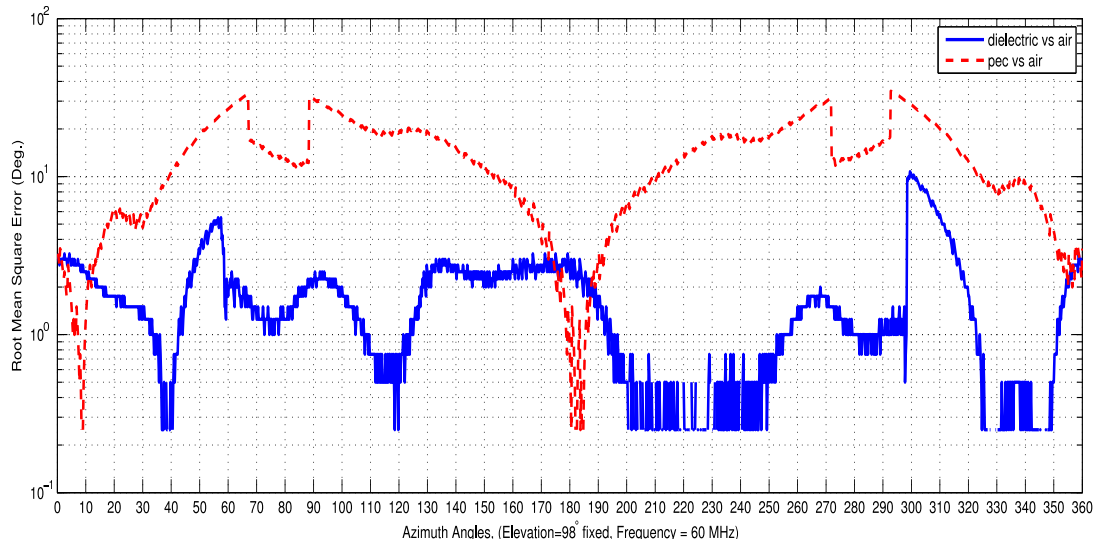


Figure 4.17: 60 MHz, Perfect Electric Conductor versus Dielectric medium, with relative permittivity  $\epsilon_r=15$  and conductivity  $\sigma=0.04$ , elevation angle is 98 degree.

In Figure 4.18, azimuth scan simulation results for frequency 100 MHz and elevation angle 92 degrees are given. In this figure, average RMSEs for dielectric medium and PEC medium are similar. For the frequency band 20 MHz-100 MHz, as frequency increases, dielectric medium's DF performance improves.

In Figure 4.19, azimuth scan simulation results for frequency 100 MHz and elevation angle 98 degrees are given. In this figure, DF performances of dielectric medium and PEC medium are similar. If we compare the results for frequencies 100 MHz and 60 MHz, DF performance of PEC medium is improved.

In Figure 4.20, azimuth scan simulation results for frequency 250 MHz and elevation angle 92 degrees are given. In this figure, average RMSE of PEC medium is two times higher than average RMSE of dielectric medium. Especially around 0 degree azimuth angle, which corresponds to the nose of the UAV; dielectric medium's DF performance is much better.

In Figure 4.21, azimuth scan simulation results for frequency 250 MHz and elevation angle 98 degrees are given. In this figure, PEC medium gives approximately 100 degrees of RMSE

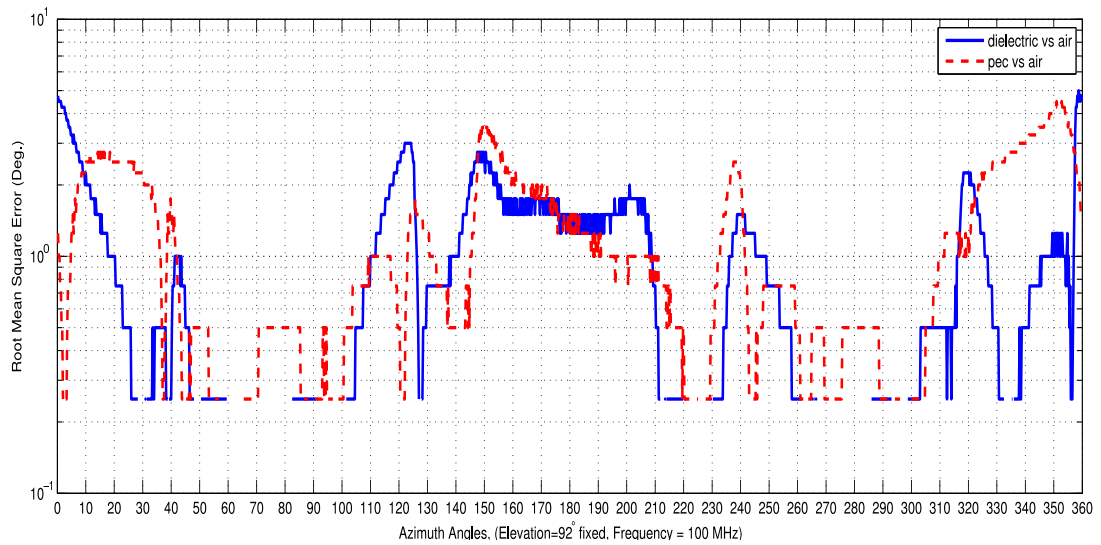


Figure 4.18: 100 MHz, Perfect Electric Conductor versus Dielectric medium, with relative permittivity  $\epsilon_r=15$  and conductivity  $\sigma=0.04$ , elevation angle is 92 degree.

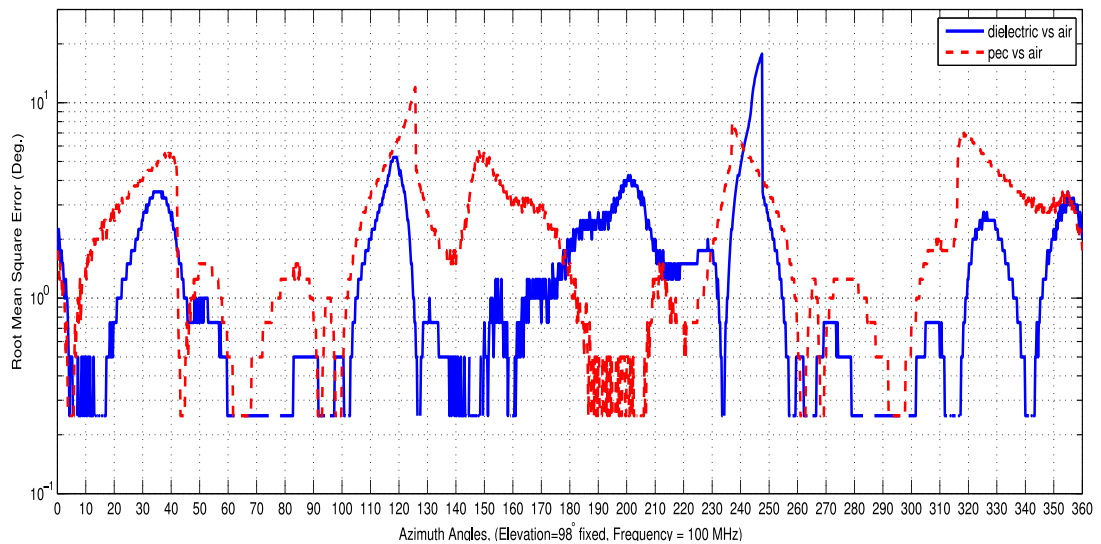


Figure 4.19: 100 MHz, Perfect Electric Conductor versus Dielectric medium, with relative permittivity  $\epsilon_r=15$  and conductivity  $\sigma=0.04$ , elevation angle is 98 degree.

in some azimuth angle regions, where dielectric medium's RMSE is around 1 degree. Thus dielectric medium's DF performance is much better than PEC medium's DF performance. High errors for PEC medium can be explained by the ground reflections. In PEC ground medium, ground reflections are more effective in elevation angle 98 degrees. In dielectric medium, fewer reflections occur so RMSE is lower.

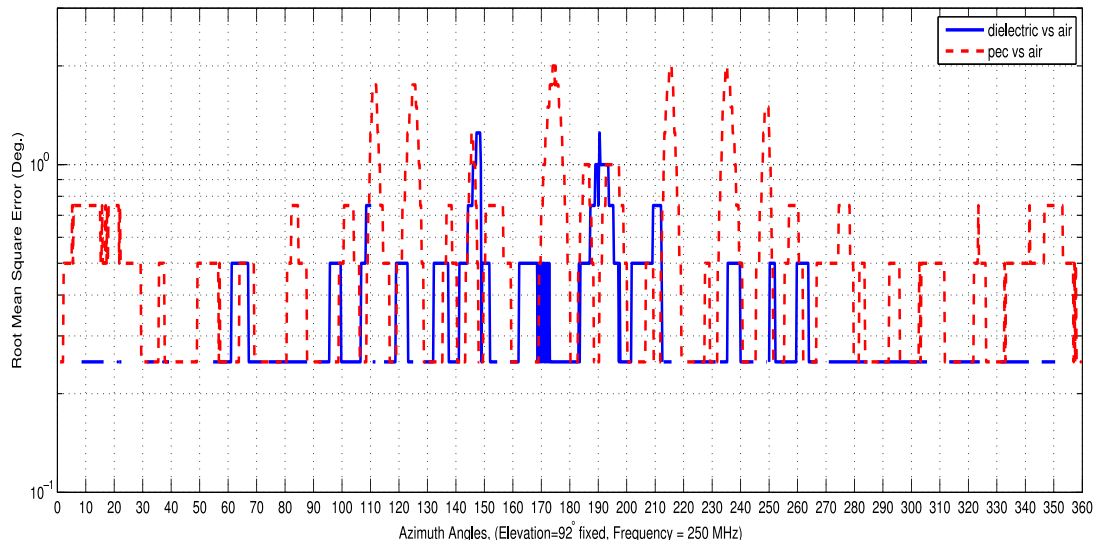


Figure 4.20: 250 MHz, Perfect Electric Conductor versus Dielectric medium, with relative permittivity  $\epsilon_r=15$  and conductivity  $\sigma=0.04$ , elevation angle is 92 degree.

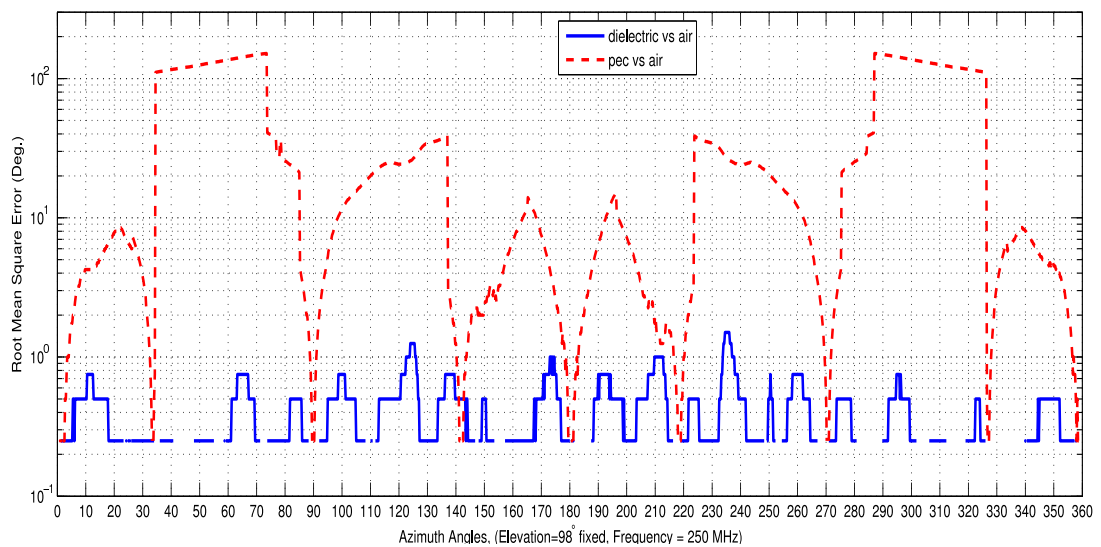


Figure 4.21: 250 MHz, Perfect Electric Conductor versus Dielectric medium, with relative permittivity  $\epsilon_r=15$  and conductivity  $\sigma=0.04$ , elevation angle is 98 degree.

In Figure 4.22, azimuth scan simulation results for frequency 375 MHz and elevation angle 92 degrees are given. In this figure, PEC medium's DF performance is better than dielectric medium's DF performance. Average RMSE for dielectric ground medium is around one degree. However average RMSE for PEC medium is 0.5 degree.

In Figure 4.23, azimuth scan simulation results for frequency 375 MHz and elevation angle

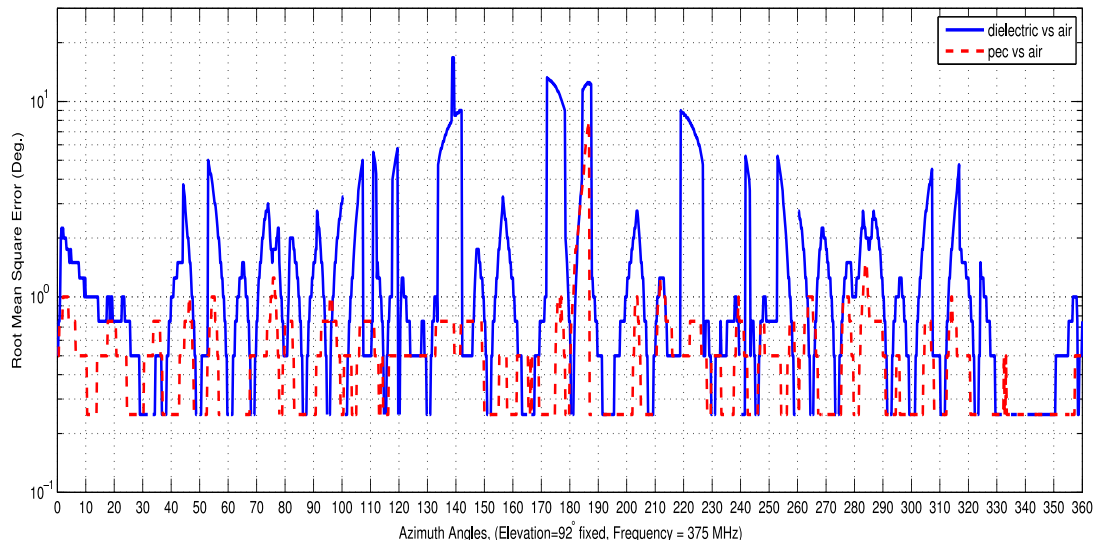


Figure 4.22: 375 MHz, Perfect Electric Conductor versus Dielectric medium, with relative permittivity  $\epsilon_r=15$  and conductivity  $\sigma=0.04$ , elevation angle is 92 degree.

98 degrees are given. In this figure, average RMSE for dielectric ground medium is around 0.5 degree. However average RMSE for PEC ground medium is around one degree. DF performance of dielectric ground medium is approximately two times better.

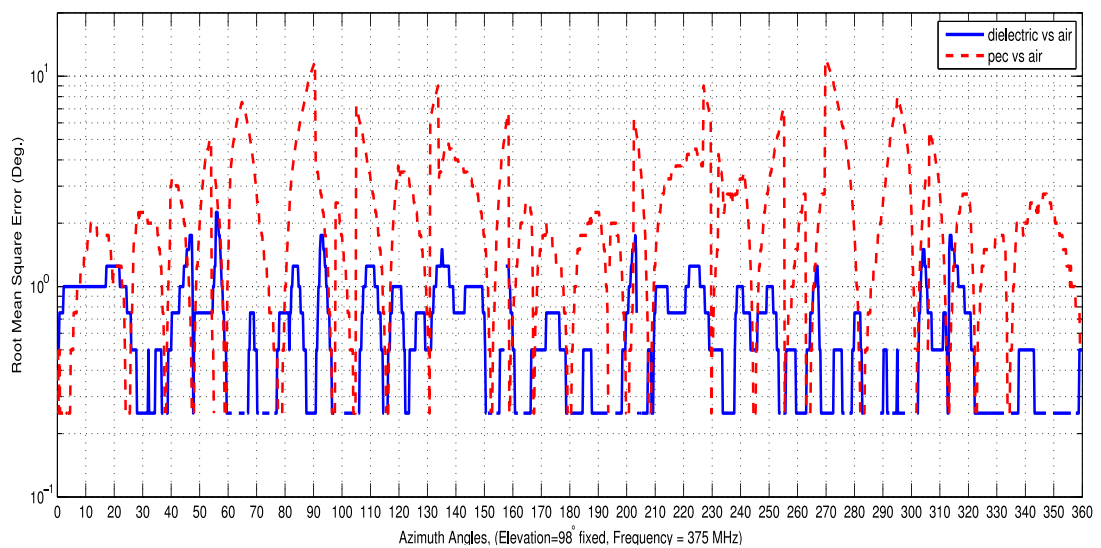


Figure 4.23: 375 MHz, Perfect Electric Conductor versus Dielectric medium, with relative permittivity  $\epsilon_r=15$  and conductivity  $\sigma=0.04$ , elevation angle is 98 degree.

In Figure 4.24, azimuth scan simulation results for frequency 500 MHz and elevation angle 92 degrees are given. In this figure, DF performances of dielectric medium and PEC medium

are similar.

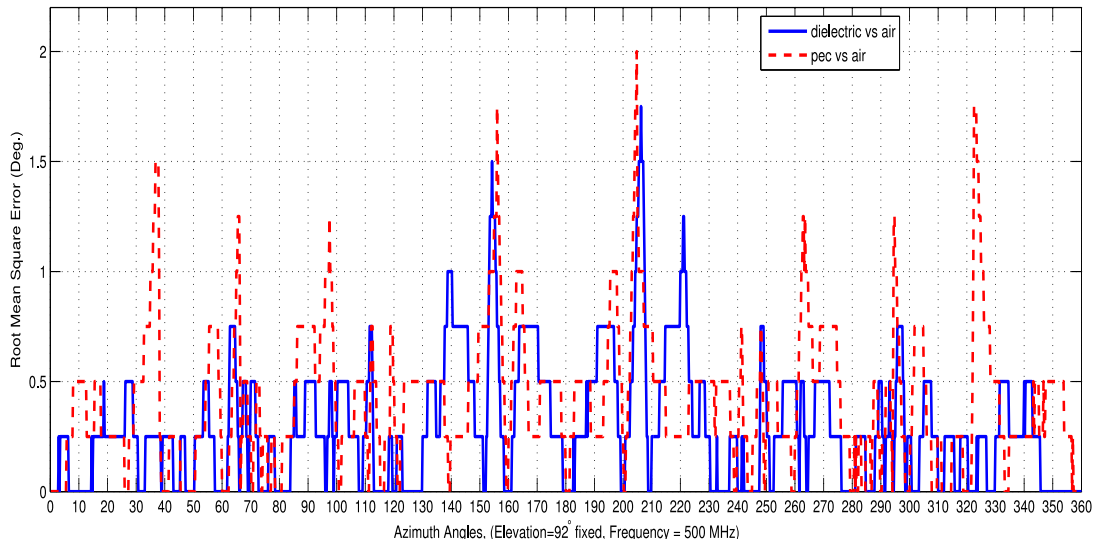


Figure 4.24: 500 MHz, Perfect Electric Conductor versus Dielectric medium, with relative permittivity  $\epsilon_r=15$  and conductivity  $\sigma=0.04$ , elevation angle is 92 degree.

In Figure 4.25, azimuth scan simulation results for frequency 500 MHz and elevation angle 98 degrees are given. In this figure, dielectric medium's DF performance is much better especially around 180 degrees of azimuth angle, which corresponds to the back of the UAV.

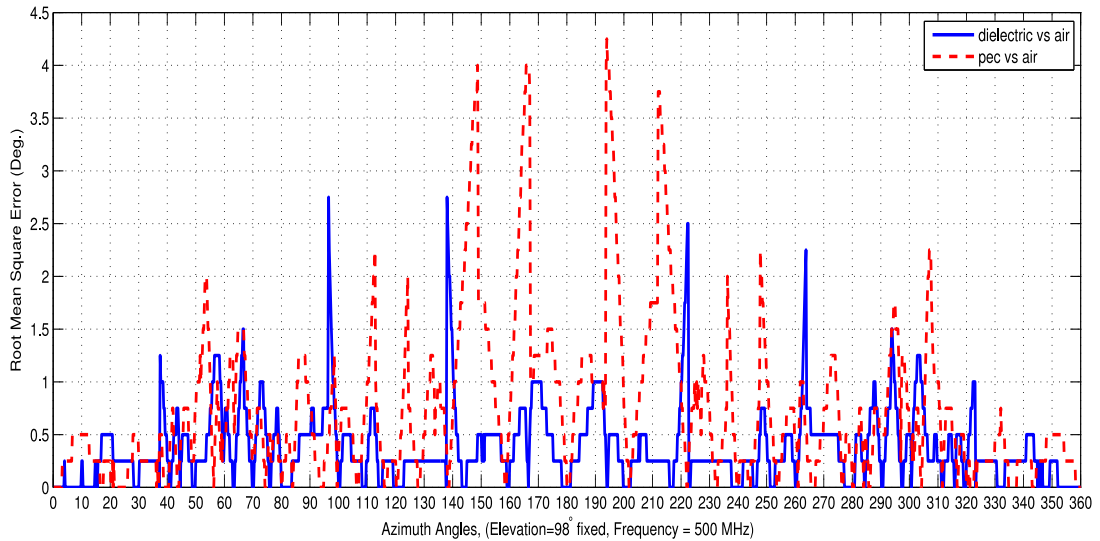


Figure 4.25: 500 MHz, Perfect Electric Conductor versus Dielectric medium, with relative permittivity  $\epsilon_r=15$  and conductivity  $\sigma=0.04$ , elevation angle is 98 degree.

## 4.2.2 Eight Antenna Model Simulation Results

In this section, eight antenna model RMSE vs. azimuth angle simulation results for frequency band 20-500 MHz are given.

In Figure 4.26, azimuth scan simulation results for frequency 20 MHz and elevation angle 92 degrees are given. If we analyze this figure, PEC medium's DF performance is still better than dielectric medium's DF performance. For eight antenna model, azimuth scan characteristic is changed as compared to four antenna model. In eight antenna model, RMSE's are lower and concentrated around 90 and 270 degrees of azimuth, which correspond to left and right wings, respectively. On the other hand, in four antenna model, RMSE is usually constant and has an average value of 10 degrees. This value is much higher than eight antenna model's RMSE, which has an average value of approximately 1-2 degrees. RMSE for eight antenna model decreases sharply around 0 and 180 degrees of azimuth, which correspond to the nose and back of the UAV, respectively.

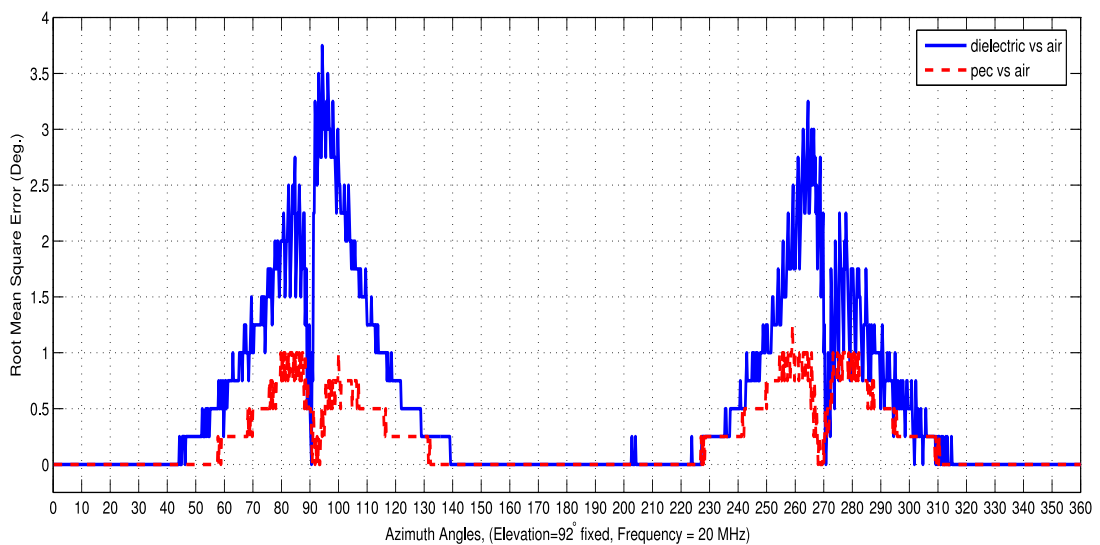


Figure 4.26: 20 MHz, Perfect Electric Conductor versus Dielectric medium, with relative permittivity  $\epsilon_r=15$  and conductivity  $\sigma=0.04$ , elevation angle is 92 degree.

In Figure 4.27, azimuth scan simulation results for frequency 20 MHz and elevation angle 98 degrees are given. In this figure DF performance of dielectric medium is better than DF performance of PEC medium. For this frequency and elevation angle settings, eight antenna model's average RMSE is still much lower than four antenna model's average RMSE.

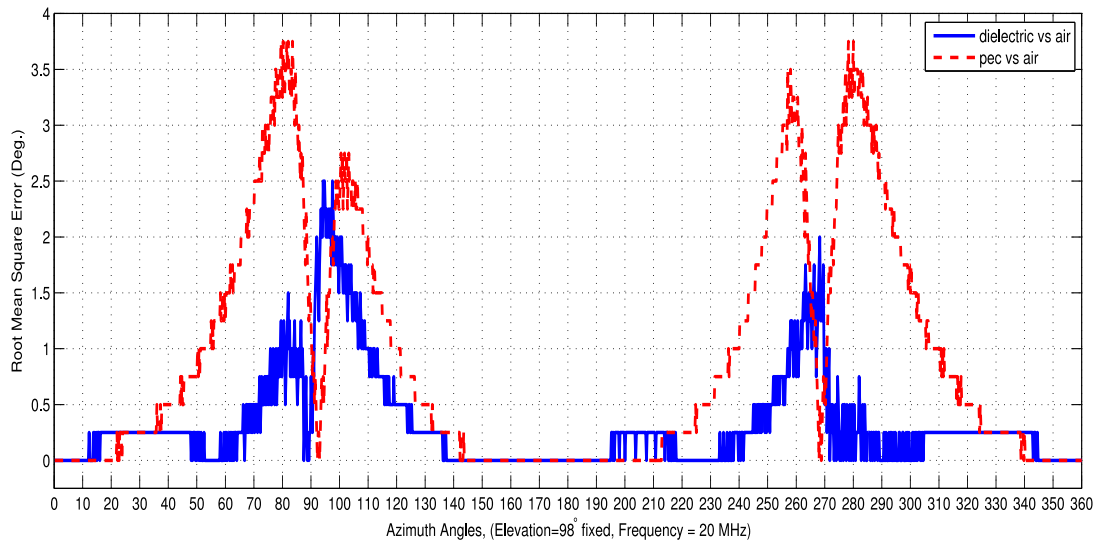


Figure 4.27: 20 MHz, Perfect Electric Conductor versus Dielectric medium, with relative permittivity  $\epsilon_r=15$  and conductivity  $\sigma=0.04$ , elevation angle is 98 degree.

In Figure 4.28, azimuth scan simulation results for frequency 60 MHz and elevation angle 92 degrees are given. In this figure, DF performances of dielectric and PEC mediums are similar. Dielectric medium's RMSE is slightly higher at some azimuth angle sections. Similar to 20 MHz case, average RMSE of eight antenna model is still much lower than average RMSE of four antenna model.

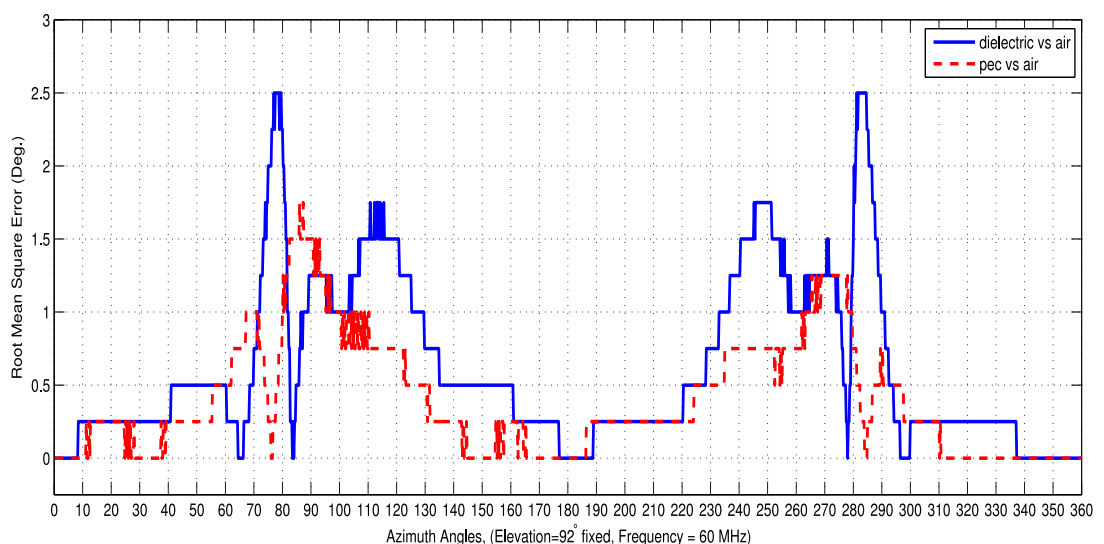


Figure 4.28: 60 MHz, Perfect Electric Conductor versus Dielectric medium, with relative permittivity  $\epsilon_r=15$  and conductivity  $\sigma=0.04$ , elevation angle is 92 degree.

In Figure 4.29, azimuth scan simulation results for frequency 60 MHz and elevation angle 98 degrees are given. In this figure, average RMSE of PEC medium is much higher (approximately 6-8 times) than dielectric medium's average RMSE. Eight antenna model's DF characteristic for PEC medium is similar to four antenna model's PEC medium's DF characteristic for 60 MHz and elevation angle 98 degrees. For 60 MHz, wavelength is 5 meters. UAV models are elevated by 10 meters from ground. This corresponds to two times wavelength for this frequency. Thus ground reflections for PEC medium are affected from the ground elevation level and high errors occur in four antenna and eight antenna models.

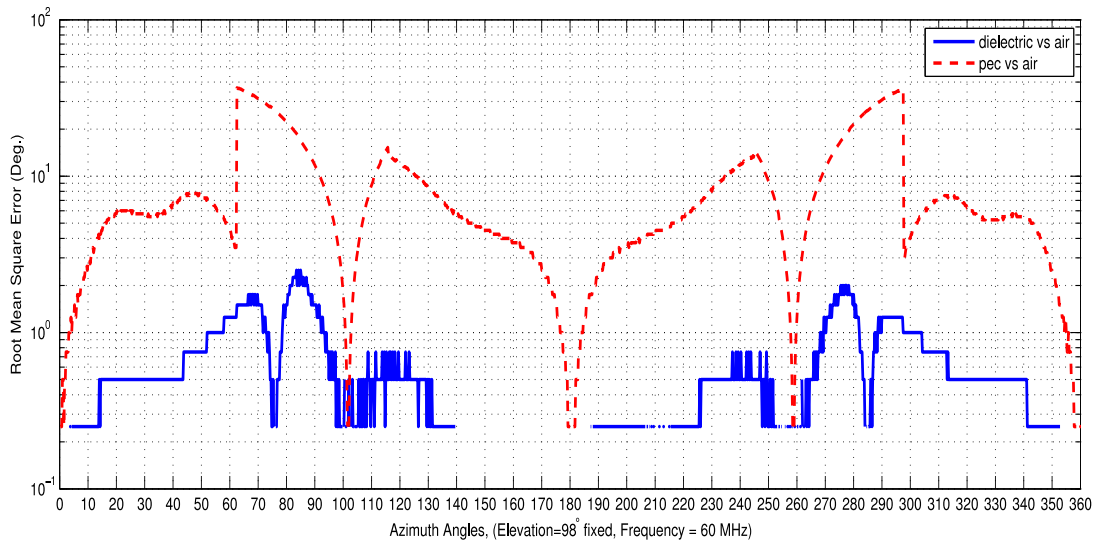


Figure 4.29: 60 MHz, Perfect Electric Conductor versus Dielectric medium, with relative permittivity  $\epsilon_r=15$  and conductivity  $\sigma=0.04$ , elevation angle is 98 degree.

In Figure 4.30, azimuth scan simulation results for frequency 100 MHz and elevation angle 92 degrees are given. In this figure, DF performances of dielectric medium and PEC medium are very similar and average RMSE is lower than 0.5 degree for both mediums. In four antenna model, average RMSE is approximately 4-6 times higher and as a result DF performance is worse than the eight antenna model's DF performance.

In Figure 4.31, azimuth scan simulation results for frequency 100 MHz and elevation angle 98 degrees are given. In this figure, PEC ground medium gives 1.5 degrees RMSE around 110 and 250 degrees azimuth. In other azimuth regions RMSE is lower than 0.8 degree for PEC medium. For dielectric ground medium, RMSE peaks are lower in the corresponding azimuths. If we compare these results with the four antenna simulations in Figure 4.19, the

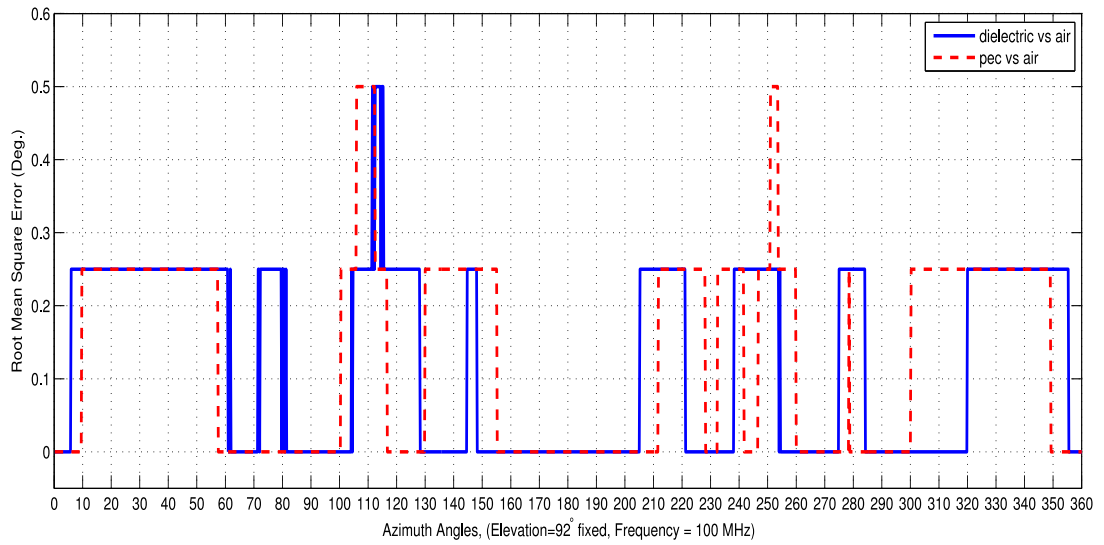


Figure 4.30: 100 MHz, Perfect Electric Conductor versus Dielectric medium, with relative permittivity  $\epsilon_r=15$  and conductivity  $\sigma=0.04$ , elevation angle is 92 degree.

average RMSE of four antenna model is approximately 3-4 times higher than the average RMSE of eight antenna model for both ground mediums.

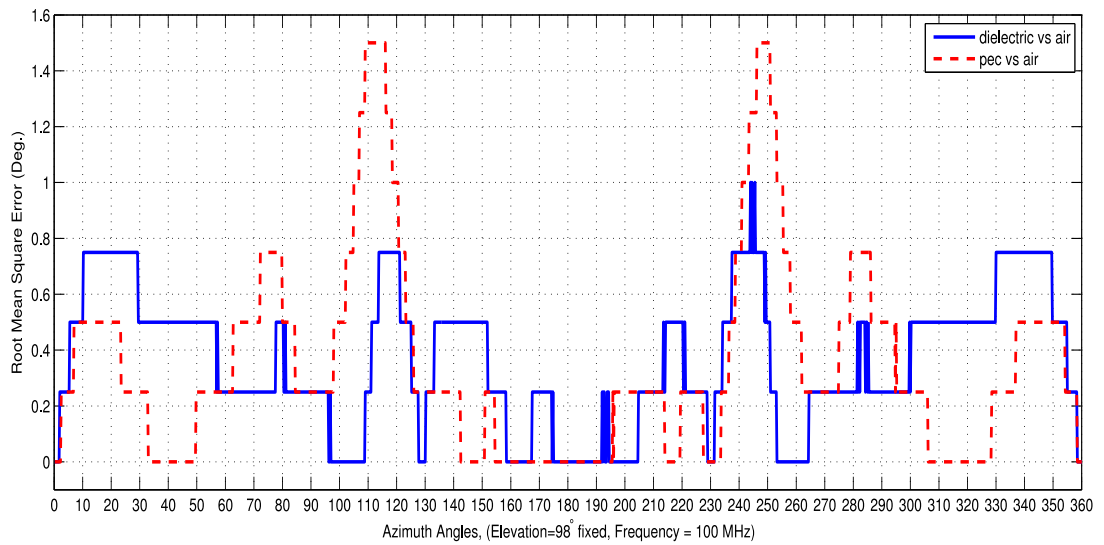


Figure 4.31: 100 MHz, Perfect Electric Conductor versus Dielectric medium, with relative permittivity  $\epsilon_r=15$  and conductivity  $\sigma=0.04$ , elevation angle is 98 degree.

In Figure 4.32, azimuth scan simulation results for frequency 250 MHz and elevation angle 92 degrees are given. In this figure, dielectric medium gives RMSE in a small azimuth angle sectors. Average RMSE of dielectric medium is lower than 0.1 degree, while it is approximately

0.3-0.4 degree for PEC. If we compare eight antenna model with the four antenna model, DF performance of 8 antenna model is still better, and the average RMSE of four antenna model is nearly two times higher than the average RMSE for eight antenna model. DF performances of two antenna models get closer as the frequency increases.

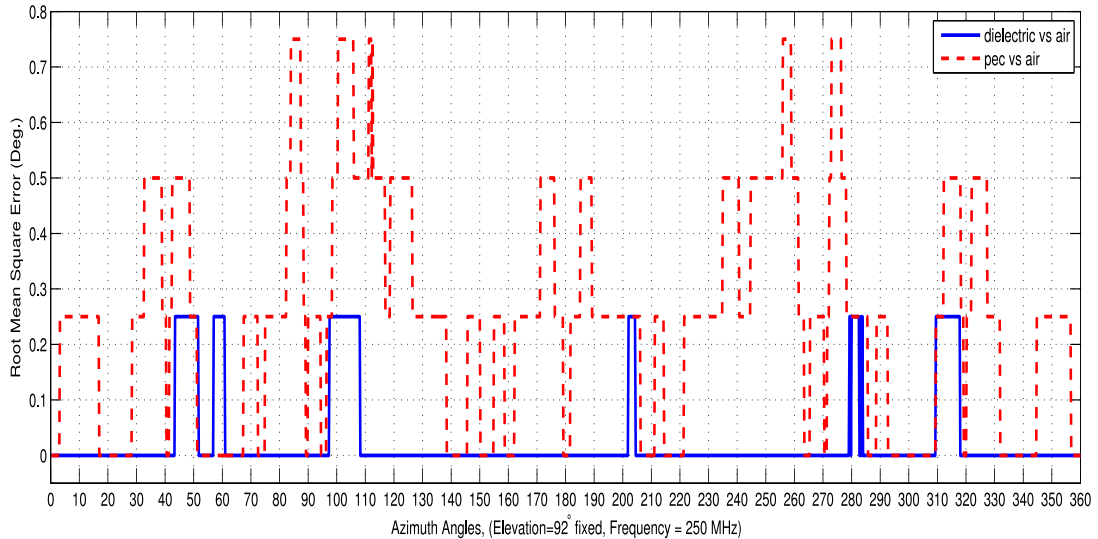


Figure 4.32: 250 MHz, Perfect Electric Conductor versus Dielectric medium, with relative permittivity  $\epsilon_r=15$  and conductivity  $\sigma=0.04$ , elevation angle is 92 degree.

In Figure 4.33, azimuth scan simulation results for frequency 250 MHz and elevation angle 98 degrees are given. In this figure, PEC medium's DF performance does not change much with the change of the elevation angle. Although dielectric medium's average RMSE increases, DF performance of the dielectric medium is nearly two times better than DF performance of the PEC medium. If we compare eight antenna model with the four antenna model, PEC medium's average RMSE is much higher (approximately 20-40 times) in four antenna model as compared to eight antenna model. But for the dielectric medium, average RMSE does not change in different antenna models.

In Figure 4.34, azimuth scan simulation results for frequency 375 MHz and elevation angle 92 degrees are given. In this figure, DF performances of dielectric medium and PEC medium are similar, but average RMSE of PEC medium is slightly higher, due to the peaks in the RMSE curve. In four antenna model given in Figure 4.22, dielectric medium makes approximately 10 times higher average RMSE than eight antenna model. For the PEC medium, average RMSE's for four antenna and eight antenna models are similar except for the peak RMSE of

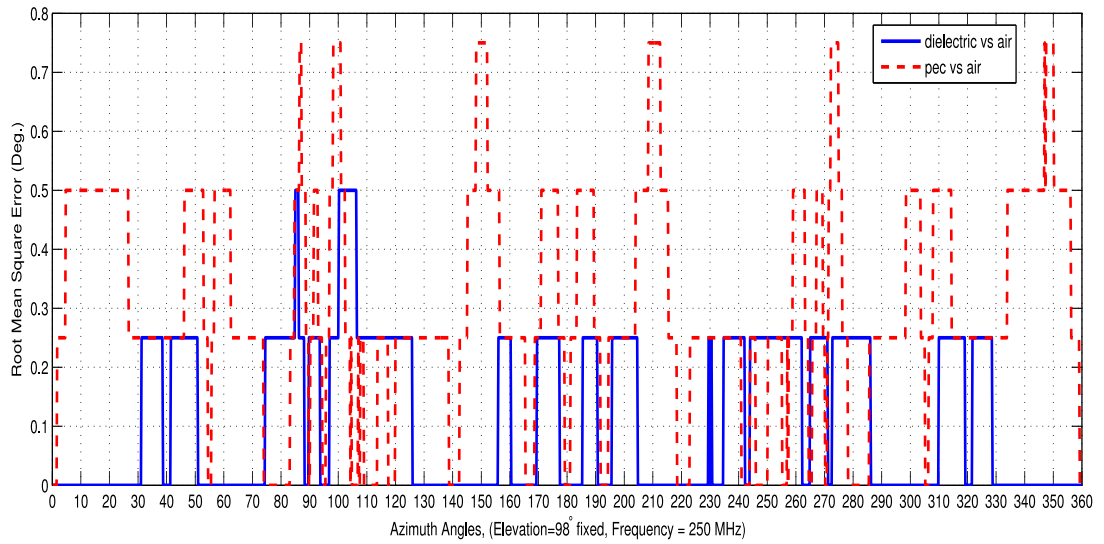


Figure 4.33: 250 MHz, Perfect Electric Conductor versus Dielectric medium, with relative permittivity  $\epsilon_r=15$  and conductivity  $\sigma=0.04$ , elevation angle is 98 degree.

7 degrees at azimuth angle 190 degrees in four antenna model.

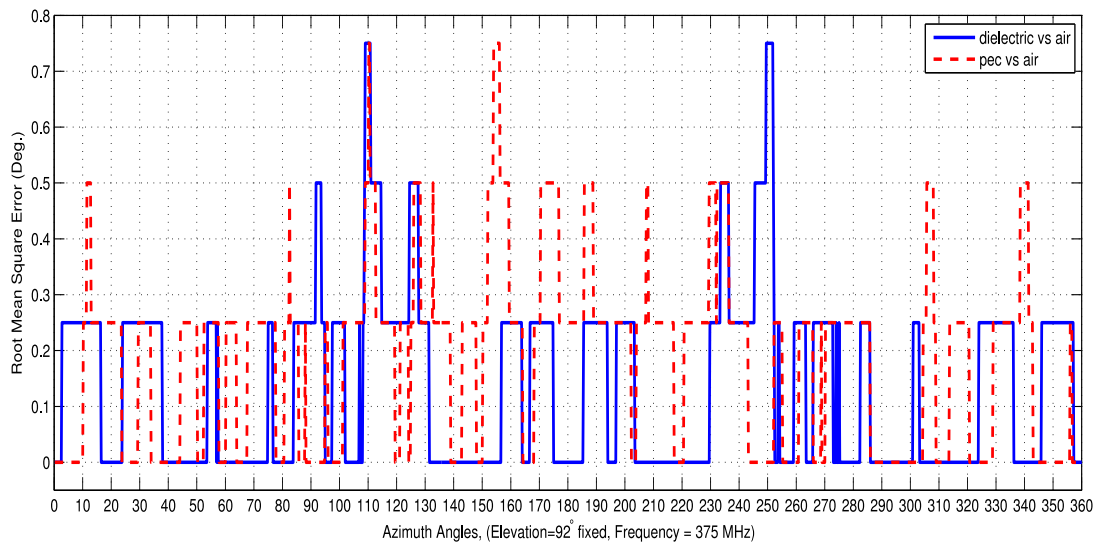


Figure 4.34: 375 MHz, Perfect Electric Conductor versus Dielectric medium, with relative permittivity  $\epsilon_r=15$  and conductivity  $\sigma=0.04$ , elevation angle is 92 degree

In Figure 4.35, azimuth scan simulation results for frequency 375 MHz and elevation angle 98 degrees are given. In this figure, PEC medium generates large RMSE's, around 100 degrees in some azimuth angle sectors. Average RMSE for the PEC medium is approximately 10 degrees, but for dielectric medium average RMSE is approximately 0.3 degree. Dielectric

medium has 30 times better DF performance compared to PEC medium. If we compare eight antenna model with four antenna model, for dielectric medium average RMSE for four antenna is two times higher, but for PEC medium average RMSE is approximately two degrees, which means for four antenna model PEC medium's DF performance is five times better than PEC medium's DF performance in eight antenna model.

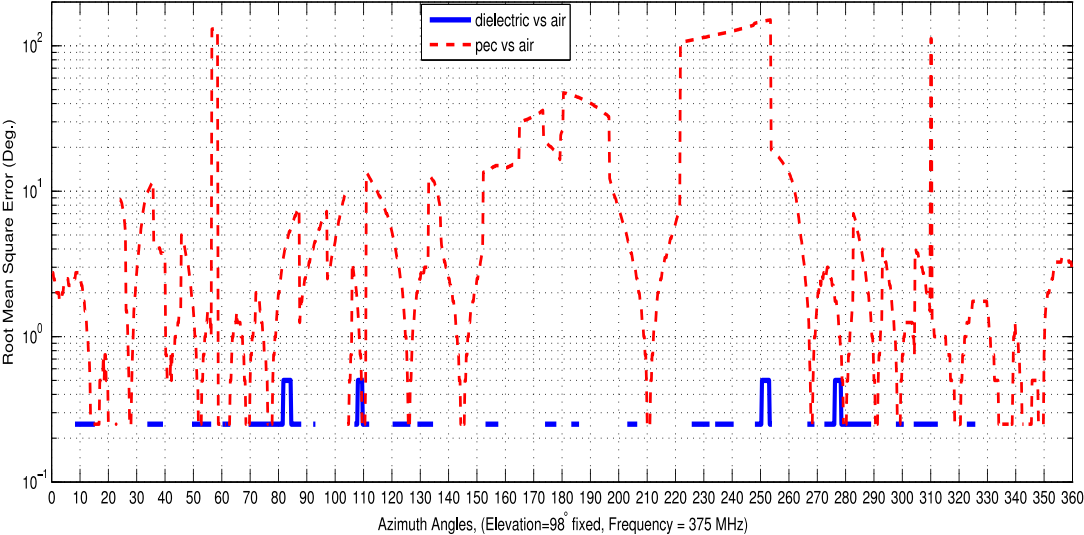


Figure 4.35: 375 MHz, Perfect Electric Conductor versus Dielectric medium, with relative permittivity  $\epsilon_r=15$  and conductivity  $\sigma=0.04$ , elevation angle is 98 degree

In Figure 4.36, azimuth scan simulation results for frequency 500 MHz and elevation angle 92 degrees are given. In this figure, DF performance of dielectric medium is slightly better than PEC medium's DF performance. If we compare eight antenna model with four antenna model, eight antenna model's DF performance is approximately two times better than that of four antenna model.

In Figure 4.37, azimuth scan simulation results for frequency 500 MHz and elevation angle 98 degrees are given. In this figure, average RMSE for dielectric medium is less than 0.2 degree but for PEC medium average RMSE is approximately 10-20 degrees, so DF performance of dielectric medium is approximately 50-100 times better. If we compare eight antenna model with four antenna model, for dielectric medium; DF performance of eight antenna model is approximately 3-4 times better. However for PEC medium average RMSE is 2 degrees in four antenna model. This means for PEC medium, DF performance of four antenna model is 5-10 times better than eight antenna model.

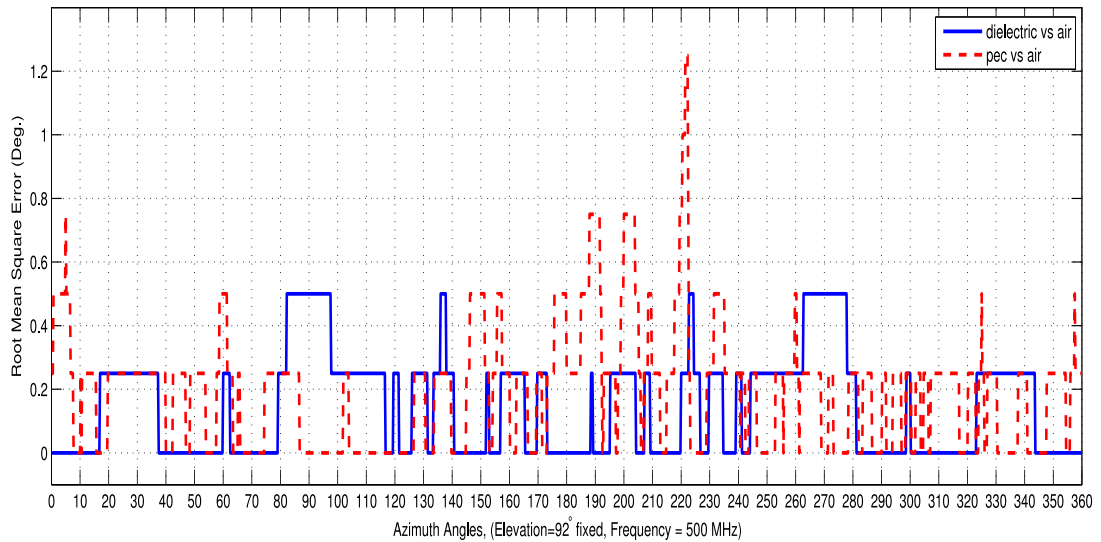


Figure 4.36: 500 MHz, Perfect Electric Conductor versus Dielectric medium, with relative permittivity  $\epsilon_r=15$  and conductivity  $\sigma=0.04$ , elevation angle is 92 degree

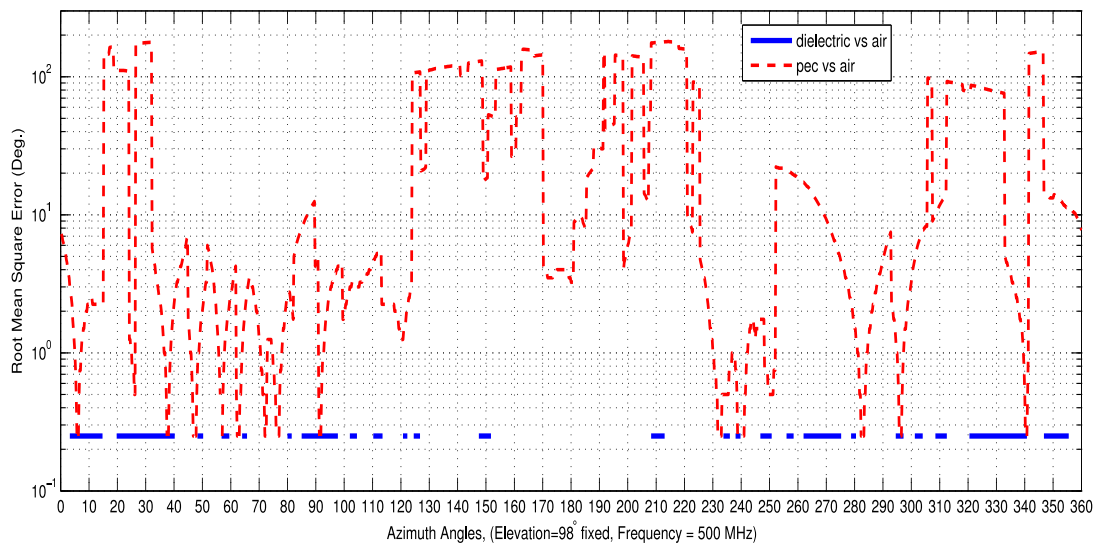


Figure 4.37: 500 MHz, Perfect Electric Conductor versus Dielectric medium, with relative permittivity  $\epsilon_r=15$  and conductivity  $\sigma=0.04$ , elevation angle is 98 degree

In Figure 4.38, comparison of ground elevation levels for frequency 500 MHz and elevation angle 92 degrees are given. In these simulations, UAV elevation level is changed to 4 meters, which is 10 meters for the previous figures. Ground medium is selected as the perfect electric conductor (PEC) in both cases. When we analyze this figure we can see that, for 4 meters of ground elevation level, there are RMSE levels higher than 100 degrees especially at 170 and 190 degrees of azimuth, which are in 10 degrees neighborhood of the back of the UAV.

Average RMSE of 4 meters of ground elevation is higher. So we can say that getting closer to the ground medium decreases the DF performance by increasing reflections from ground.

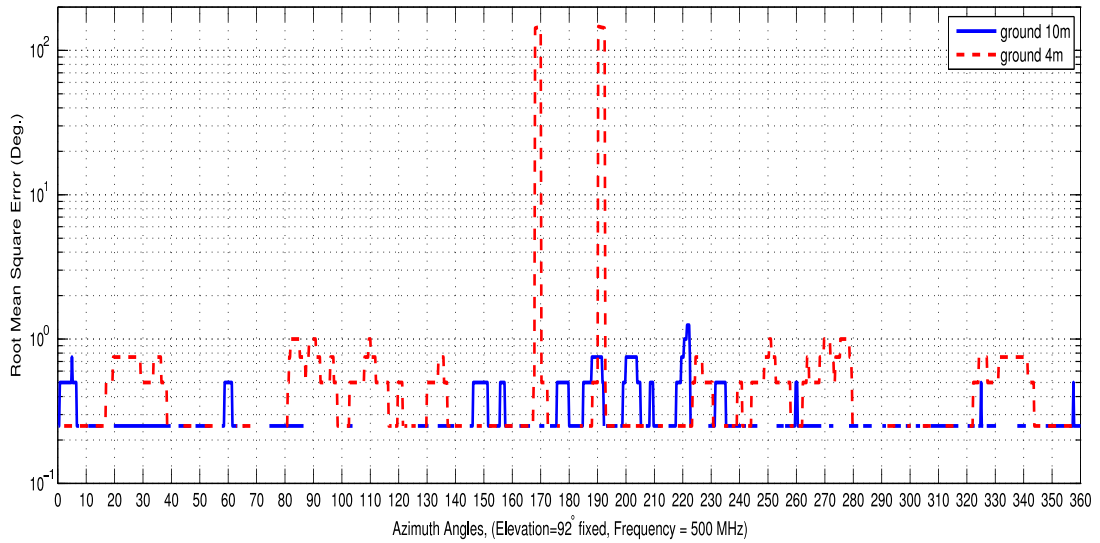


Figure 4.38: 500 MHz, Perfect Electric Conductor versus air, ground 10m vs 4m, elevation angle is 92 degree

In Figure 4.39, comparison of ground elevation level for frequency 500 MHz and elevation angle 98 degrees are given. This time, 10 meters of ground elevation makes huge RMSE's over all azimuth span. Average RMSE is approximately 10-20 degrees. For 4 meters of ground elevation case, average RMSE is lower than 0.5 degree. In that frequency and elevation angle settings, 4 meters of ground elevation has better DF performance.

### 4.3 Discussions

In this chapter, four antenna and eight antenna models are created. These two models have different positions and alignments in the UAV model in addition to change in the number of antennas, hence ground reflection effects on RMSE vs. azimuth curves are different among these models.

In the frequency band 20-500 MHz, dielectric ground medium's DF performance is generally better than perfect electric conductor (PEC) ground medium's DF performance. Exceptions occur for frequencies 20 and 60 MHz and elevation angle 92 degrees. For these cases, peak RMSE's are higher for dielectric medium. However, in elevation angle 98 degrees, PEC

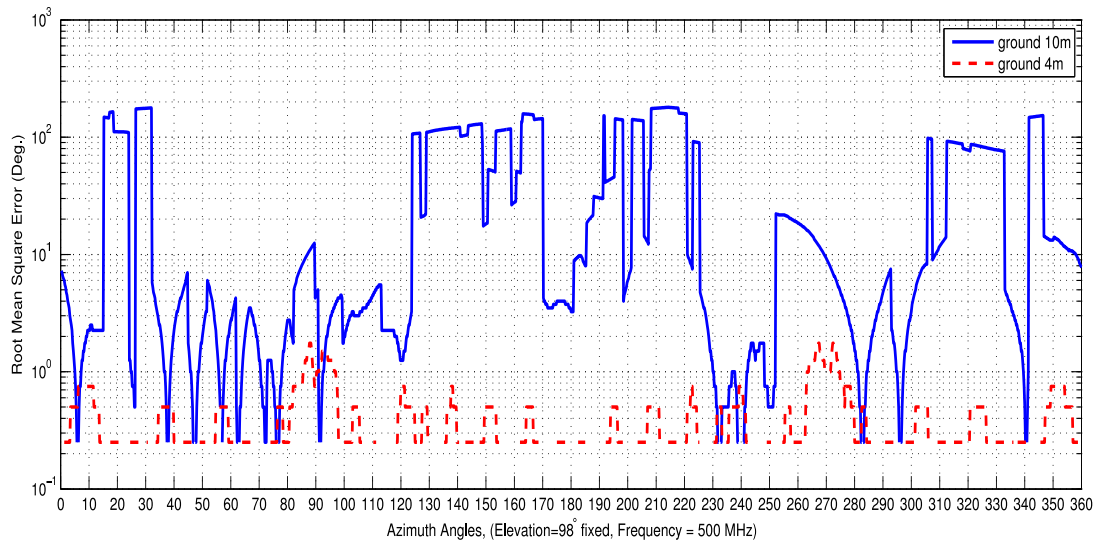


Figure 4.39: 500 MHz, Perfect Electric Conductor versus air, ground 10m vs 4m, elevation angle is 98 degree

medium's peak RMSE becomes higher than dielectric medium's peak RMSE in all frequencies in the frequency band 20-500 MHz.

In general eight antenna model's DF performance is much better than four antenna model's DF performance. Only for 375 and 500 MHz and elevation angle 98 degrees, eight antenna model has more than 100 degrees peak RMSE for PEC ground medium, while for four antenna model, peak RMSE values are 10 and 4 degrees, respectively, for 375 and 500 MHz for PEC ground medium. Similarly four antenna model has over 100 degrees peak RMSE for PEC ground medium in elevation angle 98 degrees while eight antenna model has a peak RMSE of 0.75 degree.

Root Mean Square Errors (RMSE) are higher for elevation angle 98 degrees as compared to elevation angle 92 degree, especially for perfect electric conductor (PEC) ground medium simulations. This situation can be explained with higher ground reflections for elevation angle 98 degrees. In PEC medium, signal attenuation after reflection is much less as compared to dielectric medium. As a result, ground reflected signals change the magnitude and phase characteristics of the currents collected from dipole antennas for PEC ground medium.

## CHAPTER 5

### DF SYSTEM ON SUV WITH MONOPOLE ANTENNAS

In this chapter, a DF antenna array composed of monopole antennas is investigated on a complex platform. The platform is selected as SUV more specifically Hummer. Monopole antennas are mounted on top of the passenger carrier part and centered on the ceiling of the vehicle. Antenna interelement distance for the monopole antennas is taken as 35 cm and the radius of the circular array is 25.5 cm. There are four monopole antennas in the array. Spatial aliasing can be expected at frequencies above 430 MHz for 35 cm interelement distance antennas. However, due to the fact that correlative interferometer and circular array are more resistant to spatial aliasing, simulations are done up to 500 MHz. Frequency band is selected as 20 MHz-500 MHz. Simulations are repeated for two elevation angles, namely, 72 degrees and 88 degrees. The monopole antennas are two meters above the ground.

In this chapter, two different sets of analysis are done. In the first part, perfect electric conductor and dielectric infinite ground mediums are used to obtain DF performance. Calibration data is collected when the ground medium is perfect electric conductor (PEC). In the test data, ground medium is dielectric ground medium. Three different dielectric ground mediums are used. In other words, ground mediums have different relative permittivity and conductivity values. Relative permittivity values of the dielectric mediums are selected as  $\epsilon_r=15$ , 13 and 4, respectively, and conductivity values are  $\sigma=0.04$ , 0.03 and 0.06, respectively for these mediums. In this part, effects of different ground mediums on DF performance are analyzed using the above mentioned dielectric ground mediums.

In the second part of the analysis, a new method to improve the DF performance in a multipath environment is presented. This method is based on collecting so called "bias data" which is later used to correct the DOA result. Bias data is collected during the calibration process

where the calibration source's DOA is known. Bias data is created from the above mentioned calibration and test data for the frequency band 20 MHz-500 MHz and elevation angles 72 degrees and 88 degrees. Then this bias data is used to lower the RMSE's due to differences in the calibration and test data. While using the bias data, calibration data used in the simulation is the same as that used in bias data derivation, but test data is collected with different dielectric ground medium characteristics. In addition, azimuth data set has different start and end values as compared to bias data's azimuth data set. In this part, RMSE reduction performance of bias data is tested with changing dielectric characteristics and azimuth data. In the bias analysis part, simulation settings are described in detail.

In the following section which is SUV model, monopole antenna design parameters are given. In addition, Hummer vehicle's FEKO model is given with various CAD drawings. In Hummer simulation results part, Direction Finding (DF) performance of the vehicle is tested by azimuth scan analysis with various simulation settings.

## **5.1 SUV Model**

In chapter-3 and chapter-4, dipole antennas are used for DF comparison. In this chapter monopole antennas are mounted on top of Hummer vehicle. In this section, monopole antenna model's dimensions are given first. Then CAD drawings for the FEKO model of the Hummer vehicle are given.

### **5.1.1 Antenna Model**

In Figure 5.1, dimensions of monopole antenna are given. In Table 5.1, values of the monopole antenna design parameters are given. Monopole antenna has a length of 30 centimeters. Monopole antenna's radius is 1.5 millimeters. There is a 1.4 centimeters gap between the pole of the antenna and ground plane. In the FEKO model, there is a wire line constructing a port within the gap touching the monopole antenna and ground plane. Antenna currents are measured from these ports.

In Figure 5.2, circular array structure of the monopole antenna placements is given. This structure is used through the simulations in this chapter. The radius of the array is 25.5

Table 5.1: Monopole antenna design parameters

Parameter Name	Value (cm)
Monopole Length	30
Monopole Radius	1.5
Monopole Gap	1.4

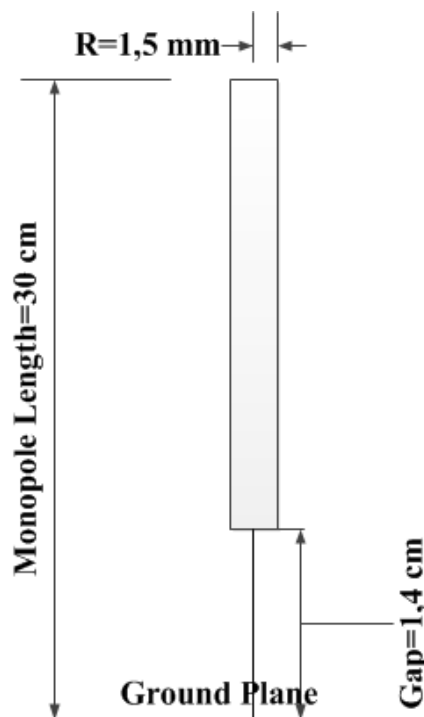


Figure 5.1: Monopole antenna dimensions

centimeters. The antenna interelement distance is 35 centimeters.

### 5.1.2 SUV Feko Model

In this section, FEKO model of Hummer vehicle is given in different perspectives. Detailed antenna view is added for clarity. In Figure 5.3, Hummer FEKO model with 4 monopole antennas can be observed. Monopole antennas are placed on the ceiling of the vehicle. Antennas are centered on the ceiling and have an antenna interelement distance of 35 centimeters. In addition, circular array has a radius of 25.5 centimeters. Perfect electric conductor (PEC) is used as the ground medium.

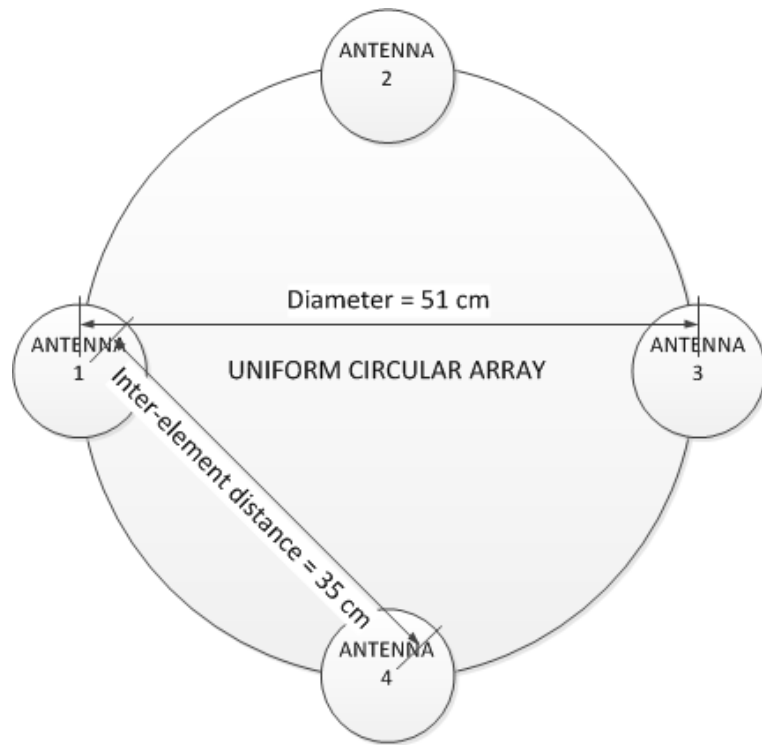


Figure 5.2: Circular array antenna pattern with antenna interelement distance 35cm

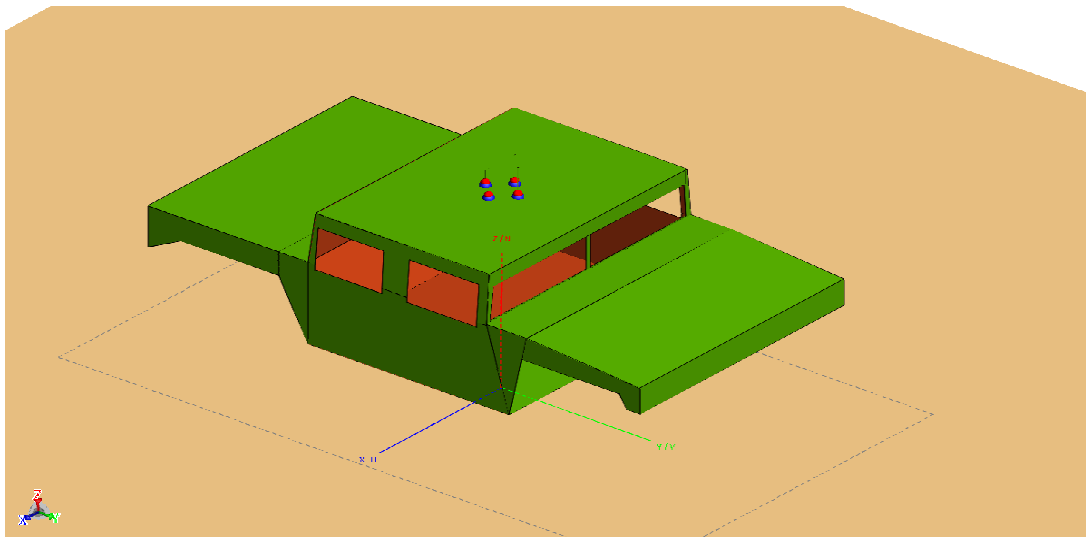


Figure 5.3: Hummer feko model isometric view. Monopole antenna interelement distance is 35cm.

In Figure 5.4, monopole antennas can be observed more clearly. Antennas are touching the ceiling without a gap. Antenna alignments according to the coordinate axes can be seen.

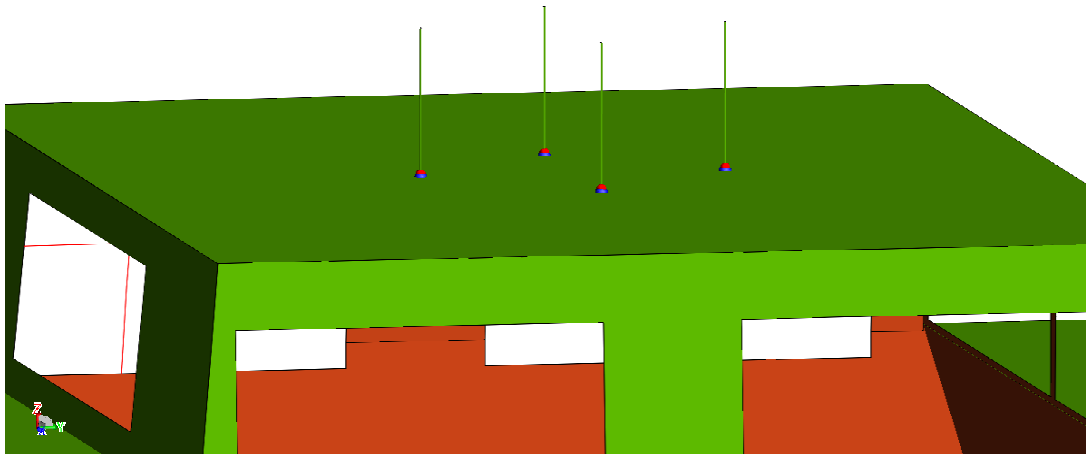


Figure 5.4: Hummer feko model detailed antenna view

In Figure 5.5, front view of the model is given. In this figure detail of the windscreen and front bumpers and bonnet of the model can be observed. In addition, elevation of the model from the ground plane can be seen.

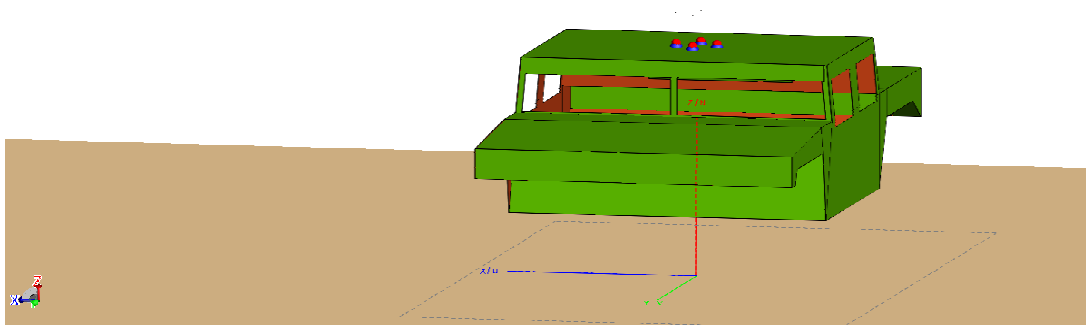


Figure 5.5: Hummer feko model front view

In Figure 5.6, side view of the model can be seen. Side front and rear bumpers and windows are clearly observable from this figure.

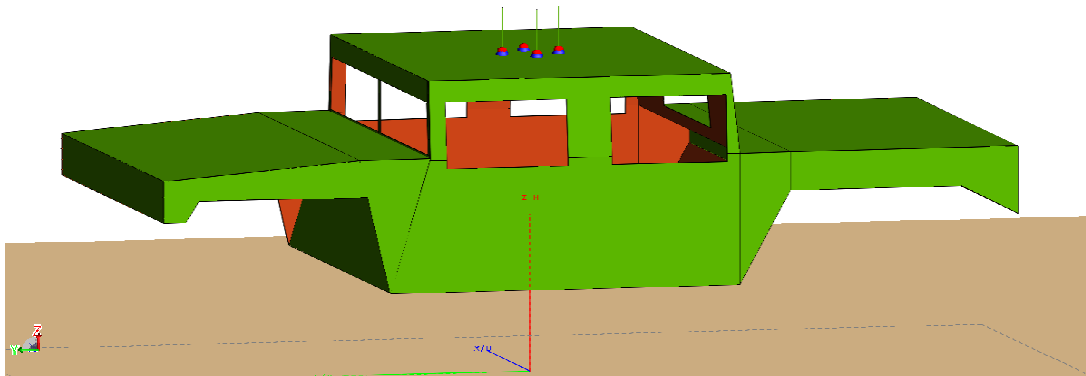


Figure 5.6: Hummer feko model side view

In Figure 5.7, back view of the model can be observed. Rear window, luggage compartment, rear bumpers can be seen from this figure.

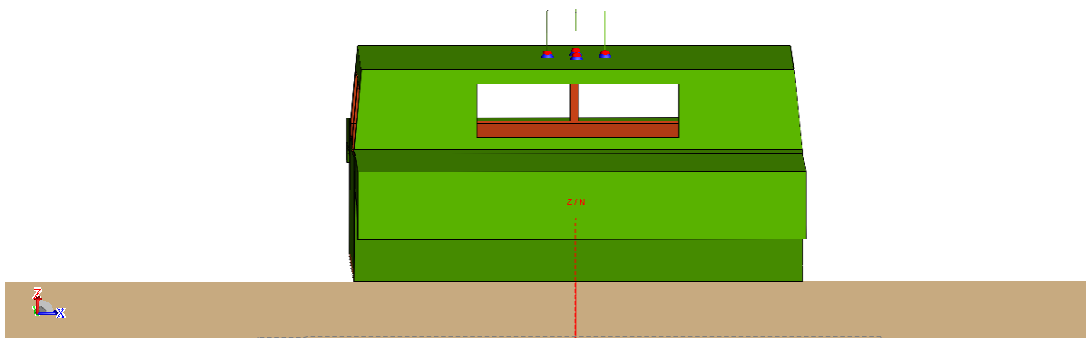


Figure 5.7: Hummer feko model back view

In Figure 5.8, bottom view of the model can be seen. In this figure, we can observe passenger cabin of the car. The cabin is closed to prevent any reflection from the ground to reach the ceiling of the model.

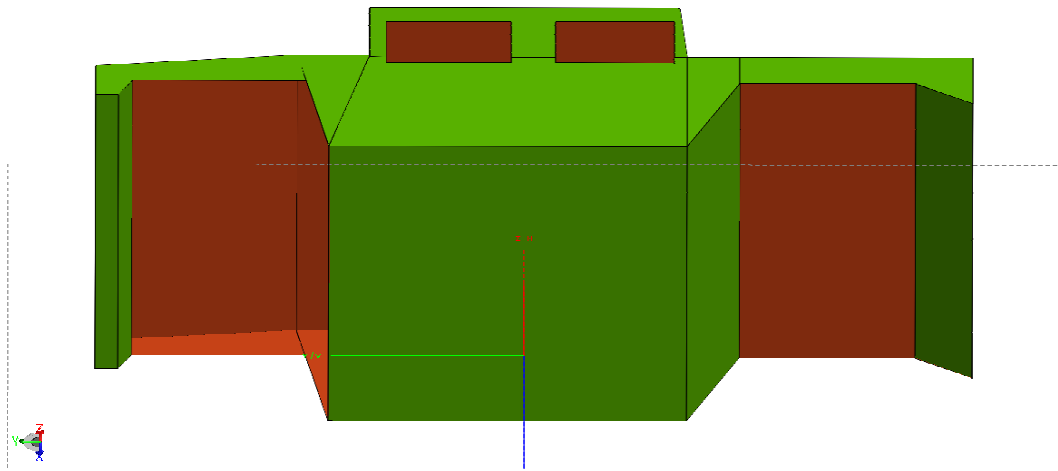


Figure 5.8: Hummer feko model bottom view

In Figure 5.9, infinite ground medium is selected as dielectric medium. Other properties of the Hummer model in this figure are the same compared to previous figures.

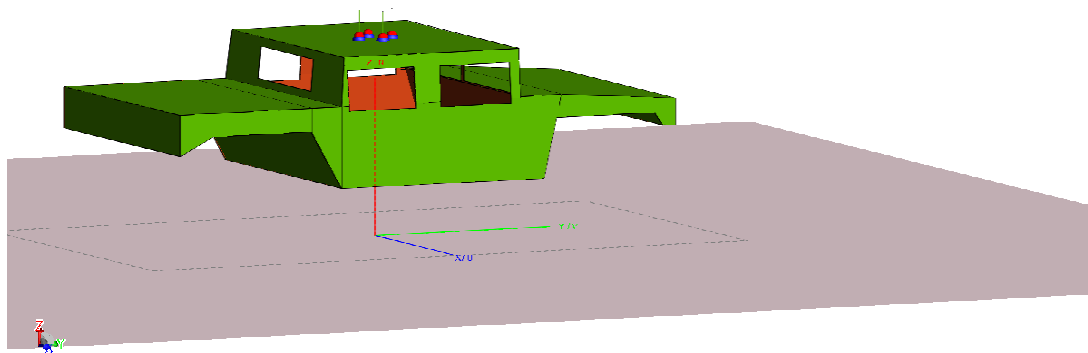


Figure 5.9: Hummer feko model above infinite dielectric ground medium

## 5.2 Simulation Results for the SUV

In the following sections, two different analyses are presented. In the first part, azimuth scan simulations are performed for both perfect electric conductor (PEC) and dielectric infinite ground mediums. The dielectric infinite ground medium has relative permittivity  $\epsilon_r=15$  and conductivity  $\sigma=0.04$ . Calibration data is collected when the ground medium is selected as PEC medium, test data is collected with dielectric ground medium. These calibration and test data settings are simulated to obtain RMSE vs. azimuth results as well as bias data. Detailed information for bias data is given in bias analysis section.

Second part of analysis is done with the use of bias data and by changing the dielectric medium's properties. Detailed information about this analysis can be found in bias analysis section.

Frequency band of 20-500 MHz is analyzed with the selected frequencies of 20 MHz, 100 MHz, 250 MHz, 375 MHz and 500 MHz. Simulations are realized in two different elevation angles of 72 and 88 degrees, which correspond to 18 and 2 degrees of inclinations from the ground plane, respectively. Notation for the elevation angle is such that ground plane is considered to be at 90 degrees of elevation angle. Elevation angle values decrease as we go above the ground plane.

Plane wave excitation is applied with vertical linear polarization. Azimuth angle is swept from 0 to 360 degrees. Two different azimuth step values are used. For the frequencies from 20 MHz to 100 MHz, azimuth step is taken as 1 degree. For the frequencies 250 MHz, 375 MHz and 500 MHz, azimuth step value is 0.25 degree. Azimuth step is decreased for high frequencies to determine if any spatial aliasing occurs in these frequencies. Antenna interelement distance is selected not to cause any spatial aliasing under the frequency of 430 MHz. 500 MHz is a candidate frequency for spatial aliasing.

SNR is taken as 150 dB in order to see only the platform effects. Since SNR is high, only a single trial is done with 100 snapshots. Interpolation is not applied in the following analyses since azimuth data steps are small enough.

### 5.2.1 Perfect Electric Conductor vs. Dielectric Medium

In this section, different comparisons with different ground mediums and calibration-test sets are done. In the simulations, calibration data is collected with a PEC ground medium, while the test data is collected with a dielectric ground medium. This comparison is expected to show the effect of different ground mediums on DF performance.

In Figure 5.10, azimuth scan simulation results for frequency 20 MHz and elevation angle of 72 degrees are given. Dielectric constants for three dielectric mediums used in the simulations are given by relative permittivity  $\epsilon_r=15,13$  and 4, respectively, and conductivity  $\sigma=0.04, 0.03$  and 0.06, respectively.

In this figure, we can say that the average RMSE of three different dielectric mediums are around 3 degrees. The dielectric medium with relative permittivity  $\epsilon_r=4$  shows better DF performance than other two mediums. Dielectric medium with  $\epsilon_r=13$  has approximately one degree higher RMSE than dielectric medium with  $\epsilon_r=15$ .

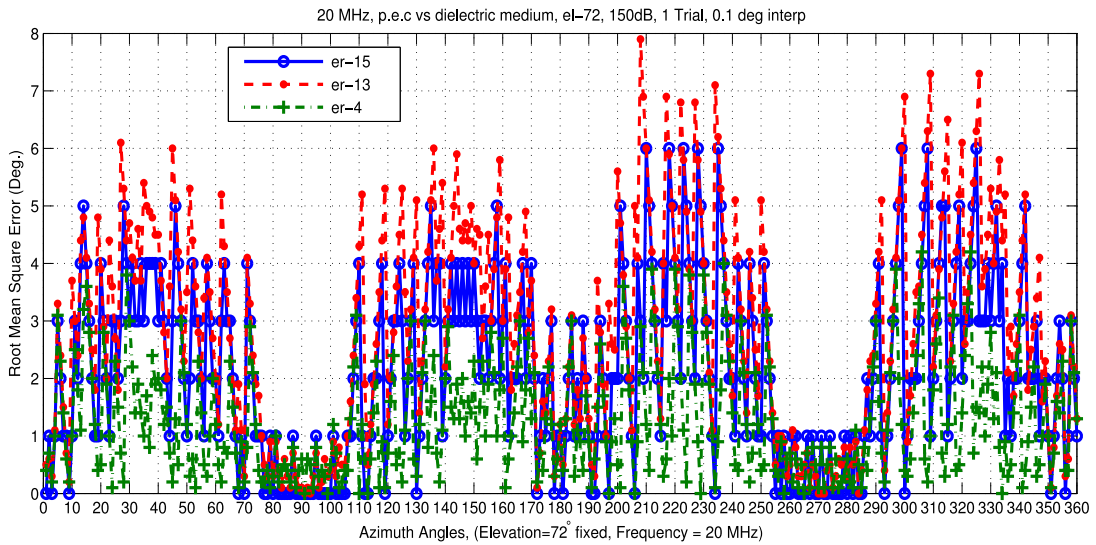


Figure 5.10: 20 MHz, Perfect Electric Conductor versus Dielectric medium, with relative permittivity  $\epsilon_r=15, 13$  and 4 respectively, and conductivity  $\sigma=0.04, 0.03$  and 0.06 respectively, elevation angle is 72 degrees.

In Figure 5.11, azimuth scan simulation results for frequency 20 MHz and elevation angle of 88 degrees are given. In this figure, average RMSE level is decreased to 1.5 degrees, which is 3 degrees for elevation angle 72 degrees. DF performance comparison of the dielectric mediums

shows that, dielectric medium with  $\epsilon_r=4$  has 0.5-1 degree of RMSE average, while dielectric medium with  $\epsilon_r=15$  has 1-1.5 degrees of RMSE average. On the other hand dielectric medium with  $\epsilon_r=13$  has 1.5-2 degrees of RMSE average.

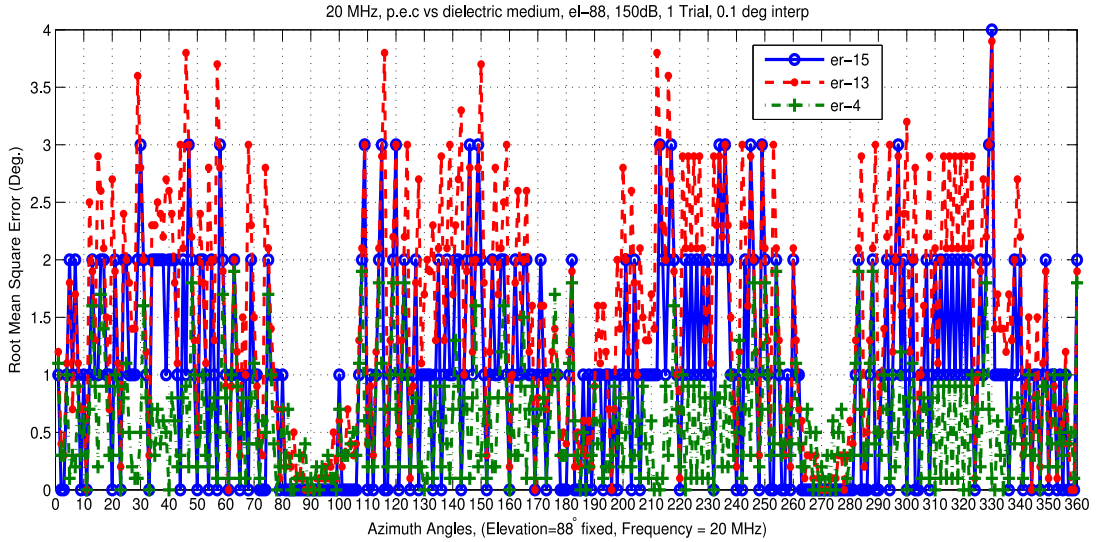


Figure 5.11: 20 MHz, Perfect Electric Conductor versus Dielectric medium, with relative permittivity  $\epsilon_r=15, 13$  and  $4$  respectively, and conductivity  $\sigma=0.04, 0.03$  and  $0.06$  respectively, elevation angle is  $88$  degrees.

In Figure 5.12, azimuth scan simulation results for frequency  $100$  MHz and elevation angle of  $72$  degrees are given. In this figure, average RMSE is around  $120$  degrees. These large errors occur due to high reflections from the PEC medium. High reflections increase the current read from antennas for the PEC medium which distorts correlation characteristics. In dielectric mediums, reflections from infinite ground medium have lower effects on the magnitude and phase of the current in the segments. In other words, calibration data is more affected from reflections than the test data. As a result, calibration and test data do not match and large errors occur. From the figure, we can not distinguish the performances of dielectric mediums.

In Figure 5.13, azimuth scan simulation results for frequency  $100$  MHz and elevation angle of  $88$  degrees are given. In this figure, average RMSE is around  $3-4$  degrees except for the azimuth regions  $200-220$  degrees and  $320-350$  degrees, where RMSE has a peak value of  $18$  degrees. Dielectric medium with  $\epsilon_r=4$  has a peak RMSE of  $18$  degrees. On the other hand, dielectric mediums with  $\epsilon_r=15$  and  $13$  have a peak RMSE of  $12$  degrees.

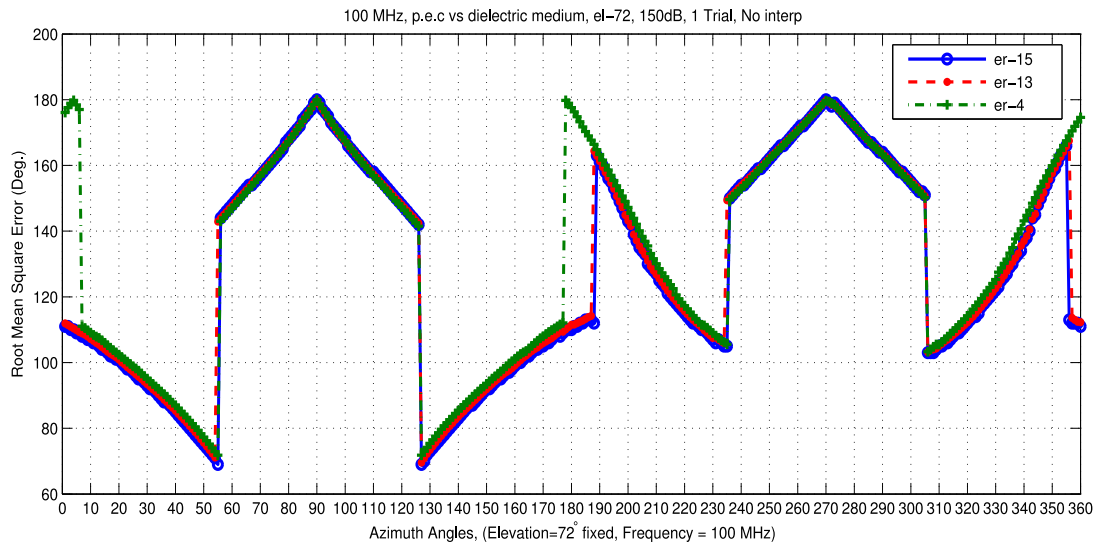


Figure 5.12: 100 MHz, Perfect Electric Conductor versus Dielectric medium, with relative permittivity  $\epsilon_r=15, 13$  and  $4$  respectively, and conductivity  $\sigma=0.04, 0.03$  and  $0.06$  respectively, elevation angle is  $72$  degrees.

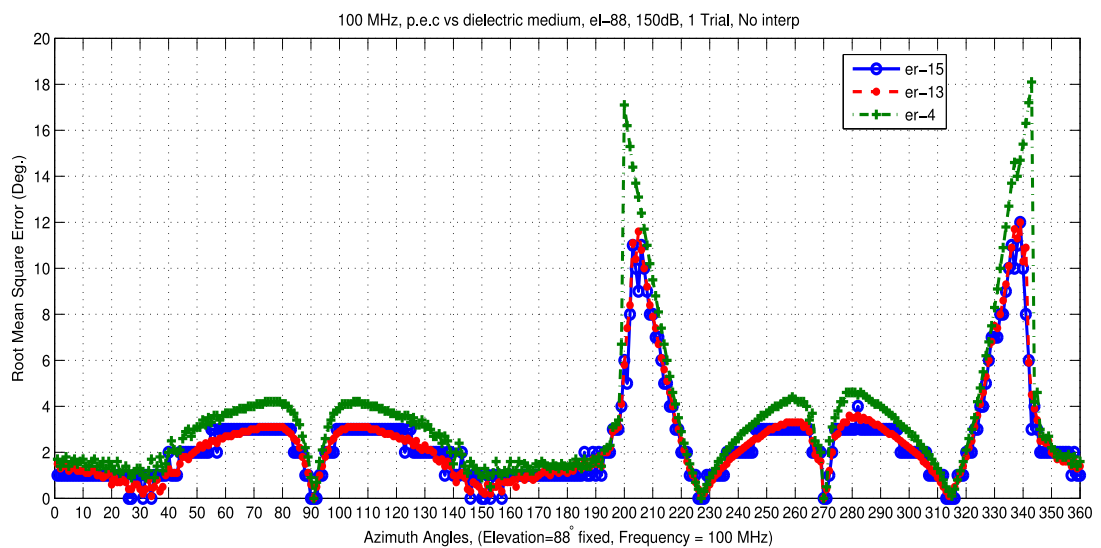


Figure 5.13: 100 MHz, Perfect Electric Conductor versus Dielectric medium, with relative permittivity  $\epsilon_r=15, 13$  and  $4$  respectively, and conductivity  $\sigma=0.04, 0.03$  and  $0.06$  respectively, elevation angle is  $88$  degrees.

In Figure 5.14, azimuth scan simulation results for frequency  $250$  MHz and elevation angle of  $72$  degrees are given. In this figure, average RMSE is around  $2-3$  degrees. DF performances of dielectric mediums with  $\epsilon_r=13$  and  $15$  are better than DF performance of dielectric medium with  $\epsilon_r=4$ , actually in this dielectric medium peaks in RMSE increase by  $2$  degrees especially

in the azimuth regions around 70, 110, 260 and 280 degrees compared to other two mediums.

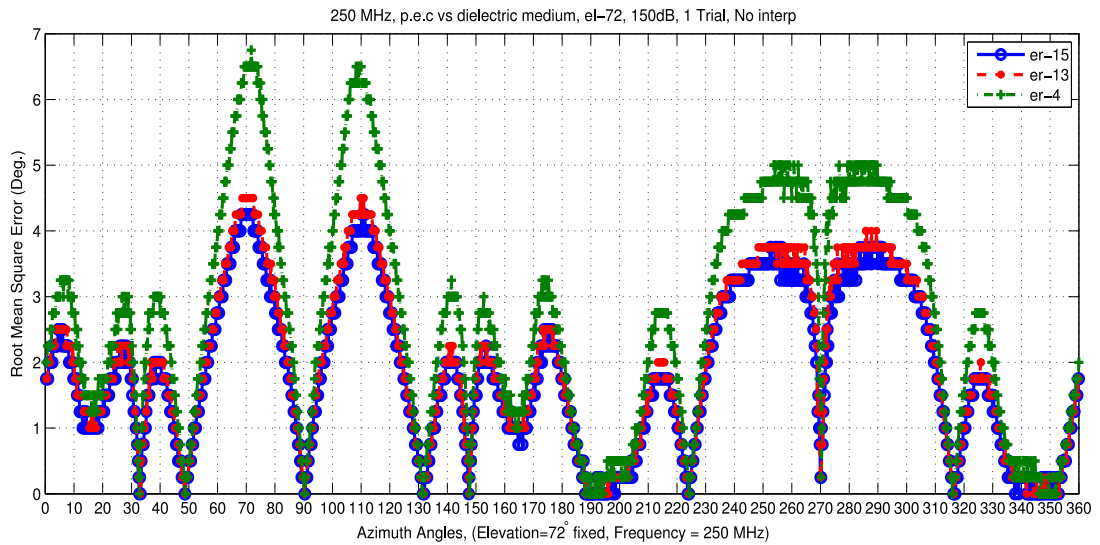


Figure 5.14: 250 MHz, Perfect Electric Conductor versus Dielectric medium, with relative permittivity  $\epsilon_r=15, 13$  and  $4$  respectively, and conductivity  $\sigma=0.04, 0.03$  and  $0.06$  respectively, elevation angle is  $72$  degrees.

In Figure 5.15, azimuth scan simulation results for frequency  $250$  MHz and elevation angle of  $88$  degrees are given. In this figure, DF performances of the three different dielectric mediums are similar. Average RMSE is around  $1-2$  degrees. RMSE has peaks of  $4.5$  degrees around  $190$  and  $350$  degrees of azimuth which have symmetric around  $270$  degrees of azimuth.

In Figure 5.16, azimuth scan simulation results for frequency  $375$  MHz and elevation angle of  $72$  degrees are given. In this figure, DF performances of the dielectric mediums are similar but dielectric medium with  $\epsilon_r=4$  has  $0.5-1$  degree higher RMSE peaks. In this frequency and elevation angle settings, DOA from the back of the vehicle is significantly less affected from reflections since RMSE level is around  $0.5$  degree for the back while it is  $2$  degrees for the front of the vehicle.

In Figure 5.17, azimuth scan simulation results for frequency  $375$  MHz and elevation angle of  $88$  degrees are given. In this figure, average RMSE is lower than  $1$  degree. DF performances of the dielectric mediums are alike.

In Figure 5.18, azimuth scan simulation results for frequency  $500$  MHz and elevation angle

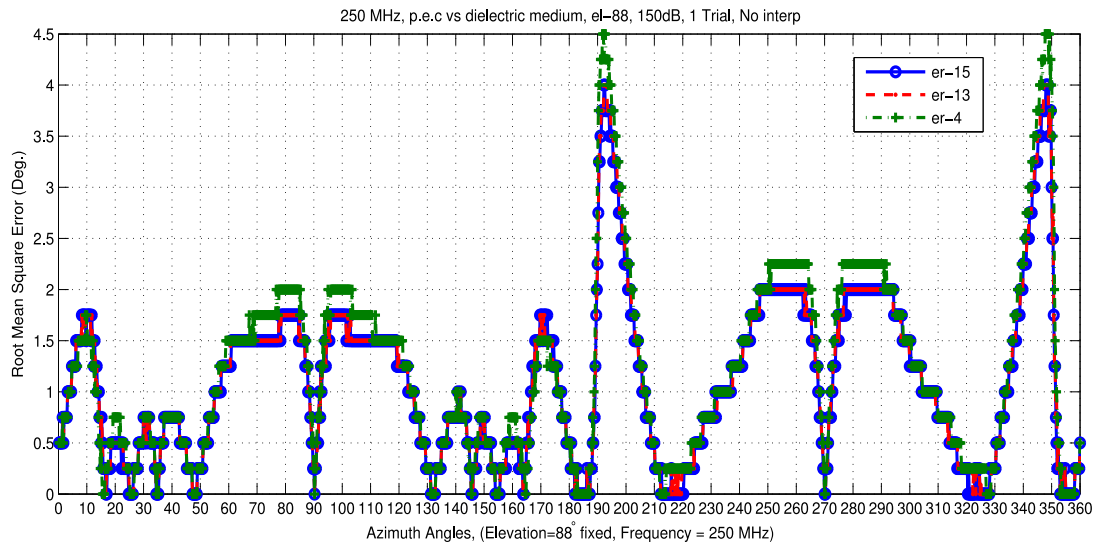


Figure 5.15: 250 MHz, Perfect Electric Conductor versus Dielectric medium, with relative permittivity  $\epsilon_r=15, 13$  and  $4$  respectively, and conductivity  $\sigma=0.04, 0.03$  and  $0.06$  respectively, elevation angle is  $88$  degrees.

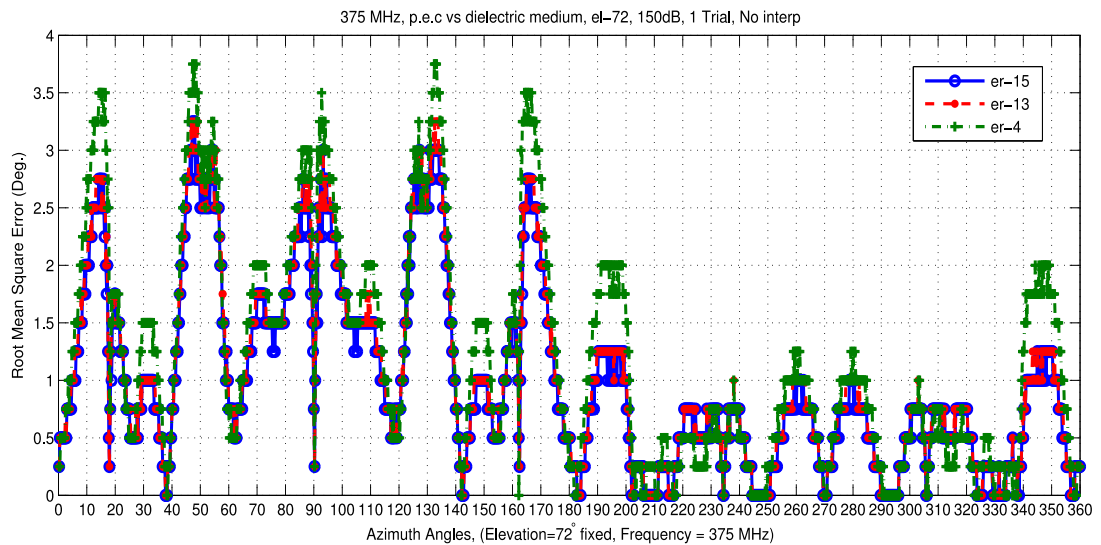


Figure 5.16: 375 MHz, Perfect Electric Conductor versus Dielectric medium, with relative permittivity  $\epsilon_r=15, 13$  and  $4$  respectively, and conductivity  $\sigma=0.04, 0.03$  and  $0.06$  respectively, elevation angle is  $72$  degrees.

of  $72$  degrees are given. In this figure, average RMSE is around  $1$  degree, but for dielectric medium with  $\epsilon_r=4$  peak RMSE over  $100$  degrees occur around  $70$  and  $110$  degrees of azimuth. This situation can be explained by spatial aliasing which happens when the antenna interelement distance is larger than half of the wavelength for that frequency setting. In our

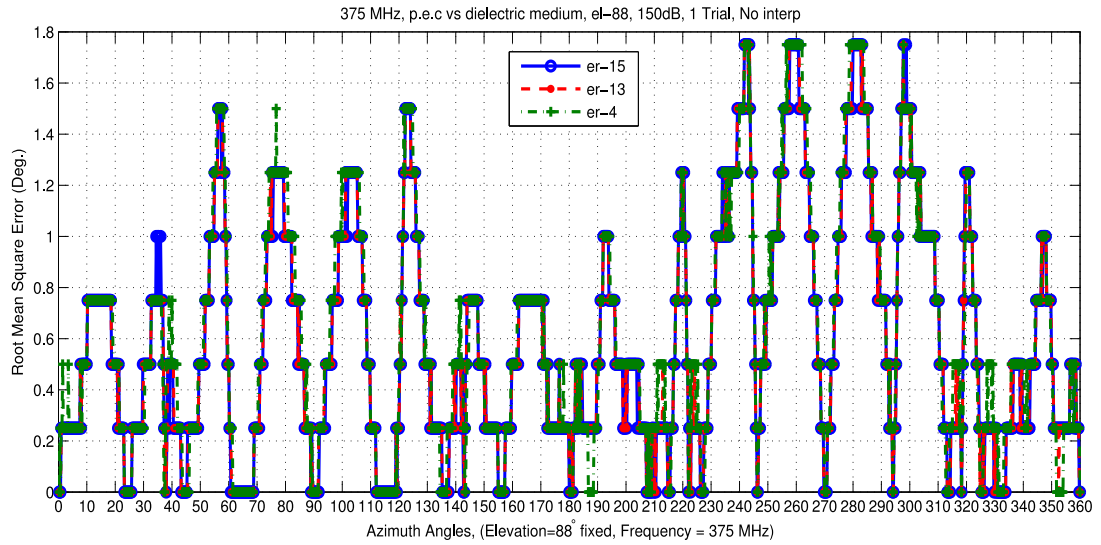


Figure 5.17: 375 MHz, Perfect Electric Conductor versus Dielectric medium, with relative permittivity  $\epsilon_r=15, 13$  and  $4$  respectively, and conductivity  $\sigma=0.04, 0.03$  and  $0.06$  respectively, elevation angle is  $88$  degrees.

case, since the interelement distance is  $35$  cm, aliasing starts after the frequency  $430$  MHz from calculations. Spatial aliasing does not occur for other two dielectric mediums. In the evaluations, the data collected with any dielectric ground medium is compared with the data collected with PEC ground medium. In the FEKO simulations, dielectric ground mediums are defined by the relative permittivity and conductivity values. Dielectric mediums with higher relative permittivity have better DF performance than the dielectric mediums with lower relative permittivity. Comparison with PEC ground medium results in lower RMSE values for dielectric ground mediums with high relative permittivity.

In Figure 5.19, azimuth scan simulation results for frequency  $500$  MHz and elevation angle of  $88$  degrees are given. In this figure, average RMSE is lower than  $1$  degree for dielectric mediums. Dielectric medium with  $\epsilon_r=4$  has a peak RMSE value over  $100$  degrees similar to the results for elevation angle  $72$  degrees, but this time RMSE peaks occur at  $80$  and  $100$  degrees of azimuth.

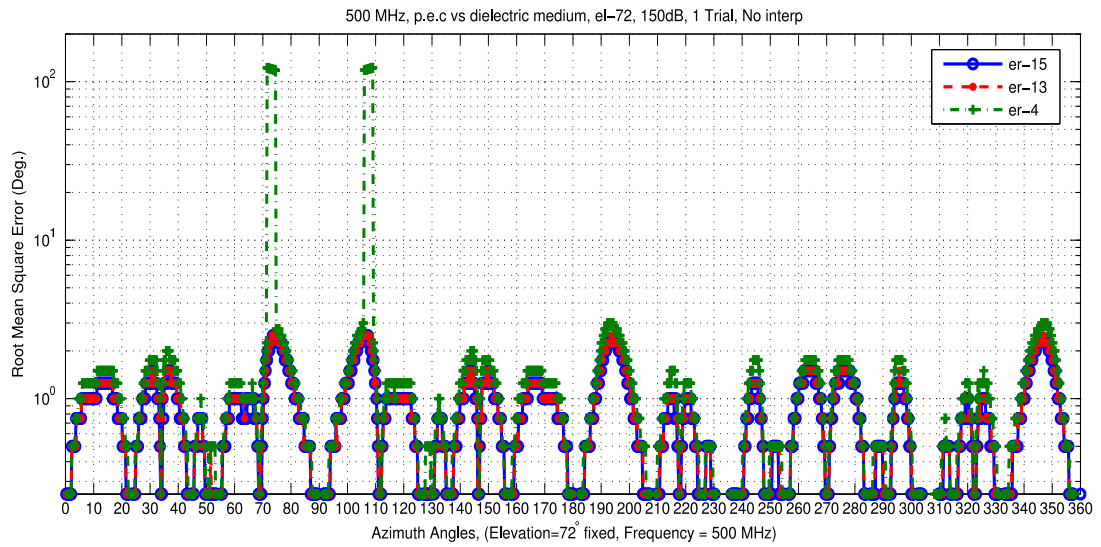


Figure 5.18: 500 MHz, Perfect Electric Conductor versus Dielectric medium, with relative permittivity  $\epsilon_r=15, 13$  and  $4$  respectively, and conductivity  $\sigma=0.04, 0.03$  and  $0.06$  respectively, elevation angle is  $72$  degrees.

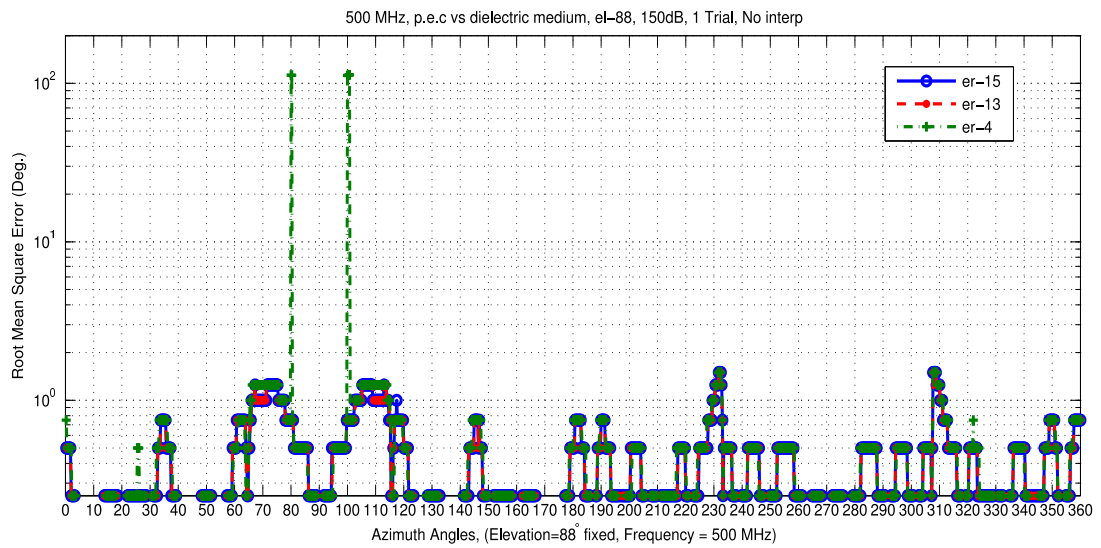


Figure 5.19: 500 MHz, Perfect Electric Conductor versus Dielectric medium, with relative permittivity  $\epsilon_r=15, 13$  and  $4$  respectively, and conductivity  $\sigma=0.04, 0.03$  and  $0.06$  respectively, elevation angle is  $88$  degrees.

### 5.3 Bias Analysis

In this section, we carry out the analyses by obtaining a bias data file first. Bias data file is used as a calibration table to overcome the errors due to changes in simulation properties such

as a shift in the azimuth data set. Bias data file is obtained for all frequency and elevation angle settings and also for the resolution of the azimuth angle scan. Resolution of the azimuth angle scan is determined by the azimuth step value selected for the test data and using the same value for the azimuth step of calibration data.

In bias analysis, azimuth resolution is selected as 0.25 degree for frequencies 250 MHz, 375 MHz and 500 MHz and 1 degree for frequencies 20 MHz and 100 MHz. Bias data file is the output of the azimuth scan analysis done by selecting the perfect electric conductor infinite ground medium as the calibration data and the dielectric infinite ground medium with relative permittivity  $\epsilon_r=15$  and conductivity  $\sigma=0.04$  as the test data.

After obtaining the bias data file for the selected frequency and elevation angle, azimuth scan simulations are accomplished with the bias data using the following settings. Calibration data remains unchanged and selected as the perfect electric conductor medium data, but test data is a different version of a dielectric ground medium whose dielectric properties are changed. Thus we use the bias data to test the robustness of the data for changes in medium properties as well as azimuth shifts in the data.

Test data is simulated in FEKO with different relative permittivity and conductivity. In addition, excitation plane wave's azimuth angle value is different from the calibration data. This is done by selecting a different start point for the azimuth scan for the test data. For 20 MHz, initial azimuth angle is 1.25 degrees, for 100 MHz, it is 0.5 degree, whereas for 250 MHz, 375 MHz and 500 MHz, the initial azimuth angle is selected as 0.3 degree. Changing the initial azimuth value shifts the test data's all azimuth values, since the azimuth increment remains unchanged.

During the analysis with the bias data, multiples of azimuth step values are selected for calibration data resolution. For 20 MHz, 1 degree of azimuth step is used in calibration data. For 100 MHz, three different azimuth step values are used in calibration data, namely, 1, 2 and 4 degrees. For 250 MHz, 375 MHz and 500 MHz, two different values namely, 0.25 degree and 1 degree are used as azimuth step or azimuth resolution in calibration data. However, for test data we use the original azimuth step value determined by the FEKO simulation's azimuth resolution, which is 1 degree of azimuth step for frequencies 20 MHz and 100 MHz, 0.25 degree of azimuth step for 250 MHz, 375 MHz and 500 MHz.

Analyses are realized for two different dielectric ground mediums and the results for different dielectric mediums are covered in two sections. For the following section, dielectric medium-1 refers to the dielectric infinite ground medium data with relative permittivity  $\epsilon_r=13$  and conductivity  $\sigma=0.03$ . In the second section named perfect electric conductor vs. dielectric medium-2, dielectric medium-2 refers to the dielectric infinite ground medium data with relative permittivity  $\epsilon_r=4$  and conductivity  $\sigma=0.06$ .

### 5.3.1 Perfect Electric Conductor vs Dielectric Medium-1

In the following analysis, perfect electric conductor is used as the ground medium for calibration data and dielectric medium with relative permittivity  $\epsilon_r=13$  and conductivity  $\sigma=0.03$  is used as the ground medium for test data. Bias data file is used to correct DF errors due to ground medium differences. The test data whose errors are to be corrected is called "correction data" through the analysis in this section. Azimuth angle set for the test data has different initial azimuth values for different frequencies. For 20 MHz, initial azimuth value is taken as 1.25 degrees, for 100 MHz initial azimuth value is taken as 0.5 degree, for 250 MHz, 375 MHz and 500 MHz initial azimuth value is taken as 0.3 degree.

In Figure 5.20, azimuth scan simulation results for frequency 20 MHz and elevation angle of 72 degrees are given. In this figure two different plots are observed. Straight line, named monopole antenna, is the azimuth scan simulation result for the PEC ground medium versus dielectric medium with relative permittivity  $\epsilon_r=15$  and conductivity  $\sigma=0.04$ , which has the same ground medium settings with the bias data file. The striped line is called "cal 1deg" in the simulation. This means calibration data is collected with 1 degree azimuth steps while obtaining the bias data file. Striped line simulation results are obtained when the calibration data is collected with PEC ground medium and test data is collected with dielectric ground medium having relative permittivity  $\epsilon_r=13$  and conductivity  $\sigma=0.03$ . In the simulation for striped line, bias data file is used as a correction tool for the analysis. From the figure we can say that, changing the properties of dielectric medium does not affect the DF performance much due to bias correction. Average RMSE is around 3 degrees in both cases.

In Figure 5.21, azimuth scan simulation results for frequency 20 MHz and elevation angle of 88 degrees are given. In this figure, average RMSE is decreased by 1.5 degrees as compared to average RMSE for elevation angle 72 degrees. DF performances are similar for both

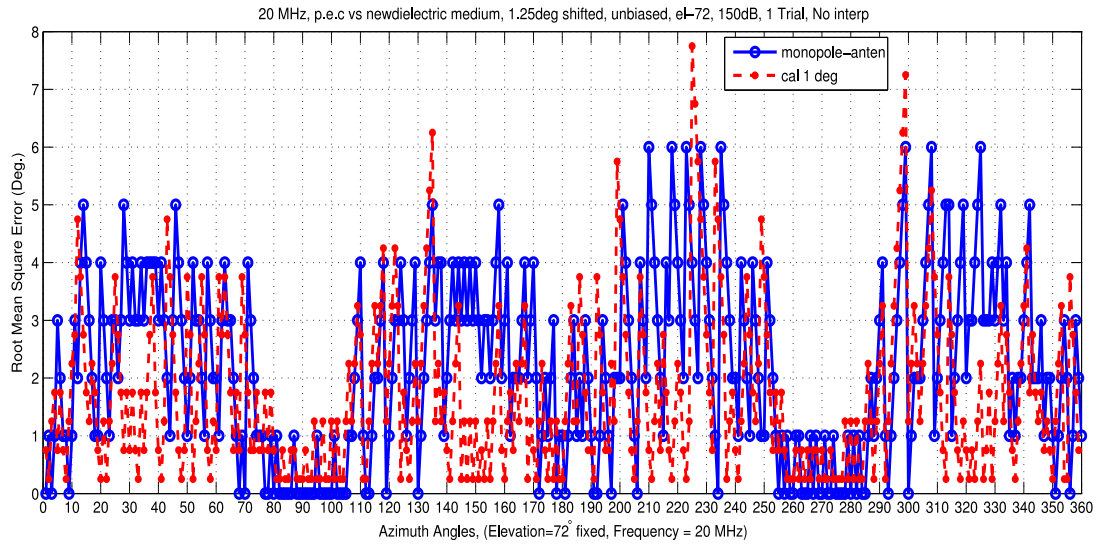


Figure 5.20: 20 MHz, Perfect Electric Conductor versus Dielectric medium, with relative permittivity  $\epsilon_r=13$ , and conductivity  $\sigma=0.03$ , elevation angle is 72 degrees.

calibration data and correction data.

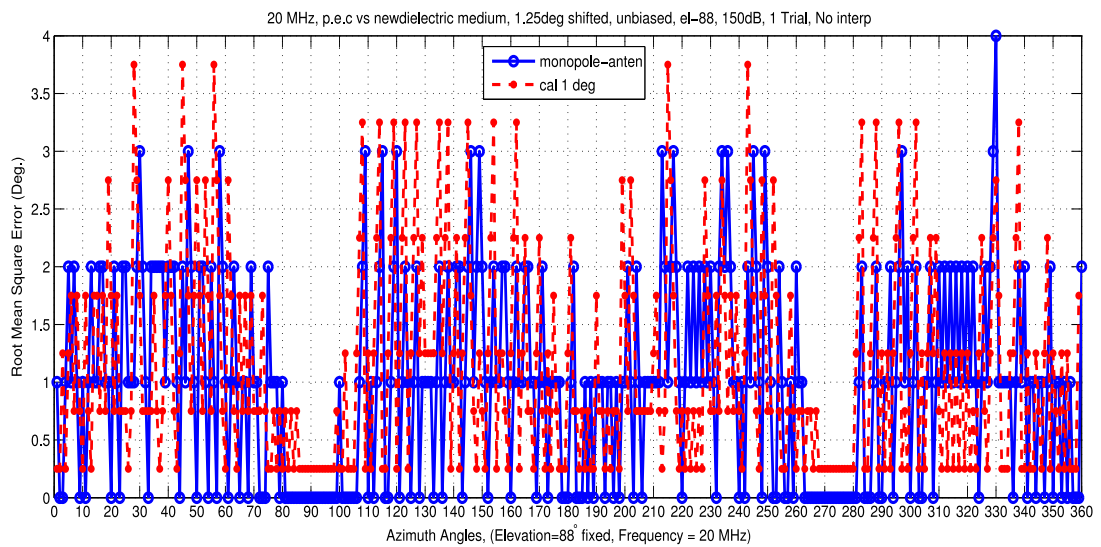


Figure 5.21: 20 MHz, Perfect Electric Conductor versus Dielectric medium, with relative permittivity  $\epsilon_r=13$ , and conductivity  $\sigma=0.03$ , elevation angle is 88 degrees.

In Figure 5.22, azimuth scan simulation results for frequency 100 MHz and elevation angle of 72 degrees are given. In this figure, straight line which corresponds to the calibration data simulation of PEC vs. dielectric with  $\epsilon_r=15$  and conductivity  $\sigma=0.04$ , gives 180 degrees RMSE in 90 and 270 degrees azimuth angles. For correction data simulations, these errors

are corrected with the use of bias data file. Average RMSE is also decreased to 60 degrees for correction data, while in calibration data, RMSE is around 120 degrees. DF performances for three azimuth steps of 1, 2 and 4 degrees are similar. In the azimuth region between 130-140 degrees, approximately 150 degrees RMSE occur for azimuth step of 2 degrees.

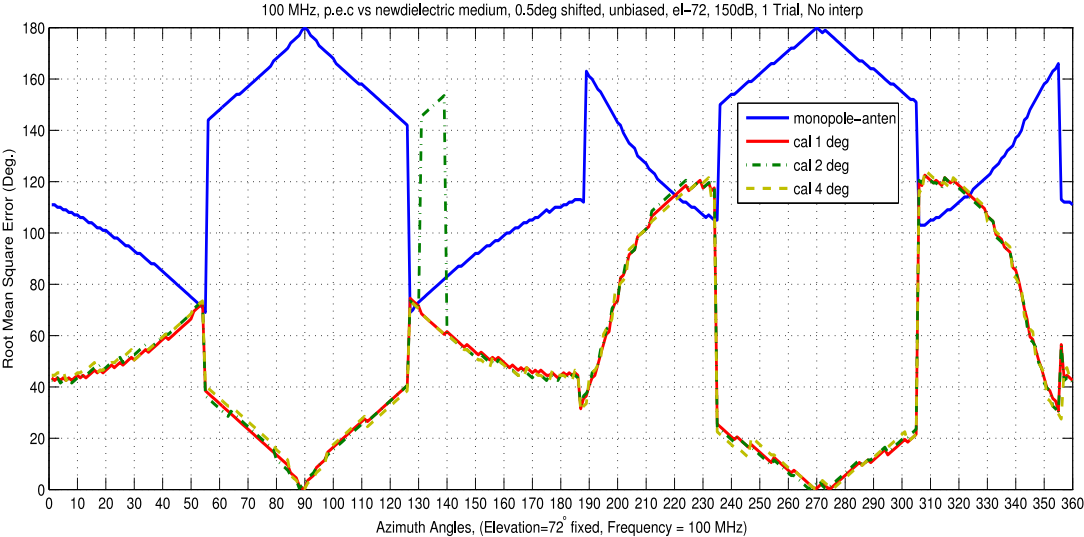


Figure 5.22: 100 MHz, Perfect Electric Conductor versus Dielectric medium, with relative permittivity  $\epsilon_r=13$ , and conductivity  $\sigma=0.03$ , elevation angle is 72 degrees.

In Figure 5.23, azimuth scan simulation results for frequency 100 MHz and elevation angle of 88 degrees are given. In this figure, straight line (calibration data), named monopole antenna in the simulation, represents analysis for PEC ground medium vs. dielectric ground medium with  $\epsilon_r=15$  and conductivity  $\sigma=0.04$ . Bias data file is not used in straight line simulations and an average RMSE of 2 degrees is obtained from the straight line except for the azimuth regions 200-220 degrees and 320-340 degrees. In these regions, RMSE is around 10 degrees. For the correction data simulations, these peak errors drop to 6 degrees RMSE for these azimuth regions. In other azimuth regions, average RMSE is below 1 degree for correction data. If we compare the results for different azimuth steps we can observe that, 1 degree of azimuth step causes lower RMSE than 2 degrees and 4 degrees of azimuth steps. However in the azimuth regions described above, RMSE levels for azimuth steps of 1 degree, 2 degrees and 4 degrees are similar.

In Figure 5.24, azimuth scan simulation results for frequency 250 MHz and elevation angle of 72 degrees are given. In this figure, straight line(calibration data) has an average of 2.5-

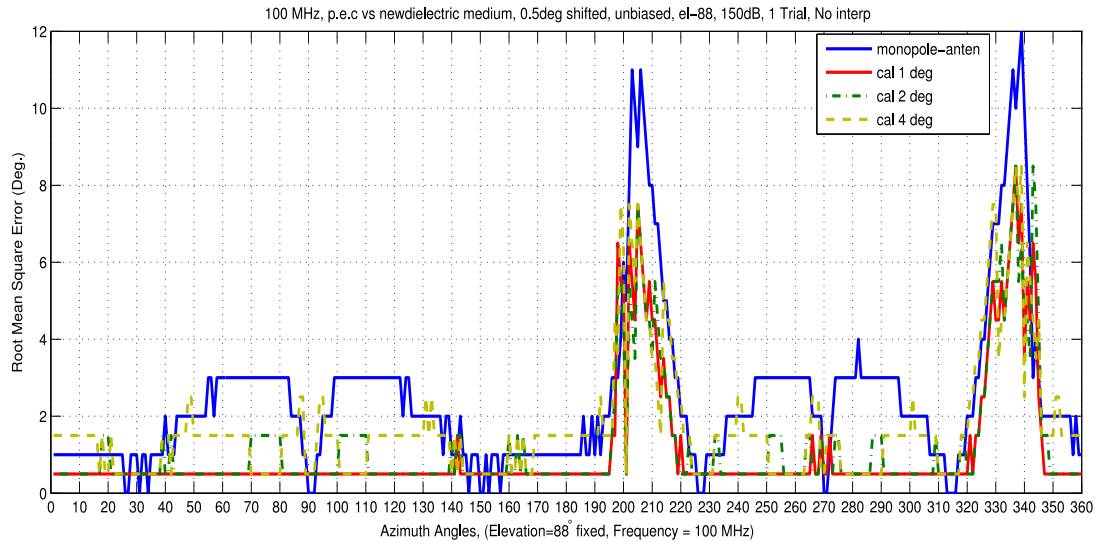


Figure 5.23: 100 MHz, Perfect Electric Conductor versus Dielectric medium, with relative permittivity  $\epsilon_r=13$ , and conductivity  $\sigma=0.03$ , elevation angle is 88 degrees.

3 degrees RMSE. However for correction data simulations with azimuth steps 0.25 and 1 degree, average RMSE is lower than 0.5 degree. Thus DF performance of correction data is at least 5-6 times better than that of calibration data. If we compare the performance of 0.25 degree azimuth step with 1 degree azimuth step we will see that, peak RMSE values for 1 degree azimuth resolution are slightly higher than peaks of 0.25 degree azimuth resolution case.

In Figure 5.25, azimuth scan simulation results for frequency 250 MHz and elevation angle of 88 degrees are given. In this figure, average RMSE of calibration data (PEC vs dielectric medium with  $\epsilon_r=15$  and conductivity  $\sigma=0.04$ ) is 1 degree, whereas average RMSE of correction data is lower than 0.5 degree. Around azimuth angle sectors of 190-210 degrees and 330-350 degrees RMSE levels of 4 degrees are reached by the calibration data, however for correction data RMSE is around 2 degrees. In other azimuth sectors RMSE is below 0.5 degree for correction data.

In Figure 5.26, azimuth scan simulation results for frequency 375 MHz and elevation angle of 72 degrees are given. In this figure, calibration data has an average RMSE of 1.5 degrees for the azimuth sector 0-180 degrees and 0.5 degree for the azimuth angles between 180-360 degrees. For the correction data, average RMSE is around 0.5 degree. Peak RMSE values for 1 degree of azimuth step are 0.5 degree higher than that of the 0.25 degree azimuth step case.

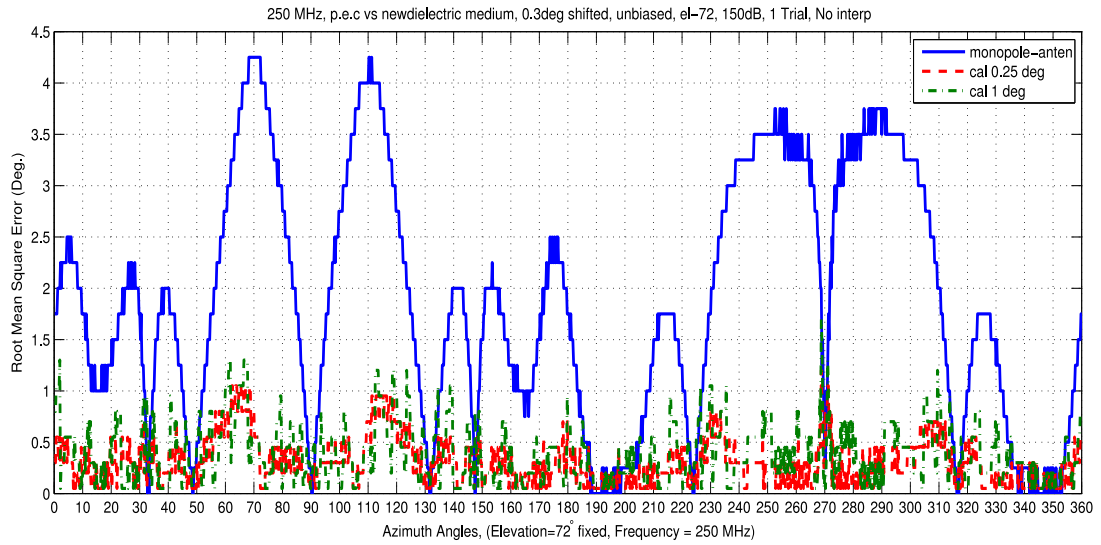


Figure 5.24: 250 MHz, Perfect Electric Conductor versus Dielectric medium, with relative permittivity  $\epsilon_r=13$ , and conductivity  $\sigma=0.03$ , elevation angle is 72 degrees.

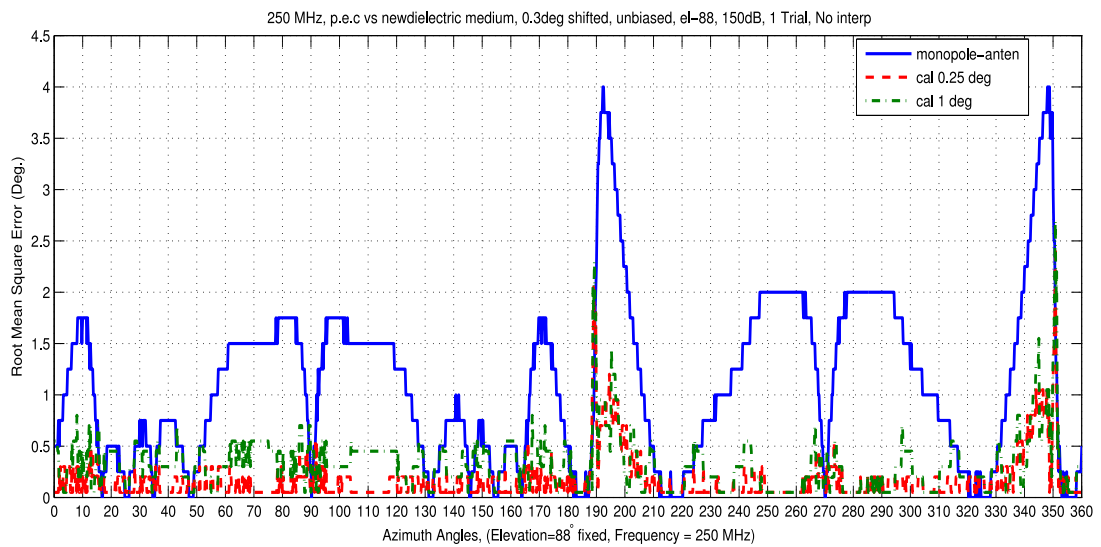


Figure 5.25: 250 MHz, Perfect Electric Conductor versus Dielectric medium, with relative permittivity  $\epsilon_r=13$ , and conductivity  $\sigma=0.03$ , elevation angle is 88 degrees.

In Figure 5.27, azimuth scan simulation results for frequency 375 MHz and elevation angle of 88 degrees are given. In this figure, average RMSE for the calibration data is below 1 degree. For the simulation with azimuth step 0.25 degree, average RMSE is lower than 0.2 degree, while for simulation with azimuth step 1 degree, average RMSE is around 0.4 degree. RMSE

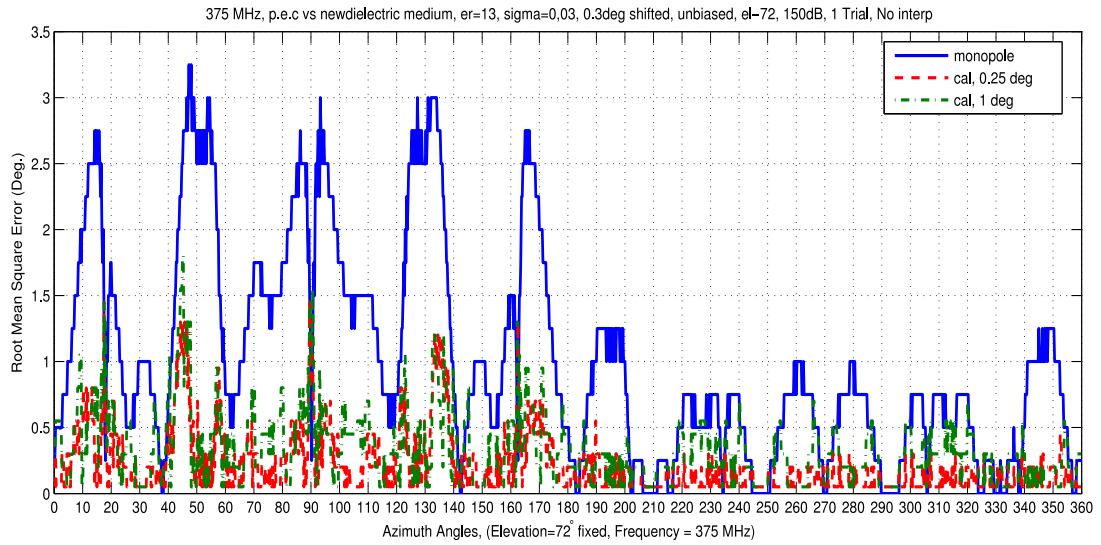


Figure 5.26: 375 MHz, Perfect Electric Conductor versus Dielectric medium, with relative permittivity  $\epsilon_r=13$ , and conductivity  $\sigma=0.03$ , elevation angle is 72 degrees.

curves of different azimuth resolutions are distinguishable in this figure.

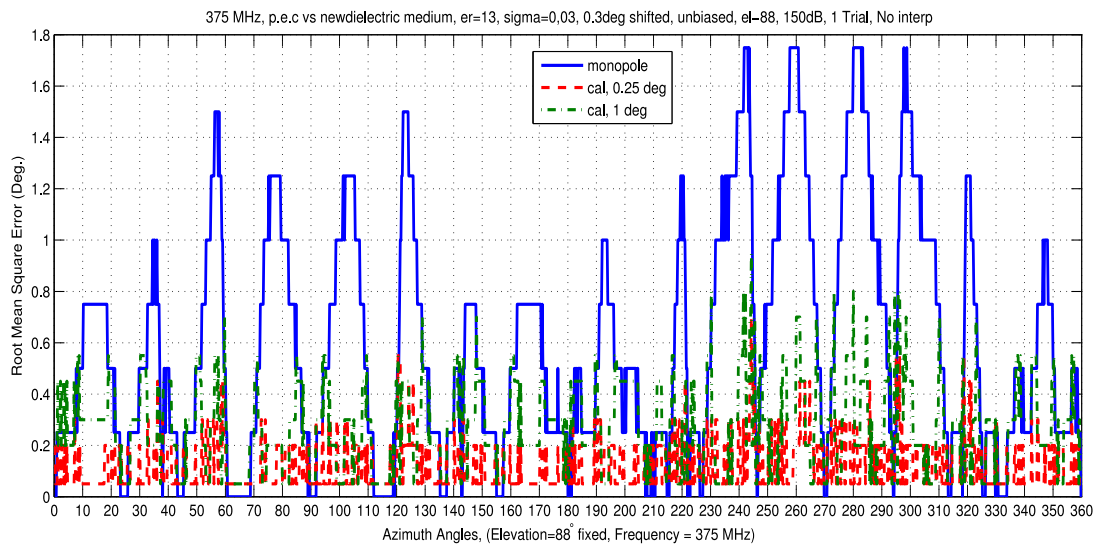


Figure 5.27: 375 MHz, Perfect Electric Conductor versus Dielectric medium, with relative permittivity  $\epsilon_r=13$ , and conductivity  $\sigma=0.03$ , elevation angle is 88 degrees.

In Figure 5.28, azimuth scan simulation results for frequency 500 MHz and elevation angle of 72 degrees are given. In this figure, RMSE distribution for the calibration data among azimuth sector is more homogenous as compared to simulations in frequency 375 MHz. Average RMSE is around 1 degree for the calibration data. For correction data, average RMSE is

lower than 0.5 degree. If we compare two azimuth steps' performances we can say that, peak RMSE levels are 0.5 degree higher in some azimuth sectors for 1 degree azimuth resolution.

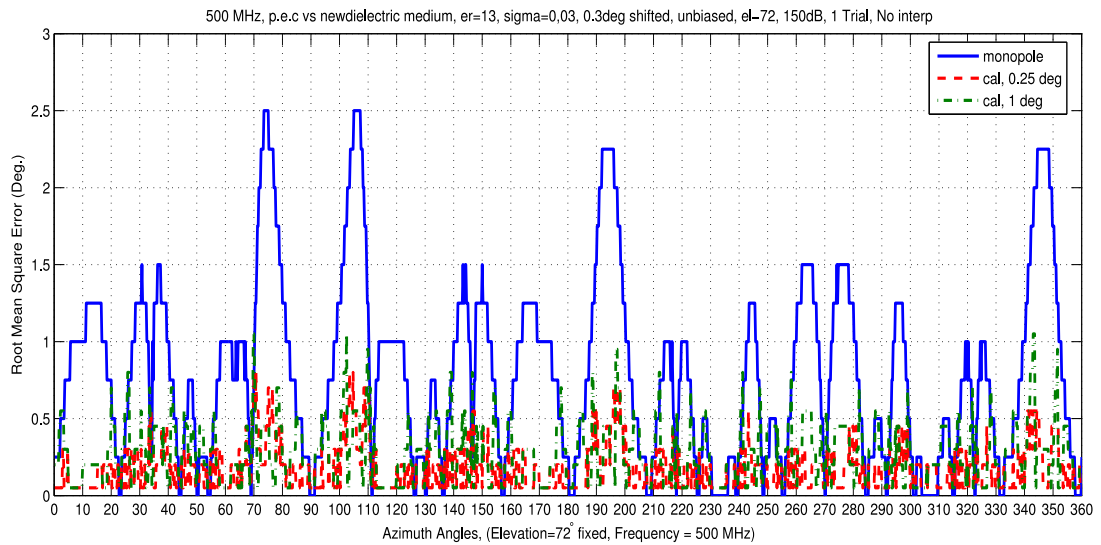


Figure 5.28: 500 MHz, Perfect Electric Conductor versus Dielectric medium, with relative permittivity  $\epsilon_r=13$ , and conductivity  $\sigma=0.03$ , elevation angle is 72 degrees.

In Figure 5.29, azimuth scan simulation results for frequency 500 MHz and elevation angle of 88 degrees are given. In this figure, average RMSE for the calibration data is around 0.6 degree. In simulations with azimuth step 0.25 degree, average RMSE is lower than 0.2 degree, whereas in simulations with azimuth step 1 degree, average RMSE is lower than 0.4 degree. As in 375 MHz, different azimuth step's RMSE curves are distinguishable for elevation angle 88 degrees.

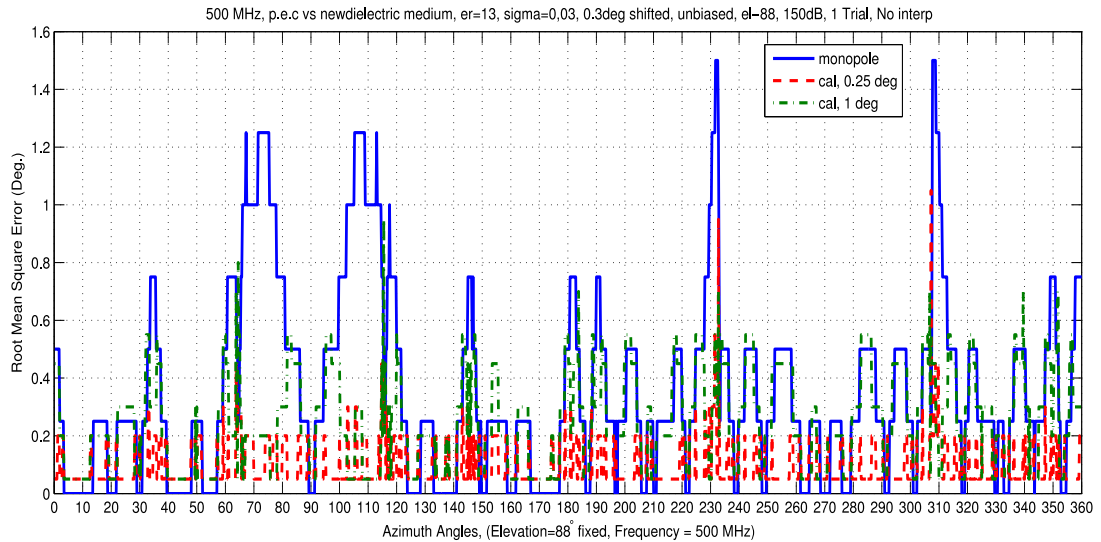


Figure 5.29: 500 MHz, Perfect Electric Conductor versus Dielectric medium, with relative permittivity  $\epsilon_r=13$ , and conductivity  $\sigma=0.03$ , elevation angle is 88 degrees.

### 5.3.2 Perfect Electric Conductor vs Dielectric Medium-2

In this section, properties of dielectric medium are changed and the same analysis applied for this new dielectric medium as well. Dielectric infinite ground medium in these simulations has a relative permittivity  $\epsilon_r=4$  and conductivity  $\sigma=0.06$ . This dielectric medium is named dielectric medium-2. In the following figures, the same bias data file is used as in the dielectric medium-1 simulations. Therefore robustness of the "bias approach" is checked during these experiments.

In Figure 5.30, azimuth scan simulation results for frequency 20 MHz and elevation angle of 72 degrees are given. In this figure, average RMSE values for calibration data (PEC vs. relative permittivity  $\epsilon_r=15$  and conductivity  $\sigma=0.04$ ) which is represented by straight line and correction data which is represented by striped line are similar and around 3 degrees. If we compare this result with the dielectric medium-1 simulations we observe that there is no significant change in RMSE curves for different dielectric mediums.

In Figure 5.31, azimuth scan simulation results for frequency 20 MHz and elevation angle of 88 degrees are given. In this figure, DF performances of calibration data and correction data are similar, average RMSE level is around 1-1.5 degrees. When this result is compared with the dielectric medium-1 simulations, it is observed that average RMSE level is 1 degree lower

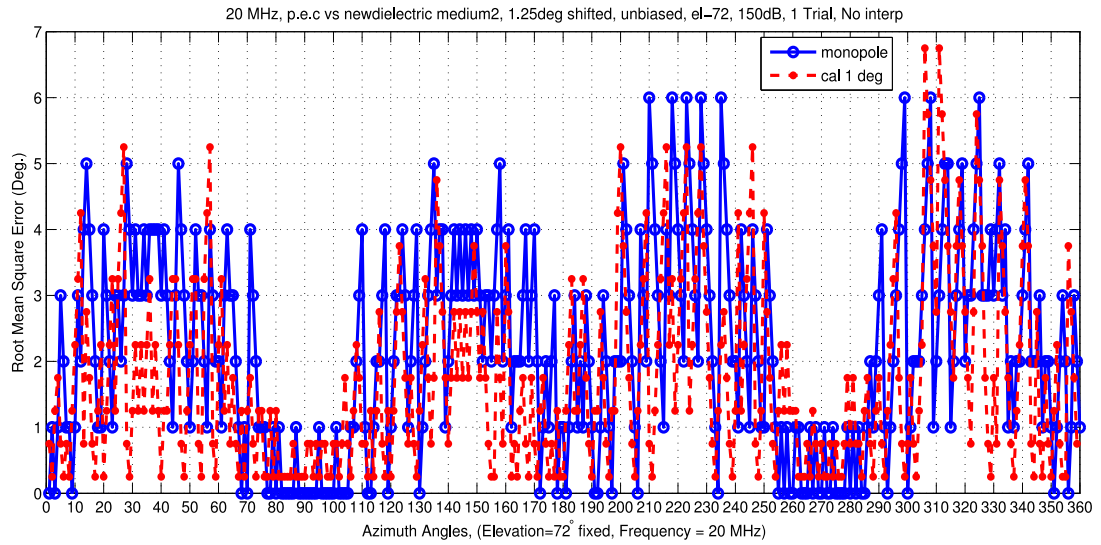


Figure 5.30: 20 MHz, Perfect Electric Conductor versus Dielectric medium, with relative permittivity  $\epsilon_r=4$ , and conductivity  $\sigma=0.06$ , elevation angle is 72 degrees.

for dielectric medium-2.

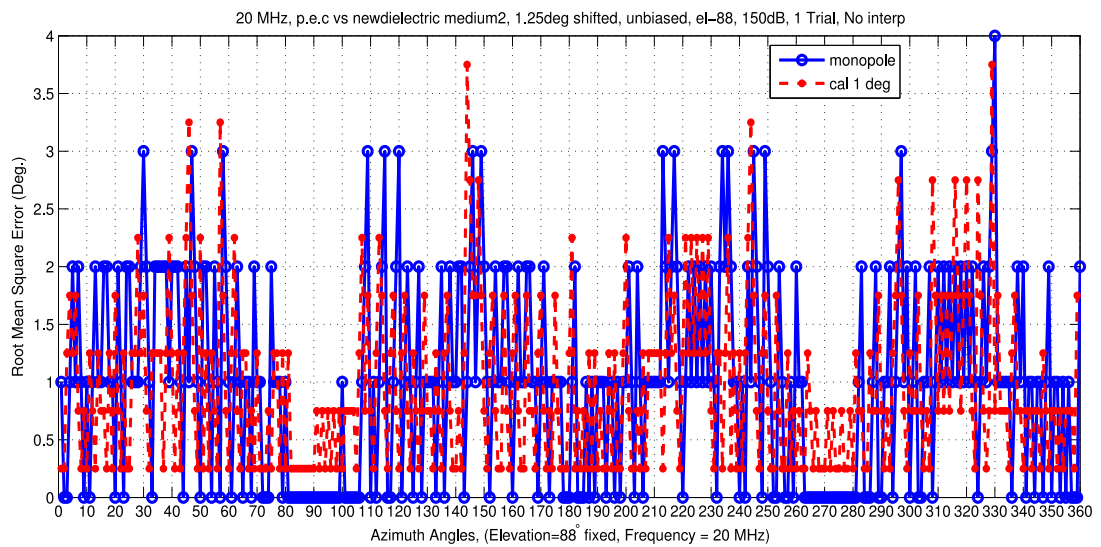


Figure 5.31: 20 MHz, Perfect Electric Conductor versus Dielectric medium, with relative permittivity  $\epsilon_r=4$ , and conductivity  $\sigma=0.06$ , elevation angle is 88 degrees.

In Figure 5.32, azimuth scan simulation results for frequency 100 MHz and elevation angle of 72 degrees are given. In this figure, average RMSE for calibration data is around 120 degrees with a peak RMSE of 180 degrees in 90 and 270 degrees azimuths. For correction data, average RMSE is around 80 degrees. If we compare this result with the dielectric medium-1

simulation with the same frequency and elevation angle, we can say that RMSE curves for different azimuth steps are similar except for the azimuth regions 30-60 degrees and 120-150 degrees, where peak RMSE level is around 160 degrees in dielectric medium-2. However in dielectric medium-1, there is 70 degrees of peak RMSE in azimuth region 30-60 degrees for all azimuth resolutions and 150 degrees RMSE for azimuth sector 120-150 degrees for only azimuth step 2 degrees, in other azimuth resolutions of 1 degree and 4 degrees, RMSE curve has a peak of 70 degrees in azimuth sector 120-150 degrees.

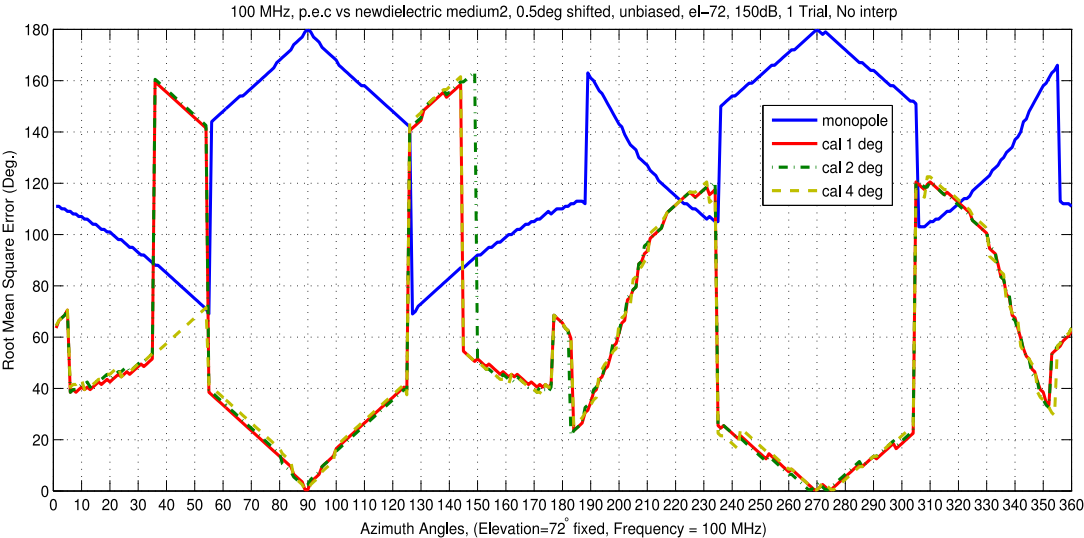


Figure 5.32: 100 MHz, Perfect Electric Conductor versus Dielectric medium, with relative permittivity  $\epsilon_r=4$ , and conductivity  $\sigma=0.06$ , elevation angle is 72 degrees.

In Figure 5.33, azimuth scan simulation results for frequency 100 MHz and elevation angle of 88 degrees are given. In this figure, DF performances of calibration data and correction data are similar especially at azimuth sectors 200-220 degrees and 320-340 degrees where peak RMSE of 10 degrees occur. In these azimuth sectors there is no difference in the RMSE levels of different azimuth steps. Around 90 and 270 degrees azimuths, calibration data makes around 3 degrees of RMSE while correction data has lower RMSE. If we compare these results with the results for dielectric medium-1 we can say that dielectric medium-1 makes lower RMSE especially at the azimuth sectors where peak RMSEs occur. At these angles RMSE level of dielectric medium-1 is 3-4 degrees lower than the results of the dielectric medium-2.

In Figure 5.34, azimuth scan simulation results for frequency 250 MHz and elevation angle

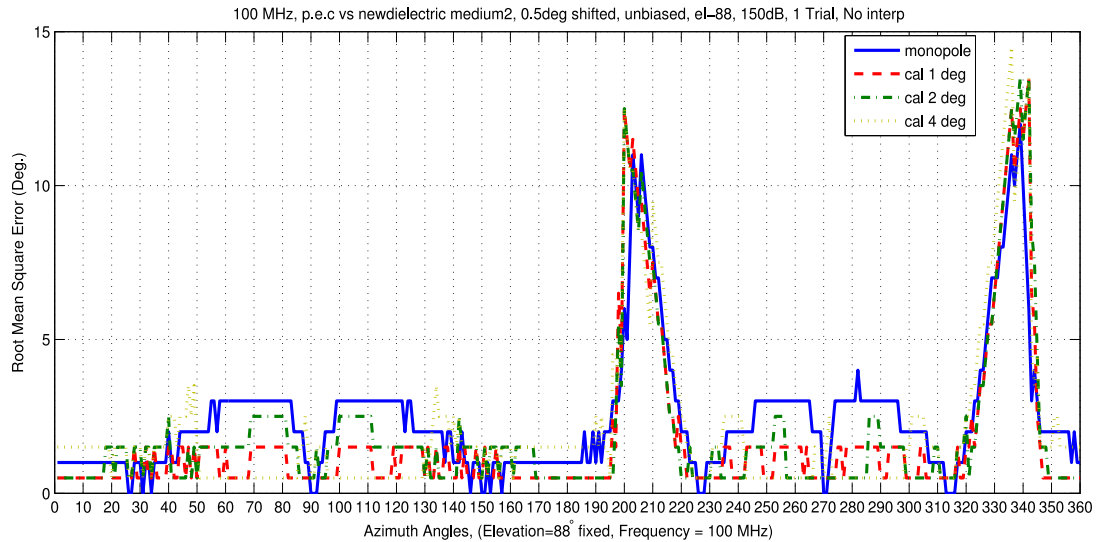


Figure 5.33: 100 MHz, Perfect Electric Conductor versus Dielectric medium, with relative permittivity  $\epsilon_r=4$ , and conductivity  $\sigma=0.06$ , elevation angle is 88 degrees.

of 72 degrees are given. In this figure, average RMSE is 2 degrees for calibration data and it is 1-1.5 degrees for correction data. In azimuth regions around 90 and 270 degrees, peak RMSE level for correction data are 3 degrees and 1.5 degrees, respectively. However, for dielectric medium-1, RMSE levels for the same azimuth sectors are 1 degree and 0.5 degree, respectively. Thus dielectric medium-1 still has better DF performance in comparison. This result is due to the resemblance of dielectric medium characteristics used in the simulations for obtaining bias data file and dielectric medium-1. Relative permittivity of dielectric medium-1's dielectric ground medium is close to the relative permittivity of dielectric medium used in bias data file. As a result, any increase in the RMSE level can be better tolerated using the data in bias data file and lower RMSE levels achieved by dielectric medium-1.

In Figure 5.35, azimuth scan simulation results for frequency 250 MHz and elevation angle of 88 degrees are given. In this figure, average RMSE for calibration data is 1 degree. For correction data, average RMSE is lower than 0.5 degree for most of the azimuth span except for the azimuth region 190-210 degrees and 330-350 degrees. In these azimuth regions, peak RMSE is 1.5 degree. If we compare these results with the simulations for dielectric medium-1 we can say that in azimuth regions defined above, peak RMSE is 0.5 degree higher in dielectric medium-2, in other azimuth angles DF performances are similar.

In Figure 5.36, azimuth scan simulation results for frequency 375 MHz and elevation angle

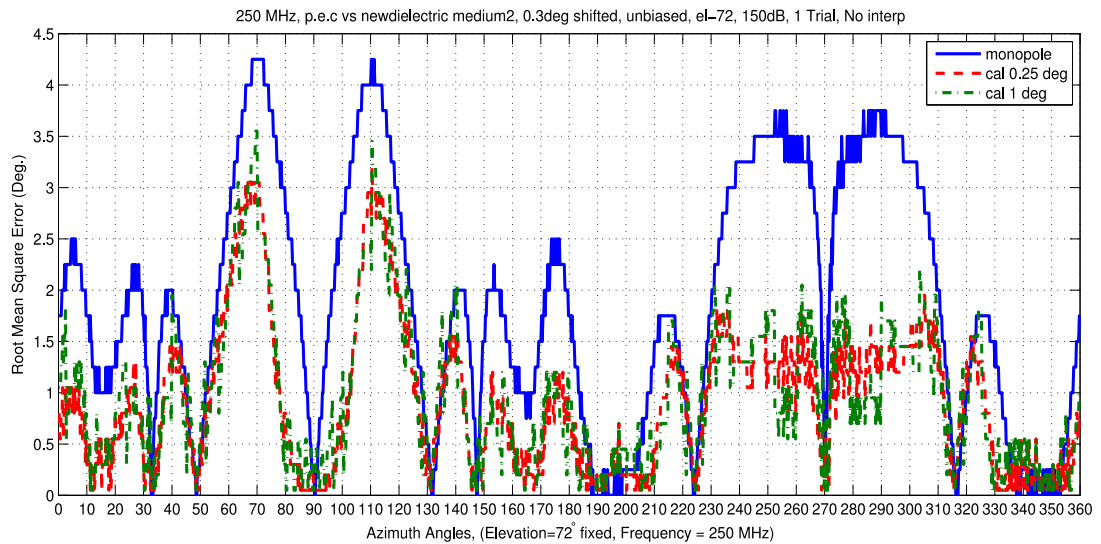


Figure 5.34: 250 MHz, Perfect Electric Conductor versus Dielectric medium, with relative permittivity  $\epsilon_r=4$ , and conductivity  $\sigma=0.06$ , elevation angle is 72 degrees.

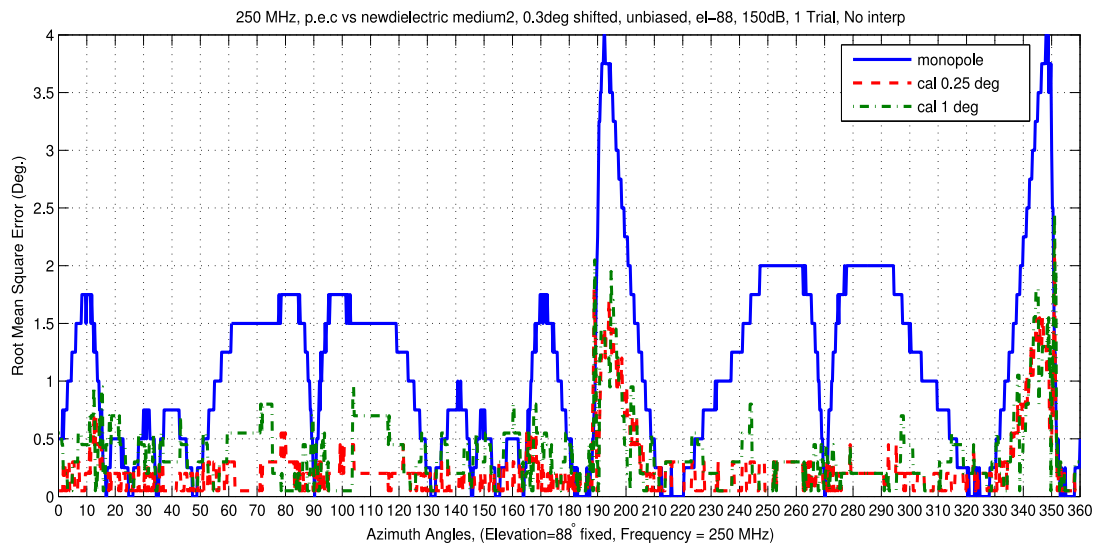


Figure 5.35: 250 MHz, Perfect Electric Conductor versus Dielectric medium, with relative permittivity  $\epsilon_r=4$ , and conductivity  $\sigma=0.06$ , elevation angle is 88 degrees.

of 72 degrees are given. In this figure, average RMSE levels of correction data is around 0.5 degree, where higher RMSE levels occur between azimuth angles of 0-180 degrees. If we compare these results with the simulations for dielectric medium-1, we can say that RMSE levels in azimuth sector between 0-180 degrees are 0.5 degree higher in dielectric medium-2.

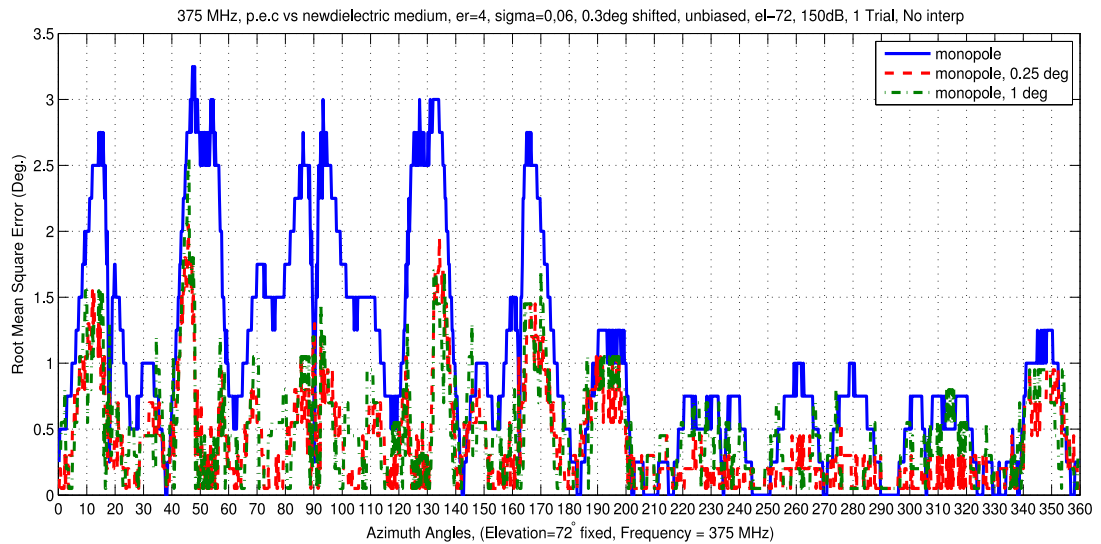


Figure 5.36: 375 MHz, Perfect Electric Conductor versus Dielectric medium, with relative permittivity  $\epsilon_r=4$ , and conductivity  $\sigma=0.06$ , elevation angle is 72 degrees.

In Figure 5.37, azimuth scan simulation results for frequency 375 MHz and elevation angle of 88 degrees are given. In this figure, average RMSE for the calibration data is around 0.8 degree. For correction data with azimuth step 0.25 degree, average RMSE is around 0.2 degree, however for azimuth step 1 degree, average RMSE is approximately 0.4 degree. If we compare these results with the simulations for dielectric medium-1, we can say that DF performances are similar for two different dielectric mediums.

In Figure 5.38, azimuth scan simulation results for frequency 500 MHz and elevation angle of 72 degrees are given. In this figure, correction data makes peak RMSE above 100 degrees in the azimuth sectors around 70 and 110 degrees. However, calibration data has RMSE of 2.5 degrees in these azimuth regions. This situation can be explained with the difference in the dielectric properties of calibration data and dielectric medium-2. If we compare this figure with the simulation for dielectric medium-1, we observe that RMSE in the azimuth sectors given above is around 0.5 degree.

In Figure 5.39, azimuth scan simulation results for frequency 500 MHz and elevation angle of 88 degrees are given. In this figure, RMSE level is above 100 degrees for correction data similar to elevation angle 72 degrees results. In this case azimuth angles where these high RMSE values occur are shifted 10 degrees toward 90 degrees azimuth as compared to result for elevation angle 72 degrees. Here peak RMSE's observed in azimuth regions around 80

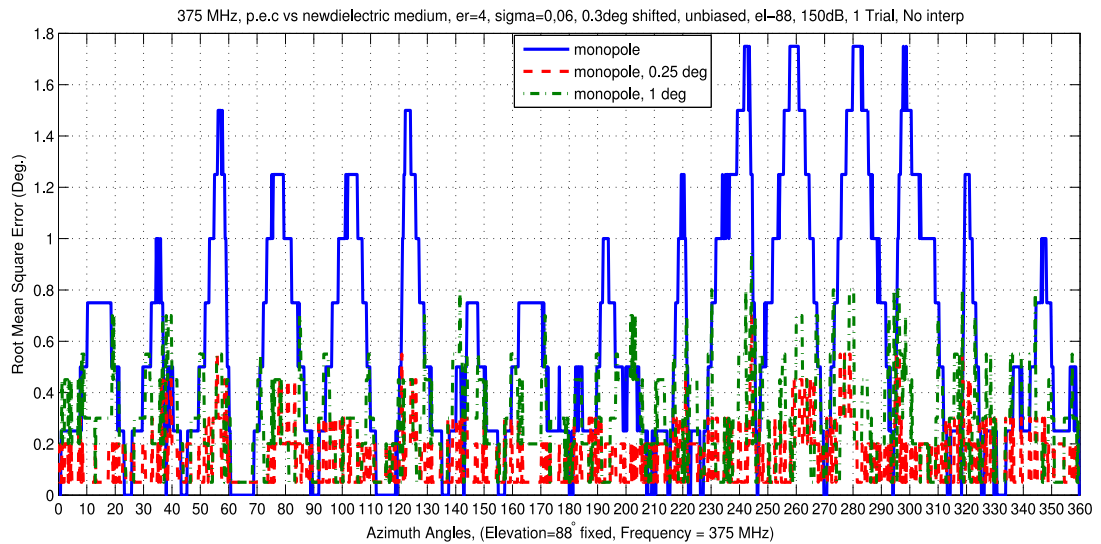


Figure 5.37: 375 MHz, Perfect Electric Conductor versus Dielectric medium, with relative permittivity  $\epsilon_r=4$ , and conductivity  $\sigma=0.06$ , elevation angle is 88 degrees.

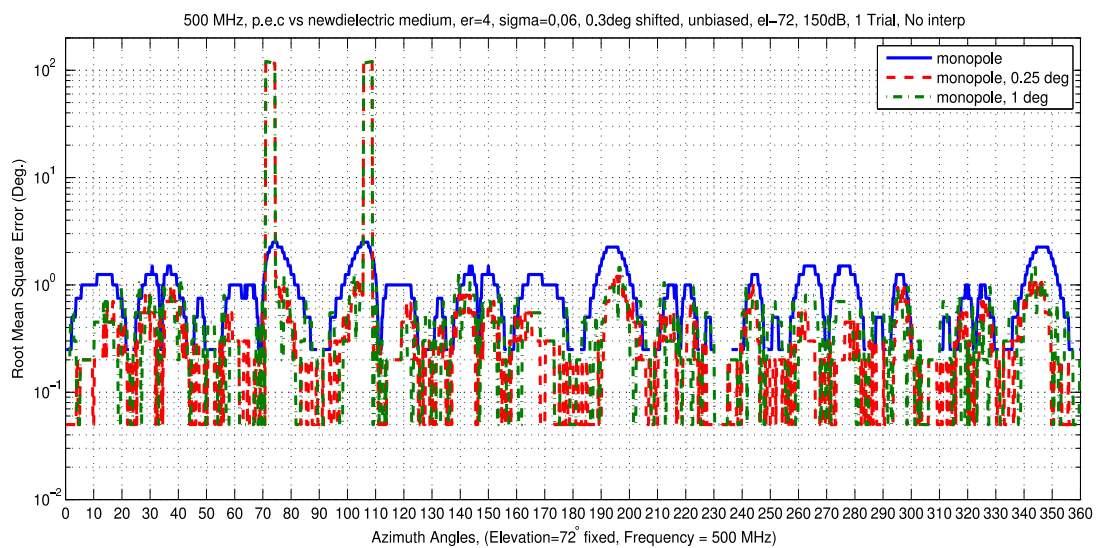


Figure 5.38: 500 MHz, Perfect Electric Conductor versus Dielectric medium, with relative permittivity  $\epsilon_r=4$ , and conductivity  $\sigma=0.06$ , elevation angle is 72 degrees.

and 100 degrees. In addition, these high RMSE levels become narrower in this figure. If we compare these results with simulations of dielectric medium-1, we can observe that RMSE level is around 0.2 degree in dielectric medium-1 for the above mentioned azimuth regions.

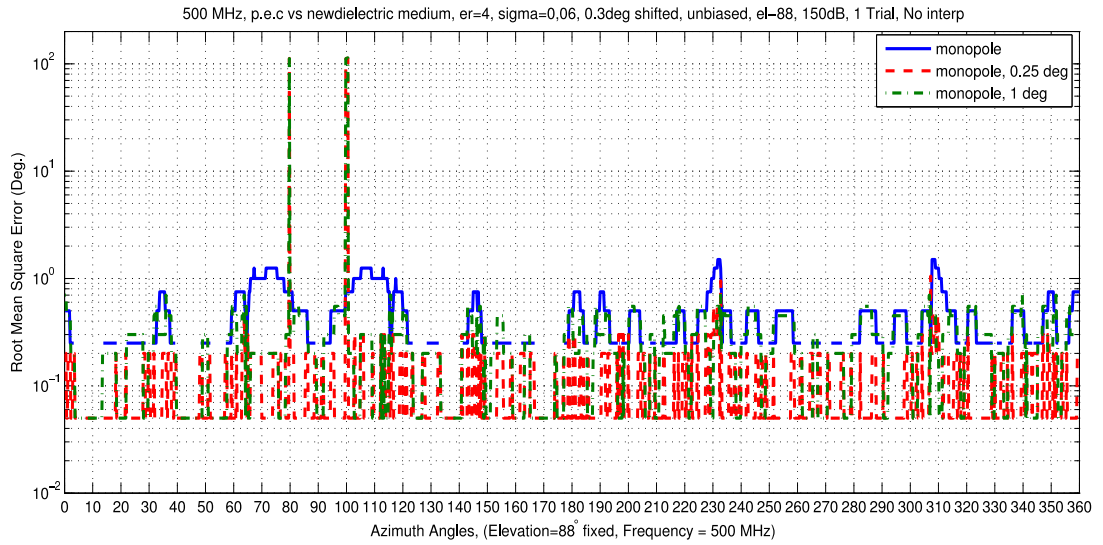


Figure 5.39: 500 MHz, Perfect Electric Conductor versus Dielectric medium, with relative permittivity  $\epsilon_r=4$ , and conductivity  $\sigma=0.06$ , elevation angle is 88 degrees.

## 5.4 Discussions

In this chapter, monopole antenna's DF performance is tested on a Hummer vehicle. Two types of analyses are accomplished. In the first type of analysis, calibration data is collected for PEC ground medium and test data is collected for dielectric medium. Three different dielectric mediums are used. RMSE vs. azimuth scan simulations show that, in the frequency band 20-500 MHz, DF performances of three dielectric mediums are similar. Single exception occurs at frequency 500 MHz and in elevation angles 72 and 88 degrees. For these settings, dielectric medium with relative permittivity  $\epsilon_r=4$  and conductivity  $\sigma=0.06$  has a peak RMSE of 100 degrees, however in the azimuth angle where this peak occurs other two dielectric mediums' RMSE is lower than 1 degree.

In the second type of analysis, bias data is used. Bias data simulations result in RMSE reduction. Bias data is collected for different azimuth steps in the calibration data. Simulations show that for dielectric medium-1, different azimuth steps result in the same RMSE reduction. However for dielectric medium-2, if calibration data is collected more dense with smaller azimuth step, RMSE reduction increases resulting in a lower RMSE level. In dielectric medium-2, RMSE levels are higher as compared to dielectric medium-1, for all frequencies in the frequency band. This result is the consequence of higher similarity between

dielectric medium-1 and dielectric medium used in bias data file. Relative permittivity and conductivity of dielectric medium-2 result in higher RMSE.

Usage of bias data file is successful in RMSE reduction especially when the fluctuations in RMSE curve is small. That is, in azimuth regions where RMSE curve has steeper slope, reduction in error is less as compared to flat RMSE regions where error cancellation can be better. In bias analysis part, correction data has an initial azimuth value different from calibration data's initial azimuth value. The difference between initial azimuth values in correction data and calibration data determines error correction. When RMSE level is the same within neighborhood of this difference, then bias data file becomes successful in error reduction. However, when RMSE curve has high fluctuations, due to difference between initial azimuth values, bias data file can not decrease errors.

## CHAPTER 6

### CONCLUSION

In this thesis work, Direction Finding (DF) performances of several antennas are tested. For this purpose antenna models are generated in a numerical electromagnetic simulation tool FEKO. Method is generated to use antenna array's current data to find DF performance. This method includes conversion of FEKO output file into a data file usable in MATLAB environment. Correlative interferometer algorithm is applied to these data files to find DF performance of antenna models on various platforms.

In chapter-3, wideband antenna model is generated. Wideband antenna model used is discone antenna. Different antenna array geometries for the discone antenna are considered. The discone model having the smallest antenna interelement distance with isotropic azimuth response is selected. DF performance of this wideband antenna is compared with narrowband antennas. Dipole antennas are used as narrowband antennas. Two frequency bands are used. In each band, different dipole antennas are used which are designed to have the optimum performance in the middle of the band. However, only a single antenna array is used for discone. The main purpose is to cover a large frequency range with only one antenna array. It is shown that, this is possible and a better DF performance than that of two dipole arrays covering the same frequency bands can be obtained.

Antenna interelement distance is a critical parameter that affects the occurrence of spatial aliasing. If the antenna interelement distance is selected lower than half the wavelength corresponding to the maximum frequency, then spatial aliasing does not occur. However if the antenna interelement distance is lower than half the wavelength, Direction Finding (DF) performance is poor in frequencies where the antenna interelement distance is too low compared to the wavelength. Thus antenna interelement distance has both a lower and an upper bound.

The best choice for antenna interelement distance is half the wavelength corresponding to the maximum frequency. In chapter-3, disccone antennas have limitations on the minimum antenna interelement distance. Disccone antenna has a cone part which limits the minimum antenna interelement distance to the base radius of the cone. Although DF performance of the disccone antenna is better than dipole antenna's DF performance in 104-1496 MHz frequency band, antenna interelement distance limitation of the disccone antenna prevents the use of this antenna in higher frequencies than 1500 MHz due to spatial aliasing. If we scale the disccone antenna to obtain lower antenna interelement distance then DF performance worsens in 104-648 MHz frequency band, thus wideband characteristics violated. Two different sets of dipole antennas are used in chapter-3. In frequency band 648-1496 MHz, smaller antenna interelement distance dipole antenna set is used, smaller antenna interelement distance prevents spatial aliasing in high frequencies, but DF performance of this dipole antenna set is worse as compared to dipole antenna set with higher antenna interelement distance at frequency 648 MHz. This frequency is used in both frequency bands and simulations are done for two different dipole antenna set. The main reason is that, when the dipole antennas get closer, DF performance worsens due to mutual coupling between antennas. High variances in RMSE curve occur for disccone antenna due to the shape and interelement distance of the antenna. Interelement distance is limited by the base radius of the cone part in the disccone antenna. This is not the case for dipole antennas, antenna interelement distance is limited to radius of dipole which is much lower than disccone antenna's base radius. However, using smaller antenna interelement distance results in higher RMSE due to mutual coupling.

In chapter-4, dipole antenna's DF performance is tested when antennas are mounted on a UAV. Two different settings are generated. In the first setting, four dipole antennas are placed under the belly of the UAV. In the second setting, two sets of four dipole antennas with a total of eight antennas are placed at right and left arms carrying the rear wings of the UAV. The same dipole antenna models are used with the same antenna interelement distance in these two settings. Calibration and test data are created and correlated to obtain RMSE curves for these two models. Calibration data is collected when the UAV model is 180 degrees rotated and 10 m elevated from the ground medium. Test data is collected when the UAV is flying and in this setting, ground medium is not used. Effects of using different ground mediums are analyzed for elevation angles 92 and 98 degrees. Perfect electric conductor and dielectric infinite ground mediums are used.

Azimuth scan simulation results show that, using eight dipole antennas improves the DF performance as compared to four dipole antenna model. DF performance is also affected from the antenna positions. Keeping the antennas near the rear wings is better than placing the antennas under the belly of the UAV. If the antennas are kept under the belly of the UAV, ground reflections and reflections from the wings and main body worsen the DF performance by increasing RMSEs.

According to the azimuth scan simulation results in chapter-4, using perfect electric conductor (PEC) as the infinite ground medium distorts the magnitude and phase of the current read from dipole antennas more than the dielectric ground medium. Ground reflections have dominant effect when PEC ground medium is used especially in elevation angle 98 degrees. For elevation angle 98 degrees, RMSE values are higher as compared to RMSE values for elevation angle 92 degrees. This situation is related to higher ground reflections for elevation angle 98 degrees.

In chapter-5, monopole antennas are placed on top of a Hummer vehicle and DF performance is tested for PEC and three different dielectric ground mediums. Two types of analyses are done. In the first type, calibration data is collected when the ground medium is perfect electric conductor. Test data is collected when dielectric ground medium is used. RMSE vs azimuth scan simulations are repeated for three different dielectric mediums. According to simulation results, DF performances of three different dielectric mediums are similar in the frequency band 20 MHz-500 MHz.

In the second type, a bias data file is used to reduce RMSE due to changes in ground medium characteristics. Actually, bias data file is successful in RMSE reduction when azimuth error has small variance.

In addition, azimuth resolution of calibration data is tested to find the highest azimuth step which results in moderate RMSE levels. It is observed that for dielectric medium-1, azimuth steps can be increased by a factor of four without increasing the RMSE levels, which means if the original azimuth step is 0.25 degree, 1 degree of azimuth step can be used for collecting calibration data. However for dielectric medium-2, lower azimuth steps result in better RMSE reduction. Thus higher azimuth steps can not be used.

Average RMSE levels for dielectric medium-2 azimuth scan simulations are higher than av-

verage RMSE levels of dielectric medium-1 azimuth scan simulations in all frequencies in the frequency band and for elevation angles 72 and 88 degrees. This situation can be explained with the similar dielectric characteristics of bias data file's dielectric medium with the dielectric medium used in dielectric medium-1 simulations.

## REFERENCES

- [1] Z. Chen, G. Gokeda, Y. Yu, "Introduction to Direction-of-Arrival Estimation," Artech House, pp 9-11,32-33, 2010.
- [2] D. Adamy, "EW101: A First Course in Electronic Warfare," Artech House, p 143, 2001.
- [3] C.S. Park, D.Y. Kim, "The Fast Correlative Interferometer Direction Finder using I/Q Demodulator," IEEE Asia Pasific Conference on Communications, pp. 1-5, August 2006.
- [4] T.E. Tuncer, B. Friedlander, "Classical and Modern Direction-of-Arrival Estimation," Burlington, MA01803, USA,Elsevier, 2009.
- [5] T. E. Tuncer, "Sensor Array Signal Processing," Course Lecture Notes, METU, 2009.
- [6] D. Adamy, "EW103: Tactical Battlefield Communications Electronic Warfare," Artech House, pp. 204-222, 2009.
- [7] A. Xiabo, F. Zhenghe, "A Single Channel Correlative Interferometer Direction Finder Using VXI Receiver," IEEE 3<sup>rd</sup> International Conference on Microwave and Millimeter wave Technology Proceedings, pp. 1158-1161, 2002.
- [8] H.W. Wei, Y.G. Shi, "Performance Analysis and Comparison of Correlative Interferometers for Direction Finding," IEEE ICSP 2010 Proceedings, pp. 393-396, 2010.
- [9] L. Qin, K. Jia, Z. He, "Performance Analysis of Correlative Interferometer Direction Finder Using Cosine Functions," IEEE ISPACS December 6-8 2010.
- [10] I. Habil, F.H. Lange, "Correlation Techniques," Iliffe Books Ltd., pp. 8-27, 1967.
- [11] Ö.Ç. Arslan, "Implementation and Performance Evaluation of a Three Antenna Direction Finding System," Msc dissertation, METU, Ankara, November 2009.
- [12] N. Burtnyk, C. W. McLeish, J. Wolfe, "Interferometer Direction Finder for the HF Band," Proceedings of the Institution of Electrical Engineers, Vol.110, No.7, July 1963.
- [13] J.S. Lim, C.G. Jung, G.S.Chae, "A Design of Precision RF Direction Finding Device Using Circular Interferometer," IEEE Intelligent Signal Processing and Communication Systems, pp. 713-716, November 2004.
- [14] D.R. Klose, W. Skudera, "A Saw Interferometer Direction Finding and Frequency Identification Method," Microwave Symposium Digest, 1981 IEEE MTT-S International, pp. 392-394, June 1981.
- [15] C.W. Mcleish, N. Burtnyk, "The Application of the Interferometer to HF Direction Finding," IEEE Proceedings of the Institution of Electrical Engineers, Vol 108, pp. 495-499, September 1961.

- [16] R. Shar, "Simulation of Polarizer Impact on Circular Interferometer Performance," IEEE 11<sup>th</sup> ICCSE Workshops, pp. 334-339, 2008.
- [17] H. Messer, G. Singal, L. Bialy, "On the Achievable DF Accuracy of Two Kinds of Active Interferometers," IEEE Transactions on Aerospace and Electronic Systems, VOL.32, NO.3, pp. 1158-1164, July 1996.
- [18] X. Yang, C.Z. Zhong, "Two-dimensional Circular Array Real-time Phase Interferometer Algorithm and Its Correction," IEEE CISP 2009, pp. 1-5, October 2009.
- [19] N. Saucier, K. Struckman, "Direction Finding Using Correlation Techniques," IEEE Antennas and Propagation Society International Symposium, Vol. 13, pp. 260-263, June 1975.
- [20] K. Struckman, "Correlation Interferometer Geolocation," IEEE Antennas and Propagation Society International Symposium, pp. 1141-1148, July 2006.
- [21] N. Burtnyk, C.W. Mcleish, J. Wolfe, "Performance of an Interferometer Direction Finder for the HF Band," IEEE Proceedings of the Institution of Electrical Engineers, Vol 112, pp. 2055-2059, November 1965.
- [22] L. Balogh, I. Kollar, "Angle of Arrival Estimation Based on Interferometer Principle," 2003 IEEE International Symposium on Intelligent Signal Processing, pp. 219-223, September 2003.
- [23] I. N. Elbehery, R. H. Macphie, "Radio Source Parameter Estimation by Maximum Likelihood Processing of Variable Baseline Correlation Interferometer Data," IEEE Transactions on Antennas and Propagation, Vol. AP-24, No.2, pp. 163-173, March 1976.
- [24] E. B. Ari, J. Remez, "Performance Verification of a Multimodal Interferometric DOA Estimation Antenna," IEEE Antennas and Wireless Propagation Letters, Vol. PP, issue: 99, pp.1-5, July 2011.
- [25] S. Murphy, P. M. Eyring, "2-18 GHz Circular Array Interferometer DF Antenna System," IEEE Antennas and Propagation Society International Symposium, Vol. 4, pp.2332-2335, June 1998.
- [26] S. Germishuizen, D.C. Baker, "Practical Accuracy Limitations in Airborne Microwave Interferometric Direction Finding," IEEE 4<sup>th</sup> Africon Conference, Vol 1., pp. 266-271, September 1996.
- [27] A. Barka, P. Caudrillier, "Domain Decomposition Method Based on Generalized Scattering Matrix for Installed Performance of Antennas on Aircraft," IEEE Transactions on Antennas and Propagation, Vol. 55, No. 6, pp. 1833-1842, June 2007.
- [28] K. A. Snyder, "A Computer Simulation of 400 MHz and 1000 MHz Antennas Located on a High Mobility Multi-Wheeled Vehicle (HMMWV)," IEEE ACES International Conference on Wireless Communications and Applied Computational Electromagnetics, pp. 495-498, April 2005.
- [29] S. P. Benham, T. J. Murphy, E. J. Totten, D. J. Knights, M. Schick, "EM Modelling Design of a Conformal IFF System on an Aircraft," IEEE Antennas and Propagation (EuCAP 2010), pp.1-4, April 2010.

- [30] S. D. Keller, W. O. Coburn, S. J. Weiss, "Efficient Electromagnetic Modeling of Bent Monopole Antenna on Aircraft Wing Using FEKO," IEEE Antennas and Propagation (EuCAP 2009), pp. 2226-2228, March 2009.
- [31] K. A. Snyder, "A Holographic Dipole from a Monopole Mounted in a Dual Parabolic Reflector," IEEE Antennas and Propagation Society International Symposium, pp. 5668-5671, June 2007.
- [32] J. Baker, M. F. Iskander, Z. Yun, M. Evans, J. Johnson, D. Elsheakh, "High Performance Compact Antenna for HF Radar," IEEE Antennas and Propagation Society International Symposium, pp. 1-4, June 2009.
- [33] H. Jiakai, S. Xiang, "Scattering Characteristic Simulation and Analysis of Two Stealth Aircrafts," IEEE International Symposium on Antennas, Propagation and EM Theory ISAPE 2006, pp. 1-5, October 2006.
- [34] H. Zhang, J. Rigelsford, L. Low, R.J. Langley, "Experimental Validation of Simulated 3D Field Distribution within a Vehicle Cabin," IEEE Computation in Electromagnetics, CEM 2008, pp. 195-196, April 2008.
- [35] C. A. Balanis, "Antenna Modeling and Performance on Complex Structures and Airframes," IEEE Antennas and Propagation (EuCAP 2010), pp. 1-5, April 2010.
- [36] S. D. Walker, D. Chatterjee, "Source-Proximity Limitations in High-Frequency Code Solvers for Modeling Conformal Cylindrical Arrays," IEEE Phased Array Systems and Technology Symposium, pp. 403-409, October 2010.
- [37] R. Bunger, F. Demmel, J. Ritter, "Installed Performance Analysis of a Direction Finding System on Board of a Large Aircraft Platform," IEEE 33<sup>rd</sup> European Microwave Conference, Vol. 2, pp. 695-697, October 2003.
- [38] V. Turgul, M. Dirim, S. B. Bilgin, H. I. Gok, T. Nesimoglu, "Broadband Signal Search and Direction Finding at UHF Frequencies," Mediterranean Microwave Symposium, pp. 288-291, August 2010.
- [39] S. Clarke, U. Jakobus, "Dielectric Material Modeling in the MoM-Based Code FEKO," IEEE Antennas and Propagation Magazine, Vol. 47, Issue.5, pp. 140-147, October 2005.
- [40] W. L. Lippincott, T. Pickard, R. Nichols, "Loop-Dipole Antenna Modeling using the FEKO code," IEEE ACES International Conference on Wireless Communications and Applied Computational Electromagnetics, pp. 507-510, April 2005.
- [41] B. F. Dawson, S. S. Lockwood, "Revisiting Mediumwave Ground System Requirements," IEEE Antennas and Propagation Magazine, Vol. 50, Issue.4, pp. 111-114, August 2008.
- [42] H. J. Delgado, J. T. Williams, S. A. Long, "Antenna Pattern Measurement Techniques for Infinite Ground Plane Simulation," IEEE Antennas and Propagation Society International Symposium, Vol. 1, pp. 339-342, June 1989.
- [43] R. G. Fitzgerrell, "Limitations on Vertically Polarized Ground-Based Antennas as Gain Standards," IEEE Transactions on Antennas and Propagation, Vol. 23, Issue.2, pp. 284-286, March 1975.

- [44] J. W. Duncan, "The Effect of Ground Reflections and Scattering on an Interferometer Direction Finder," *IEEE Transactions on Aerospace and Electronic Systems*, Vol. 3, No. 6, November 1967.
- [45] S. R. Best, "The Significance of Ground-Plane Size and Antenna Location in Establishing the Performance of Ground-Plane-Dependent Antennas," *IEEE Antennas and Propagation Magazine*, Vol. 51, No. 6, pp. 29-43, December 2009
- [46] S. Henault, Y.M.M. Antar, S. Rajan, R. Inkol, S. Wang, "Impact of a Finite Ground Plane on the Accuracy of Conventional Wideband Direction Finding Systems for Signals of Unknown Polarization," *IEEE Canadian Conference on Electrical and Computer Engineering*, pp. 1111-1116, May 2009.
- [47] E. I. Muehldorf, "The Effect of Multipath Reflections on Spaceborne Interferometer Accuracy," *IEEE Transactions on Aerospace and Electronic Systems*, Vol. 7, No. 1, pp. 122-131, January 1971.
- [48] M. U. Rehman, Y. Gao, X. Chen, C. G. Parini, Zhinong Ying, "Analysis of GPS Antenna Performance in a Multipath Environment," *IEEE Antennas and Propagation Society International Symposium*, pp. 1-4, July 2008.
- [49] Ç. H. Başçiftçi, "Direction Finding with TDOA in a Multipath Land Environment," Msc dissertation, METU, Ankara, September 2007.
- [50] D. K. Barton, H. J. Albrecht, "Multipath Error in a Vertical Interferometer," *Proceedings of the IEEE*, Vol. 53, Issue.5, pp. 543-544, May 1965.
- [51] P. Stoica, R. Moses, "Spectral Analysis of Signals," Pearson Prentice Hall, p 283, 2005.
- [52] M. Unser, "Splines a perfect fit for signal and image processing," *IEEE Signal Processing Magazine*, pp. 22-38, 1999
- [53] N. Sun, T. Ayabe, T. Nishizaki, "Efficient spline interpolation curve modelling," *Proceedings of the Third International Conference on International Information Hiding and Multimedia Signal Processing*, Vol 2, 2007.
- [54] S.A. Dyer, J.S. Dyer, "Cubic spline interpolation: part-1," *IEEE Instrumentation and Measurement Magazine*, pp. 44-46, 2001
- [55] R. Poisel, "Introduction to Communication Electronic Warfare Systems," Norwood MA:Artech House, p 35, 2002.
- [56] D.L. Adamy, "Tactical Battlefield Communications Electronic Warfare," Norwood MA:Artech House, pp. 129-136, 2009.
- [57] J.W. Duncan, "The Effect of Ground Reflections and Scattering on an Interferometer Direction Finder," *IEEE Transactions on Aerospace and Electronic Systems*, vol AES-3, no.6, pp. 922-932, November 1967.
- [58] E.I. Muehldorf, "The Effect of Multipath Reflections on Spaceborne Interferometer Accuracy," *IEEE Transactions on Aerospace and Electronic Systems*, vol AES-7, no.1, pp. 122-131, January 1971.
- [59] D.K. Barton, H.J. Albrecht, "Multipath Error in a Vertical Interferometer," *Proceedings of the IEEE*, pp. 543-544, March 1965.

- [60] FEKO Users Manuel, EM Software and Systems, S.A. (Pty) Ltd., July 2008, (Online). Available: <http://www.feko.info>
- [61] Y. Huang, K. Boyle," Antennas from Theory to Practice," Wiley,p 218, 2008.
- [62] J.L. Volakis, " Antenna Engineering Handbook", Mc Graw Hill,p 59, 2007.
- [63] S. Clarke, U. Jacobus, " Dielectric Material Modelling in the MoM-based Code FEKO," IEEE Antennas and Propagation Magazine, Vol. 47, No. 5, pp. 140-147, October 2005 .
- [64] Wikipedia (Online). Available: <http://www.wikipedia.org>
- [65] T. Filik, " Planar Array Structures for Two Dimensional Direction of Arrival Estimation," Phd dissertation, METU, Ankara, April 2010.